

Diss. ETH No 15006

**Adsorption and Catalytic Oxidation of Nitrogen Monoxide in
Lean Exhaust for Future Automotive DeNO_x Techniques**

A dissertation submitted to the
SWISS FEDERAL INSTITUTE OF TECHNOLOGY ZURICH
for the degree of
DOCTOR OF TECHNICAL SCIENCES

presented by
JOEL DESPRES
Dipl. Chem., University Louis Pasteur, Strasbourg (France)
born March 9, 1973
in Saint-Rémy, France

accepted on the recommendation of
Prof. Dr. A. Wokaun, examiner
Prof. Dr. A. Baiker, co-examiner
Dr. M. Koebel, co-examiner

2003

Diss. ETH No

**Adsorption and Catalytic Oxidation of Nitrogen Monoxide in
Lean Exhaust for Future Automotive DeNO_x Techniques**

A dissertation submitted to the
SWISS FEDERAL INSTITUTE OF TECHNOLOGY ZURICH
for the degree of
DOCTOR OF TECHNICAL SCIENCES

presented by
JOEL DESPRES
Dipl. Chem., University Louis Pasteur, Strasbourg (France)
born March 9, 1973
in Saint-Rémy, France

accepted on the recommendation of
Prof. Dr. A. Wokaun, examiner
Prof. Dr. A. Baiker, co-examiner
Dr. M. Koebel, co-examiner

2003

*à mes parents,
à Bernard et Christine*

Acknowledgments

I would like to thank Prof. Dr. A. Wokaun for the scientific supervision of this thesis. His support, his broad knowledge and his interest in my work gave me a great help to complete this thesis.

I would like to express my thanks to Prof. Dr. A. Baiker who is the co-examiner for devoting his kind attention in refereeing this thesis.

I am indebted to Dr. M. Koebel for his kind guidance in all aspects throughout the entire thesis and for valuable discussions on the application of future aftertreatment techniques. I also appreciated his strong attachment to the French culture and to the languages.

I express my gratitude to Dr. O. Kröcher for fruitful discussions during the writing of the thesis and for proofreading the publications resulted from this thesis.

Thanks are due to Mr. M. Elsener for his kind help and for the fruitful discussions on technical aspects during the thesis.

My special thanks are due to Dr. B. Schnyder for carrying out XPS measurements and for his valuable guidance in analysis of the measurements. Thanks are also due to Mrs. F. Geiger for carrying out BET measurements, to Mr. A. Frey for performing XRD analysis, to Dr. R. Schaüblin and Dr. S. Abolhassani-Dadras for the TEM analysis and to Mr. R. Keil for the ICP-AES analysis.

The financial support of the Swiss Federal Office of Energy (BFE) is also gratefully acknowledged.

Many thanks are due to the doctoral students of the Exhaust Gas Aftertreatment group, the past members (Mickaël and Giuseppe) and the present members (Mukundan, Kirill and Gaia). I hope to find again this international atmosphere in my future.

I would like also to associate thanks to those who became my friends during my studies: Olivier, Lionel, Loïc, François, Régis, and the “international French connection” at the Paul Scherrer institute.

At last but not the least, I would like to thank my parents for their support during my studies and for their affection.

Table of Contents

Summary	1
Résumé	3
1 Introduction	6
1.1 The ecological awareness.....	6
1.2 Formation of nitrogen oxide and soot.....	7
1.2.1 Formation of NO	7
1.2.2 Definition and formation of soot.....	8
1.3 Impact of pollutants on health and environment.....	9
1.3.1 Oxides of nitrogen.....	9
1.3.2 Particulate matter	10
1.4 European diesel emissions standards	10
1.5 Technologies to meet future emission standards	11
1.5.1 Primary measures	11
1.5.2 Aftertreatment techniques	12
1.6 Catalytic methods for NO _x reduction.....	12
1.6.1 SCR with N-containing reducing agent	13
1.6.2 SCR with hydrocarbons	14
1.6.3 NO _x storage and reduction (NSR) catalysts	15
1.7 Particulate filters for the removal of soot.....	15
1.7.1 Principle	15
1.7.2 Filter regeneration	16
1.8 Scope of the thesis	17
1.9 References	18
2 Literature review	20
2.1 Adsorption and desorption of nitrogen oxides.....	20
2.1.1 Adsorption of NO _x on zeolites	20
2.1.2 Adsorption and desorption of NO _x on NO _x storage catalysts	23

2.2	Oxidation of NO to NO ₂	27
2.2.1	Gas phase equilibrium	27
2.2.2	Gas phase oxidation of NO	27
2.2.3	Catalytic oxidation of NO over supported platinum catalysts	28
2.3	Surface reactions on platinum	32
2.3.1	Adsorption and desorption of oxygen on platinum	32
2.3.2	Formation of platinum oxide	33
2.3.3	Adsorption of NO on platinum	34
2.4	Conclusions for the present thesis	35
2.5	References	36
3	Characterization methods and experimental setup	39
3.1	Physico-chemical characterization	39
3.1.1	X-ray diffraction (XRD)	40
3.1.2	X-ray photoelectron spectroscopy (XPS)	41
3.2	Experimental setup	42
3.2.1	Gas dosing system	42
3.2.2	Reactors	44
3.2.3	Gas analyzer	45
3.3	Evaluation of the adsorption and the oxidation tests	47
3.3.1	Gas hourly space velocity	47
3.3.2	Adsorption tests	48
3.3.3	Oxidation tests	49
3.4	References	49
4	Adsorption and desorption of NO and NO₂ on Cu-ZSM-5	51
4.1	Introduction	51
4.2	Experimental	53
4.2.1	Catalyst preparation	53
4.2.2	Characterization	53
4.2.3	Adsorption tests	54
4.3	Results	56
4.3.1	Adsorption and oxidation of NO in dry and humid base feeds	56
4.3.2	Adsorption of NO ₂ in dry and humid base feeds	58

4.3.3	Influence of NO on the adsorption of NO ₂	59
4.3.4	Effect of temperature on the adsorption of an equimolar mixture of NO and NO ₂	60
4.3.5	Influence of NO on the desorption of adsorbed NO _x -species	62
4.4	Discussion	64
4.4.1	Adsorption of NO on Cu-ZSM-5	64
4.4.2	Adsorption of NO ₂ on Cu-ZSM-5 and desorption of the adsorbed species	64
4.5	Conclusions	67
4.6	References	67
5	Adsorption and desorption of NO and NO₂ on BaO/TiO₂	69
5.1	Introduction	69
5.2	Experimental	70
5.2.1	Sample preparation	70
5.2.2	Sorption experiments	70
5.2.3	X-ray diffraction analysis	71
5.3	Results	71
5.3.1	Adsorption	71
5.3.2	Desorption	75
5.4	Discussion	80
5.4.1	Adsorption and desorption of NO ₂ in the absence of NO and CO	80
5.4.2	Influence of CO and NO	81
5.5	Proposed mechanism for the NO _x adsorption-desorption process on NO _x storage catalysts	83
5.6	Conclusions	85
5.7	References	85
6	Screening of supported platinum catalysts for the oxidation of NO	87
6.1	Introduction	87
6.2	Experimental	88
6.2.1	Sample preparation	88
6.2.2	Catalytic tests	91

6.3	Results	92
6.3.1	Influence of calcination and reduction temperatures	92
6.3.2	Influence of the platinum precursor	93
6.3.3	Influence of the platinum loading	95
6.3.4	Activity of platinum catalysts supported on various supports	96
6.4	Discussion	97
6.5	Conclusions	98
6.6	References	99
7	The unexpected kinetic behavior of platinum catalysts for the oxidation of NO	100
7.1	Introduction	100
7.2	Experimental	100
7.2.1	Sample preparation	100
7.2.2	Transmission electron microscopy (TEM) measurements	101
7.2.3	X-ray diffraction (XRD) measurements	101
7.2.4	Catalytic tests	101
7.2.5	Calculations	102
7.3	Results	103
7.3.1	Determination of the platinum particle size	103
7.3.2	Influence of the oxygen concentration	105
7.3.3	Influence of the NO concentration	107
7.3.4	Influence of water	108
7.3.5	Influence of the NO ₂ concentration	110
7.4	Discussion	113
7.5	Conclusions	115
7.6	References	115
8	Deactivation and regeneration of Pt/SiO₂	117
8.1	Introduction	117
8.2	Experimental	118
8.2.1	Catalyst sample	118
8.2.2	Pretreatments of the samples	119
8.2.3	Experimental setup and oxidation tests	119

8.2.4	X-ray photoelectron spectroscopy measurements.....	119
8.3	Results.....	120
8.3.1	Oxidation of NO over reduced and pretreated samples	120
8.3.2	Pretreatment with NO ₂	120
8.3.3	Regeneration of the samples	123
8.3.4	XPS analysis.....	126
8.4	Discussion	129
8.5	Conclusions.....	131
8.6	References	132
9	Oxidation of NO over Pt/Al₂O₃ and Pt/ZrO₂	133
9.1	Introduction.....	133
9.2	Experimental	134
9.2.1	Catalyst samples.....	134
9.2.2	NO ₂ adsorption experiments	134
9.2.3	NO oxidation tests.....	134
9.2.4	X-ray photoelectron spectroscopy.....	135
9.3	Results.....	135
9.3.1	NO ₂ adsorption experiments	135
9.3.2	Oxidation of NO over reduced and pretreated samples	138
9.3.3	X-ray photoelectron spectroscopy analysis.....	140
9.4	Discussion	143
9.5	Conclusions.....	145
9.6	References.....	146
10	Proposed mechanisms for the oxidation of NO to NO₂ over supported platinum catalysts	147
10.1	Introduction.....	147
10.2	Langmuir-Hinshelwood or Eley-Rideal mechanism ?.....	148
10.3	Proposed mechanisms	149
10.3.1	Mechanism of NO oxidation over Pt/Al ₂ O ₃ and Pt/ZrO ₂	149
10.3.2	Mechanism of NO oxidation over Pt/SiO ₂	150
10.4	Conclusions.....	151
10.5	References	151

Conclusions and outlook	152
Annex 1	154
List of publications	159
Curriculum vitae	160

Summary

The main goals of the present work were the evaluation of possible adsorbents for nitrogen monoxide, and its oxidation to nitrogen dioxide. The oxidation of NO is an important reaction to improve the removal of NO_x and soot from lean exhaust. Various powdered catalysts were prepared and tested under laboratory conditions with synthetic gas mixtures matching lean exhaust.

The adsorption of NO was investigated on Cu-ZSM-5. It was shown that NO must first be oxidized to NO₂ before it can be adsorbed. However, the oxidation of NO is inhibited by water at low temperatures, thus impeding the storage of NO. NO₂ can be adsorbed from both dry and humid feeds. This involves the disproportionation of three NO₂ molecules, yielding two stored nitrate species and one molecule of NO released to the gas phase. However, NO lowers the adsorption of NO₂ significantly, by reacting with stored nitrates at temperatures as low as 150 °C.

Further adsorption and desorption experiments were performed on BaO/TiO₂. NO₂ disproportionates also on this sample, yielding NO and surface nitrates on TiO₂ and on BaO, as well as crystalline barium nitrate. NO again reduces the stability of nitrates causing the formation of NO₂. The evolution of NO₂ was observed at various temperatures reflecting the stability of the different nitrates: surface nitrate on TiO₂ decomposed at 200 °C, surface nitrates on BaO decomposed at 280 °C, while the decomposition of more stable bulk nitrate was observed at 510 °C.

The catalytic oxidation of NO was studied on various supported platinum catalysts prepared by incipient wetness impregnation. Screening tests showed that samples of Pt/SiO₂ prepared from Pt(NH₃)₄Cl₂ had the highest activity. Samples consisting of Pt/Al₂O₃ and Pt/ZrO₂ showed lower activities.

The kinetic behavior of Pt/SiO₂ with a platinum loading of 2.5 wt.% was investigated in both dry and humid feeds at various concentrations of oxygen, nitrogen monoxide and nitrogen dioxide. The oxidation of NO is only weakly inhibited by the presence of water in the feed. The conversion of NO to NO₂ rises when the O₂ concentration is

increased from 0.1 to 10 %, and becomes independent of O_2 at higher concentrations. Increasing feed concentrations of NO lead to a decreasing conversion to NO_2 . The formation of NO_2 is also depressed by adding NO_2 to the feed. Therefore, both observations suggest that the oxidation of NO on this catalyst is autoinhibited by the product NO_2 .

Further experiments have shown that the inhibition caused by NO_2 is mostly irreversible, i.e. a deactivation of the catalyst occurs. In order to understand the deactivation process, Pt/SiO₂ was pretreated in different feeds containing either oxygen alone, or mixtures of oxygen and NO_2 . Pretreatment at 450 °C with oxygen had no effect on the oxidation of NO, whereas a pretreatment at 250 °C in the feed containing NO_2 showed a strong decrease in activity. The analysis using X-ray photoelectron spectroscopy (XPS) revealed that platinum remains mainly in a metallic form, and that the Pt particles size was unchanged after the pretreatment. Attempts to regenerate the catalyst showed that the initial activity can be recovered by thermal regeneration at 650 °C in air or by regeneration under reducing conditions at 250 °C in a feed containing either NH_3 or NO. This suggests that the deactivation by NO_2 can be attributed to the formation of a thin layer of platinum oxide covering a fraction of the platinum surface.

Samples of Pt/Al₂O₃ and Pt/ZrO₂ with a platinum loading of 2.5 wt.% showed a very different behavior. Pretreatment at 250 °C in the feed containing NO_2 did not influence the activity for NO oxidation. On the other hand, pretreatment in the feed containing oxygen caused an enhanced activity of both samples. The analysis of Pt/ZrO₂ using XPS evidenced the oxidation of platinum into platinum oxide after pretreatment. The improved activity after pretreatment with oxygen was attributed to a rearrangement of platinum oxide due to temperature.

The better activity of Pt/SiO₂ for the oxidation of NO can be attributed to its ability of keeping platinum longer in the reduced state. The oxidation of NO over Pt/SiO₂ can best be described by an Eley-Rideal mechanism involving adsorbed oxygen atoms on Pt and nitrogen monoxide reacting from the gas phase or from a weakly adsorbed state. On the other hand, platinum supported on γ -Al₂O₃ or ZrO₂ tends to form platinum oxide. Because oxygen is more strongly bound in platinum oxide than on metallic platinum, its reactivity is lower, leading to lower conversions of NO to NO_2 on Pt/Al₂O₃ and Pt/ZrO₂.

Résumé

Les principaux objectifs de cette étude ont été l'évaluation de potentiels adsorbants de monoxyde d'azote, et son oxydation en dioxyde d'azote. L'oxydation de NO est une réaction importante pour améliorer l'élimination des NO_x et des suies contenus dans les gaz d'échappement pauvres. Plusieurs catalyseurs sous forme de poudre ont été préparés, puis testés dans des conditions de laboratoire avec des mélanges de gaz synthétiques simulant des mélanges pauvres.

L'adsorption de NO a été étudiée sur Cu-ZSM-5. Il a été montré que NO doit d'abord être oxydé avant de pouvoir être adsorbé. Cependant, l'oxydation de NO est inhibée par la vapeur d'eau à basses températures, empêchant ainsi l'adsorption de NO. NO₂ peut être adsorbé aussi bien sous flux sec ou humide. Cela implique la disproportion de trois molécules de NO₂, donnant deux espèces nitrates adsorbées et une molécule de NO libérée dans la phase gazeuse. Cependant, NO diminue de façon significative l'adsorption de NO₂, en réagissant avec les nitrates à des températures aussi basses que 150 °C.

Des expériences d'adsorption et de désorption ont également été effectuées avec BaO/TiO₂. NO₂ disproporctionne également, en formant NO et des nitrates adsorbés à la surface de TiO₂ et de BaO, ainsi que des espèces cristallines de nitrate de baryum. NO réduit aussi la stabilité des nitrates, entraînant la formation de NO₂. Cette formation a été observée à différentes températures reflétant la stabilité des espèces nitrate sous flux de NO : les nitrates adsorbés à la surface de TiO₂ se sont décomposés à 200 °C, ceux adsorbés en surface de BaO à 280 °C, tandis que la décomposition de Ba(NO₃)₂ plus stable a été observée à 510 °C.

L'oxydation catalytique de NO a été étudiée sur catalyseurs à base de platine déposé sur un support, préparés par imprégnation à sec. Une série de tests a montré que les échantillons de Pt/SiO₂ préparés à partir de Pt(NH₃)₄Cl₂ avait l'activité la plus élevée. Les échantillons de Pt/Al₂O₃ et Pt/ZrO₂ étaient eux moins actifs.

Le comportement cinétique de Pt/SiO₂ contenant 2.5 % en poids de platine a été étudié sous flux sec et humide avec différentes concentrations d'oxygène, de monoxyde d'azote et de dioxyde d'azote. L'oxydation de NO est alors seulement faiblement inhibée par la présence de vapeur d'eau dans le flux gazeux. La conversion de NO en NO₂ augmente quand la concentration en oxygène croît de 0.1 à 10 %, et devient indépendante de O₂ à des concentrations plus élevées. L'augmentation de la concentration de NO dans le flux induit une diminution de la conversion en NO₂. La formation de NO₂ est aussi abaissée par l'ajout de NO₂ dans le mélange gazeux. Par conséquent, ces deux observations suggèrent que l'oxydation de NO sur ce catalyseur est auto-inhibée par le produit de réaction NO₂.

D'autres expériences ont montré que l'inhibition occasionnée par NO₂ est principalement irréversible, c'est-à-dire qu'une désactivation du catalyseur est observée. Afin de comprendre le processus de désactivation, Pt/SiO₂ a été prétraité sous flux contenant soit uniquement de l'oxygène, soit un mélange d'oxygène et de NO₂. Un prétraitement à 450 °C avec de l'oxygène n'a pas d'effet sur l'oxydation de NO, tandis qu'un prétraitement à 250 °C sous flux contenant NO₂ induit une forte diminution de l'activité. Une analyse par spectroscopie de photoélectron X (XPS) a révélé que le platine restait principalement dans un état réduit, et que la taille des particules restait inchangée après prétraitement. Les tentatives pour régénérer le catalyseur ont montré que l'activité initiale peut être restaurée par régénération thermique sous air à 650 °C ou par régénération sous atmosphères réductrices à 250 °C dans un flux contenant NH₃ ou NO. Ceci suggère que la désactivation par NO₂ peut être attribuée à la formation d'une fine couche d'oxyde de platine recouvrant une fraction de la surface de platine.

Les échantillons de Pt/Al₂O₃ et Pt/ZrO₂ contenant 2.5 % en poids de platine ont montré un comportement très différent. Pour ces catalyseurs, le prétraitement à 250 °C sous flux de NO₂ n'a pas eu d'effet sur l'oxydation de NO. Par contre, le prétraitement sous flux contenant de l'oxygène conduit à une augmentation de l'activité des deux catalyseurs. L'analyse XPS de Pt/ZrO₂ a mis en évidence la formation d'oxyde de platine après prétraitement. L'amélioration de l'activité après le prétraitement sous oxygène a été attribuée à un réarrangement de l'oxyde de platine sous l'action de la température.

La plus forte activité de Pt/SiO₂ pour l'oxydation de NO peut être attribuée à sa capacité à garder le platine plus longtemps dans un état réduit. L'oxydation de NO sur Pt/SiO₂ peut être décrite par un mécanisme de type Eley-Rideal impliquant des atomes d'oxygène adsorbés sur Pt, et du monoxyde d'azote réagissant de la phase gazeuse ou d'un état faiblement adsorbé. Par contre, le platine supporté sur γ -Al₂O₃ ou ZrO₂ tend à former de l'oxyde de platine. Comme l'oxygène est plus fortement lié dans l'oxyde de platine que sur le platine métallique, sa réactivité est plus faible, induisant des conversions de NO en NO₂ plus faibles sur Pt/Al₂O₃ et Pt/ZrO₂.

Introduction

1.1 The ecological awareness

“... Pollution alert in the region of Bas-Rhin, especially in Strasbourg, after the measurement of high concentrations of ozone in air; the prefect asks the drivers to use their car only in case of absolute necessity. ... Asthma cases on the rise in the region of Ile-de-France: the quality of air is in question ...”. This is a selection of main news heard on the radio or television in the last years when the weather in France was hot or foggy. These words in combination with the corresponding images have led the people to realize that they have to control the concentrations of pollutants in air. This ecological awareness is not restricted to a few states, but is extended to all the industrialized countries, for example to the European community or to Switzerland. The organization for economic cooperation and development (OECD) reported in 1998 [1] on the ambitious environmental politics initiated in Switzerland during the seventies, leading to a considerable decrease of the emissions of atmospheric pollutants, especially of sulfur dioxide and carbon monoxide. However, the abatement of volatile organic compounds, nitrogen oxides and soot proved to be more difficult. In order to reduce these emissions further, the OECD recommended *inter alia* to increase the fuel taxes in order to reduce the emissions of NO_x (implementation of the “polluter-pays” principle, and pressure on the monthly fuel cost of the car drivers), and to define a strategy against fine particles emitted by mobile sources.

In the last thirty years, the contribution of the mobile sources to the global emission of toxic air pollutants has grown significantly. The road traffic has strengthened and wares producers have placed more reliance on trucks for the transport of goods. Light-, medium- and heavy-duty trucks are all equipped with diesel engines. The passenger cars market offers both the diesel and the gasoline technologies. However, the share of diesel vehicles in France has been consolidated by attractive low fuel taxes. In 2001, more than 50 % of the passenger cars sold in France were diesel vehicles [2].

1.2 Formation of nitrogen oxide and soot

The formation of NO and soot occurs during the combustion process and involves mainly chemical reactions between radical species. Various mechanisms are postulated to describe their formation. Reference [3] gives a large overview on the subject.

1.2.1 Formation of NO

Three different mechanisms may be responsible for the formation of NO: the “Thermal NO” or “Zeldovich mechanism” postulated by Y.A. Zeldovich in 1948 [4], the “prompt NO” mechanism suggested by C.P. Fenimore in 1979 [5], and the conversion of fuel nitrogen compounds to NO [3].

“Thermal NO” or “Zeldovich NO”

Thermal NO are produced according to the following elementary reactions:



Under fuel rich conditions, OH radicals can react with nitrogen radicals according to:

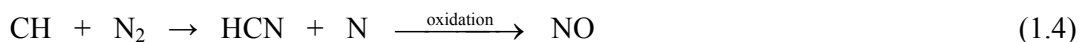


The overall rate of “thermal NO” formation is proportional to the concentrations of molecular nitrogen and oxygen. Reaction (1.1) is the rate-limiting step. Its high

activation energy, i.e. 319 kJ/mol, restricts the occurrence of this mechanism to high temperatures, above 1400 K [3,4].

“Prompt NO” or “Fenimore NO”

The Fenimore mechanism involves the reaction of CH radicals with nitrogen according to the following reaction scheme:



The initial step is the formation of hydrocyanic acid by the attack of CH radicals on molecular nitrogen. This reaction occurs in the flame front of fuel rich flames. HCN and nitrogen radicals are oxidized by O₂, O or OH radicals to form NO.

The formation of HCN is the rate-limiting step. Its activation energy (i.e. 57 kJ/mol) is much lower than the energetic barrier of reaction (1.1). Therefore, the “prompt NO” is produced at a much lower temperature than the “thermal NO”, and is formed already at 1000 K [3,5].

Conversion of fuel nitrogen compounds to NO

The formation of NO from fuel nitrogen compounds takes place mainly during the combustion of coal. The coal contains typically more than 1 % of bound nitrogen, hence the expression “fuel nitrogen compounds”. These compounds react fast to form ammonia and HCN, and finally nitrogen containing radicals. These radicals are further oxidized to NO [3].

1.2.2 Definition and formation of soot

The term “soot” is a general word to define a complex carbon-based solid matter. A chemical analysis of a typical diesel soot reveals the following composition: 83 % C, 1 % H, 0.2 % N, 10.5 % O, 1.1 % S and traces of other elements. The particle sizes of soot vary from 10 nm up to 100 μm. The biggest particles (100 μm) are composed of smaller particles (0.1-1 μm), which themselves are formed by agglomeration of spherules (about a few 10 nm) [6].

Soot is formed during the combustion in regions with oxygen deficiency, i.e. in lean air-fuel mixtures, or under poor fuel mixing conditions. The formation of soot first involves the pyrolysis of aliphatic and aromatic molecules contained in the fuel into soot precursors like acetylene. Subsequently, these precursors build small soot nuclei by repeated oligomerization and dehydration. These nuclei grow by surface addition of acetylene or polyacetylene to form spherule-type networks [7].

The spherules can collide outside the cylinder to form larger agglomerates. In the colder exhaust pipe, the agglomerates have the propensity to adsorb hydrocarbon materials or soluble organic fractions (SOF) contained in the exhaust on their surface [7]. They can also adsorb inorganic compounds, especially sulfuric acid leading to the formation of sulfates. This explains the presence of sulfur in the elemental analysis [6].

1.3 Impact of pollutants on health and environment

1.3.1 Oxides of nitrogen

Oxides of nitrogen emitted by mobile sources are mainly in the form of NO. The fraction of NO₂ is usually less than 10 %. However, once emitted, NO reacts slowly with oxygen contained in the atmosphere to form nitrogen dioxide, a highly toxic pollutant. Nitrogen dioxide is a respiratory irritant [8], which contributes to the increase of the number of asthma cases. It also increases the susceptibility to infections.

In the atmosphere, chemical reactions between nitrogen oxides and volatile organic compounds in the presence of sunlight cause the formation of ozone. Ozone is one of the harmful ingredients of urban smog, a major problem for bigger cities.

Nitrogen oxides can also react with water to form nitric acid, which is washed out in the next rainfall. This phenomenon has been called acid rain, due to the low pH values between 3 and 5 instead of 5.5. Acid rain contains also sulfuric acid due to the presence of SO₂ and SO₃ in the air. It contributes to the acidification and the impoverishment of the soils.

1.3.2 Particulate matter

Once emitted, soot can further agglomerate in the atmosphere. The injuries caused to the humans' health are related to the particle size. Small particles are more harmful for human health than big ones, since they can easily reach the lungs [7], where they are a source of irritation or cancer. Larger particles should normally deposit on the ground, or be trapped in the nose, thus preventing their penetration into the lungs.

The deposition of the particles in the environment is mainly an esthetic problem. The accumulation of particles is observed on glaciers in the Alps, or near roads, on leaves or on the facade of buildings.

1.4 European diesel emissions standards

In 1992, the European community (EU) initiated a collaboration with the European car manufacturers and the oil industry in order to establish a technical programme for tightened vehicle emissions. The European Union sets the emission requirements for the next years, taking into account the time necessary for industry to develop new technologies for meeting these emissions standards [9].

European directives deal with all types of vehicles, from passenger cars to heavy-duty trucks, including also motorcycles [9,10]. Figure 1-1 shows the NO_x and particulate emissions standards applicable to heavy-duty trucks for the Euro II stage from January 1996, the Euro III stage from January 2000, the future Euro IV stage from January 2005 and the Euro V stage from January 2008.

In addition to tightened emission standards, the EU forces the enhancement of fuel quality, in particular the sulfur and aromatics contents of petrol and of diesel [9]. Improved fuel qualities will help to reach lower emission standards (primary emissions as well as the feasibility of new aftertreatment techniques).

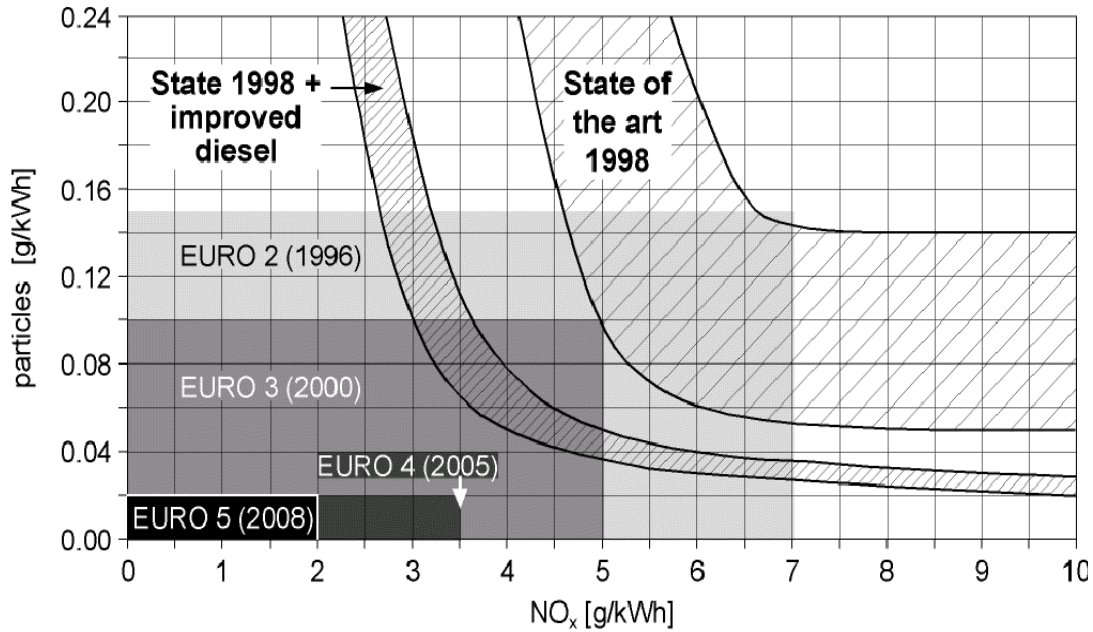


Figure 1-1: Trade-off between particulate matter and NO_x for heavy-duty truck engines, and prospected European emission standards.

1.5 Technologies to meet future emission standards

Vehicle manufacturers have investigated several strategies to reach the forthcoming emission standards. Nowadays, it is generally assumed that the forthcoming standards will no longer be feasible by primary measures at the engine alone, but will require additional aftertreatment techniques.

1.5.1 Primary measures

In order to reduce the raw emissions of diesel engines, primary measures may be adapted to obtain either

- 1) low NO_x emissions, leading to a high emission of unburned material (soot, CO, hydrocarbons), or
- 2) low emissions of unburned hydrocarbons, leading to a high emission of NO_x. This option is preferred due to a better fuel economy.

A reduction of the raw emissions of NO_x can be achieved by using the common rail system and by controlling the injection of the exact amount of fuel [11]. Exhaust gas recirculation (EGR) and the injection of a water-fuel mixture can be implemented to reduce the NO_x emissions further. These processes lower the maximum combustion temperature and improve the air-fuel mixing.

1.5.2 Aftertreatment techniques

If the combustion is optimized by primary measures to lower the NO_x emissions, this requires the use of an oxidation catalyst for the abatement of hydrocarbons and carbon monoxide. Additionally, a particulate filter (DeSoot system) is necessary.

Contrary, if the combustion is optimized to minimize the emissions of unburned material, an efficient De NO_x system for reducing nitrogen oxides selectively to nitrogen is required.

1.6 Catalytic methods for NO_x reduction

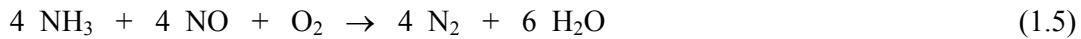
The removal of NO_x from lean exhaust gases is a major challenge. Nitrogen oxides must be reduced selectively to molecular nitrogen in the presence of excess of oxygen. There, the classical three-way catalyst used for the abatement of pollutants from gasoline engines cannot be utilized in such highly oxidizing conditions. The following three solutions have attracted much interest for practical application [12]:

- 1) selective catalytic reduction of NO_x by ammonia (ammonia-SCR),
- 2) selective catalytic reduction of NO_x by hydrocarbons (HC-SCR),
- 3) NO_x storage and reduction (NSR) catalyst.

1.6.1 SCR with N-containing reducing agent

Ammonia-SCR

The selective catalytic reduction of NO_x using ammonia as a reducing agent can efficiently remove nitrogen oxides from lean exhaust gases in the temperature range 300-450 °C [13]. Typical catalysts for NH_3 -SCR are V_2O_5 - WO_3 - TiO_2 ternary catalysts. The vanadium oxide provides sites for the activation of ammonia [14], which can subsequently react with NO according to reaction (1.5). Tungsten oxide increases both the thermal stability of the titania support and the adsorption of the ammonia, thus serving as an NH_3 -buffer for the NO_x reduction [15]:



The removal of NO_x (DeNO_x) at temperatures below 300 °C can be improved substantially by feeding a mixture of NO and NO_2 [16]. The SCR-reaction with a stoichiometric ratio of NO and NO_2 (reaction (1.6)) is much faster than the “standard” SCR-reaction (1.5) [17]:



As has already been mentioned, the NO_x emissions from diesel engines are mainly composed of nitrogen monoxide. Therefore, a strong platinum-based oxidation catalyst is positioned upstream of the SCR catalyst [18]. Figure 1-2 provides a schematic representation of the system.

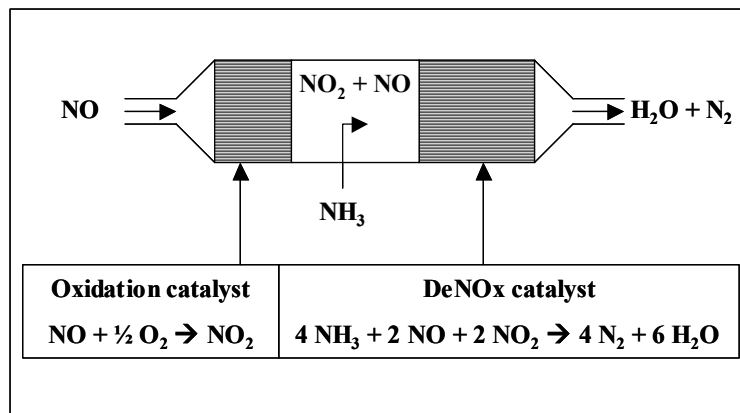
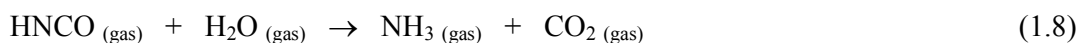


Figure 1-2: Schematic representation of an advanced DeNO_x system.

Urea-SCR

For automotive applications, urea is preferred for reasons of safety and toxicity [19]. This compound may be considered as a solid storage compound for ammonia. Instead of spraying ammonia ahead of the SCR catalyst, an aqueous solution of urea can be atomized into the hot exhaust gas stream. After evaporation of the water from the droplets, solid urea will thermally decompose to NH_3 and isocyanic acid according to reaction (1.7). This decomposition reaction takes place either in the gas stream or on the SCR catalyst itself. On the surface of the SCR catalyst, hydrolysis of HNCO occurs easily, leading to ammonia and carbon dioxide according to reaction (1.8) [20,21].



Ammonia formed during these two reactions can subsequently adsorb on the SCR catalyst. It reacts with NO_x contained in the exhaust stream as described for ammonia-SCR.

1.6.2 SCR with hydrocarbons

In this process, the nitrogen oxides are converted catalytically using hydrocarbons as a reducing agent. Typical catalysts for HC-SCR contain noble metals (e.g. platinum) finely dispersed on supports like Al_2O_3 [22,23]. Promising alternatives to noble metal catalysts are metal-exchanged zeolites, especially Cu-ZSM-5 [24], Co-ZSM-5 [23] and Fe-ZSM-5 [25].

The main disadvantages of these materials are the narrow temperature window where high NO_x conversions are possible, and the very low selectivity of the NO_x reduction. The main fraction of hydrocarbons reacts with oxygen and is burned to CO , CO_2 and water. Therefore, high amounts of reducing agent are required to reach an efficient conversion. Additionally, side reactions leading to the formation of appreciable amounts of undesired products like N_2O are observed in the case of noble metal catalysts. In view of these disadvantages, the practical application of the HC-SCR process is unlikely.

1.6.3 NO_x storage and reduction (NSR) catalysts

NO_x storage and reduction catalysts utilize the addition of a basic oxide (e.g. barium oxide) to the classical three-way catalyst thus providing sites able to store NO_x in the form of nitrates during the normal, lean operation of the engine [26]. For a short period, the exhaust is made rich thereby enabling the reduction of NO_x with hydrocarbons on the platinum sites of the catalyst according to the following scheme.



The principal problem of these NO_x adsorbers remains the formation of stable sulfates with the basic oxides, leading to an increased loss of adsorption capacity. This is due to the much higher thermal stability of sulfates compared to the nitrates. Therefore, the practical use of this method calls for an additional regeneration procedure. This requires very high temperatures (600 to 650 °C) and reducing conditions (air/fuel ratio = 0.95, 15 minutes [27]). The practical application in Europe is feasible only if the sulfur content in fuel decreases below the typical limit of 5 ppm. The application of this aftertreatment technique to heavy-duty trucks is unlikely due to the operative conditions.

1.7 Particulate filters for the removal of soot

1.7.1 Principle

In order to remove soot from diesel exhaust gases, different types of filters showed promising results for soot removal. Conventional ceramic materials like cordierite are used in form of monoliths, but with alternatively blocked channels. The exhaust gas is forced through the walls of a closed-end channel into the adjacent open-end channel. Consequently, the soot is efficiently trapped in the closed-end channel depositing on the channel wall. In the alternative foamed filters, the soot deposits inside the porous wall itself. Different kinds of foam provide sufficient high porosity and structural strength for an automotive application.

For both types of filters, an efficient regeneration is required to avoid an increase of the pressure drop over the filter unit. For this purpose, the oxidation of the particulates

is supported *inter alia* by feeding special organometallic additives or with a highly oxidizing agent like NO_2 .

1.7.2 Filter regeneration

Non-catalytic soot oxidation with oxygen necessitates temperatures above $650\text{ }^\circ\text{C}$ [28]. Electrical heaters can help to ignite the soot by raising the temperature. However, in order to regenerate the filter at lower temperatures, current aftertreatment technology aims at the utilization of catalysts for the combustion of soot.

Regeneration with additives

One way to get soot and catalyst into close contact is the addition of the catalyst precursors to the fuel. These precursors are burned in the combustion chamber together with the fuel, forming the final catalyst, which is homogeneously distributed in the produced soot particles. Among different stable organometallic compounds, cerium-, iron- and copper-based additives showed a high efficiency for the regeneration. For environmental reasons, cerium additives are preferred to copper additives [6]. The first passenger car equipped with a particle trap and commercialized by PSA Peugeot Citroën operates with a cerium additive [29] to lower the soot combustion temperature to $450\text{ }^\circ\text{C}$.

Continuously regenerating trap (CRT)

The CRT system from Johnson Matthey [30] is an aftertreatment system based on a soot filter, which is continuously regenerated without any additive. An oxidation catalyst (e.g. $\text{Pt}/\text{Al}_2\text{O}_3$) positioned upstream of the particle filter converts part of the NO from the exhaust to NO_2 . Figure 1-3 provides a schematic representation of the system. The news of this invention is the utilization of NO_2 as a more powerful oxidizing agent compared to oxygen.

A possible drawback of this system is the emission of unreacted nitrogen dioxide due to some operative conditions. Therefore, the CRT system may be combined with a urea-SCR system, thus leading to the decrease of the emissions of soot and of nitrogen oxides.

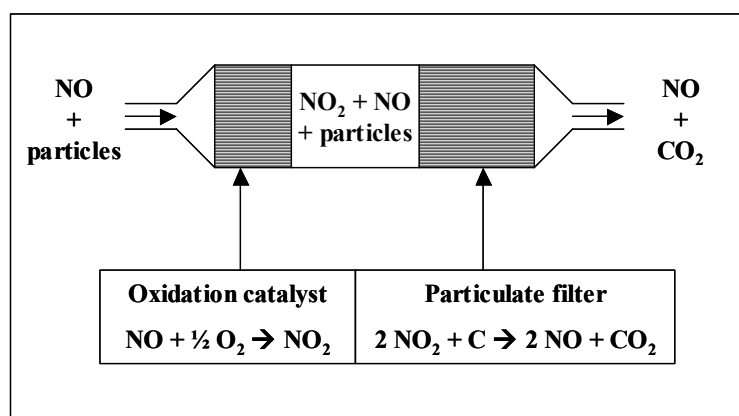


Figure 1-3: Schematic representation of the continuously regenerating trap system.

1.8 Scope of the thesis

The aim of this study is to investigate the adsorption of nitrogen oxides on various possible adsorbing materials, and to study the catalytic oxidation of nitrogen monoxide to NO_2 on supported platinum catalysts. The oxidation catalyst shall exhibit high activity in the temperature range $150\text{ }^\circ\text{C}$ to $300\text{ }^\circ\text{C}$, where NO_2 is required to enhance the removal of NO_x or soot emitted by diesel engines.

Zeolites will be investigated as possible adsorbers for NO . The study shall consider the adsorption of mixtures of NO and NO_2 as well. The adsorption properties of zeolites will be compared with the adsorption behavior of typical NO_x storage materials containing supported barium oxide.

In order to prepare an oxidation catalyst with high intrinsic activity, screening experiments with platinum supported on various supports have to be carried out. Kinetic investigations with powder catalysts, combined with physical characterization of the catalyst surface, will provide insight into the mechanism of the reaction. Attention must be paid to the influence of the platinum particle size on the activity. The oxidation state of platinum in feeds containing strongly oxidizing components like oxygen or NO_2 shall be investigated. On the basis of the experimental results, a reaction mechanism will be proposed to describe the oxidation of NO over platinum catalysts.

1.9 References

- [1] “Switzerland – Environmental Performance Review (1st Cycle) – Conclusions & Recommendations” – 10-01-98, OECD Documents, URL://www.oecd.org
- [2] *Flottes Automobiles*, No. **74**, December 2001 / January 2002, URL://www.flotauto.com/magazine
- [3] J. Warnatz and U. Maas, *Technische Verbrennung*, Springer-Verlag, New York, (1993), pp. 201-218
- [4] Y.A. Zeldovich, *Acta Physicochim. USSR* **21** (1946), 577
- [5] C.P. Fenimore, *17th Int. Symp. on Combustion*, Pittsburgh, The Combustion Institute, Pittsburgh (1979), p. 661
- [6] B.R. Stanmore, J.F. Brilhac and P. Gilot, *Carbon* **39** (2001), 2247
- [7] J.P.A. Neeft, M. Makkee and J.A. Moulijn, *Fuel Process Technol.* **47** (1996), 1
- [8] A. Fritz and V. Pitchon, *App. Catal. B: Environ.* **13** (1997), 1
- [9] P. Greening, *Top. Catal.* **16** (2001), 5
- [10] G. Emmerling and F.I. Zuther, in: A. Leipertz (Ed.), *Motorische Verbrennung - aktuelle Probleme und moderne Lösungsätze*, Berichte zur Energie- und Verfahrenstechnik, Schriftenreihe Heft 99.1, Erlangen (1999), p. 581
- [11] W. Kind, *Beitrag zur NO_x-Verminderung im Abgas von Dieselmotoren durch selektive katalytische Reduktion mit Harnstoff*, Fortschritts-Bericht VDI, Reihe 12, Nr. 355, VDI-Verlag, Düsseldorf (1998)
- [12] V.I. Pârvulescu, P. Grange and B. Delmon, *Catal. Today* **46** (1998), 233
- [13] M. Kleemann, *Beschichtung von Cordierit-Wabenkörpern für die selective katalytische Reduktion von Stickoxiden*, Thesis ETH Nr. 13401, ETH Zurich, (1999)
- [14] G. Ramis, G. Busca, F. Bregani and P. Forzatti, *Appl. Catal.* **64** (1990), 259
- [15] M. Koebel, G. Madia and M. Elsener, *Catal. Today* **73** (2002), 239
- [16] E. Jacob, G. Emmerling, A. Döring, U. Graf, M. Harris, J.A.A. van den Tillaart and B. Hupfeld, *NO_x-Verminderung für Nutzfahrzeugmotoren mit Harnstoff-SCR Kompaktsystemen*, 19. Internationale Wiener Motorensymposium, Vienna, 7-8 May 1998
- [17] G. Madia, *Measures to enhance the NO_x conversion in urea-SCR systems for automotive applications*, Thesis ETH Nr. 14595, ETH Zurich, (2002)

- [18] G. Madia, M. Koebel, M. Elsener and A. Wokaun, *Ind. Eng. Chem. Res.* **41** (2002), 3512
- [19] B. Maurer, E. Jacob and W. Weisweiler, *MTZ* **60** (1999), 308
- [20] M. Koebel, M. Elsener and M. Kleemann, *Catal. Today* **59** (2000), 335
- [21] M. Koebel, M. Elsener and G. Madia, *Recent advances in the development of urea-SCR for automotive applications*, International Fall fuels and Lubricants, San Antonio, Texas, 24-27 September 2001, SAE paper No. 2001-01-3625
- [22] P. Denton, A. Giroir-Fendler, H. Praliaud and M. Primet, *J. Catal.* **189** (2000), 410
- [23] Y. Traa, B. Burger and J. Weitkamp, *Micropor. Mesopor. Mater.* **30** (1999), 3
- [24] M. Shelef, *Chem. Rev.* **95** (1995), 209
- [25] H.Y. Chen and W.M.H. Sachtler, *Catal. Today* **42** (1998) 73
- [26] N. Takahashi, H. Shinjoh, T. Iijima, T. Suzuki, K. Yamazaki, K. Yokota, H. Suzuki, N. Miyoshi, S. Matsumoto, T. Tanizawa, T. Tanaka, S. Tateishi and K. Kasahara, *Catal. Today* **27** (1996), 63
- [27] S. Brandt, U. Dahle, J.K. Hochmuth and M. Deeba, *Entwicklungsfortschritte bei NO_x-Adsorber Katalysatoren für magerbetriebene Ottomotoren*, in *Kraftfahrwesen und Verbrennungsmotoren*, 3. Stuttgarter Symposium, Stuttgart, 23-25 February 1999, Expert Verlag, p. 82
- [28] D.W. McKee, *The catalyzed gasification reactions of carbon*, in: P.L. Walker, Jr. and P.A. Thrower (Eds.), *Chemistry and physics of carbon*, Vol. 16, (1981), p. 11
- [29] B.A.A.L. van Setten, M. Makkee and J.A. Moulijn, *Catal. Rev.* **43(4)** (2001), 489
- [30] B.J. Cooper, H.J. Jung and E.J. Thoss, US Patent 4,902,487 (1990), Assignee: Johnson Matthey Inc.

Literature review

2.1 Adsorption and desorption of nitrogen oxides

2.1.1 Adsorption of NO_x on zeolites

Description of zeolites

Zeolite materials are defined as a crystalline aluminosilicate having a unit cell $M_{(x/n)}[(AlO_2)_x(SiO_2)_y] \cdot H_2O$, where M is a metal cation with a positive charge n that can be exchanged. The zeolite structure is built up of oxygen ion tetrahedra with either Si^{4+} or Al^{3+} at the center. The assemblage of secondary built units such as double-6 ring or single-4 ring gives tridimensional structures displaying channels. Zeolites are characterized by their pore (or channel) diameters in the range of a few Angström, by their pore structure, and by their silica to alumina molar ratio (also called module). The dimensions of the channels are of particular interest for the catalytic activity of the material. The channel opening controls the access of the reactants to the active sites [1,2].

The SiO_2/Al_2O_3 ratio determines the amount of ions that can be exchanged into the zeolite. The lower this ratio, the larger the loading of exchangeable ions. The hydrophilic character of a zeolite is also a function of the silica to alumina ratio. Zeolites with higher module display strong hydrophobic properties [3] and their

hydrothermal stability is increased [4]. Therefore, the choice of the module is a compromise between the hydrothermal stability and the amount of exchanged cations.

The as-synthesized zeolites have sodium ions to counterbalance the negative charge of the framework. These ions can be exchanged with protons or other cations such as Cu^{2+} , Fe^{2+} or Ce^{3+} . Exchanged cations are essential to improve the hydrothermal stability of the material [5]. Proton exchanged zeolites display a poor resistance towards steaming. In fact, protons catalyze the dealumination, i.e. the removal of aluminum from the zeolite framework [4]. Copper [5] or cerium [6] ions have a beneficial effect.

NO_x adsorption

Zeolites have been reported as possible NO_x adsorbents [7,8,10]. Arai and Machida [7] investigated the adsorption of NO on various zeolites. The zeolite structure, the silica to alumina ratio and the cation counterbalancing the negative charge of the zeolite framework were found to be important parameters. Among the available zeolites, MFI type zeolites adsorbed the highest amount of NO at 0 °C (435 $\mu\text{mol/g}_{\text{cat}}$) [8]. Figures 2-1 and 2-2 shows a schematic representation of the structure and the channels of MFI type zeolites (also called ZSM-5) [2,9]. In ZSM-5, the oxygen tetrahedra are linked into five-membered rings, which form two kinds of intersecting channels: a straight channel with elliptical aperture of dimensions (5.1 × 5.7 Å) and a “zigzag” channel with an aperture of dimensions (5.3 × 5.6 Å) [1].

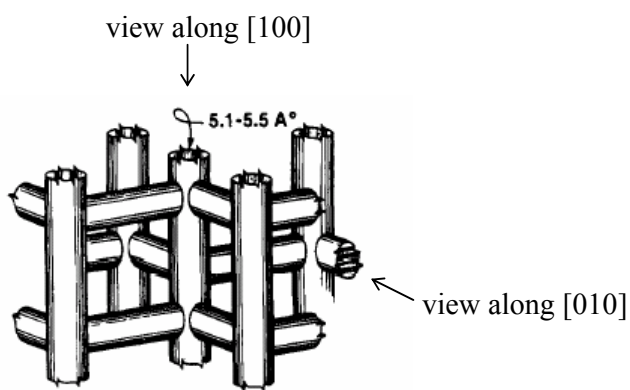
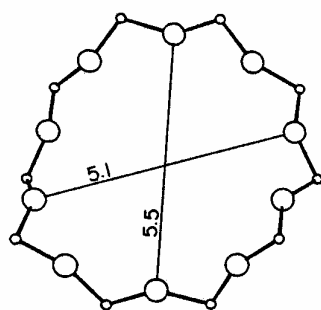
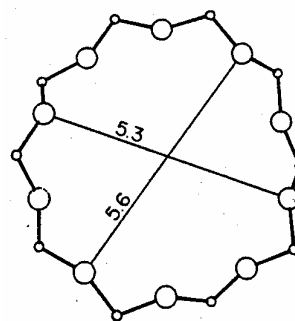


Figure 2-1: Schematic view of MFI-type zeolites, from [2].



10-ring viewed along [100]



10-ring viewed along [010]

Figure 2-2: Channels of ZSM-5 zeolite from [9]. The distances are in Angström. Large spheres symbolize the Al or Si atoms. Small spheres symbolize the O atoms.

The presence of cobalt or copper cations enhanced the adsorption considerably. Adelman et al. [10] reported on the adsorption of NO and NO₂ on Na-Y, Na-ZSM-5 and Cu-ZSM-5 in the absence and presence of oxygen at room temperature. After adsorbing NO₂ and subsequently NO from a dry gas sample, they observed the simultaneous desorption of NO and NO₂ during a temperature programmed desorption. They suggested the formation of a complex with the overall formula N₂O₃. The pre-adsorption of NO₂ provided new sites for the adsorption of NO on Cu-ZSM-5. Hadjiivanov et al. [11] proposed the following reaction sequence for the adsorption of NO on Cu-ZSM-5 in the presence of oxygen at room temperature:



The IR spectra also gave evidence for the intermediate formation of nitrosyl species (NO⁺), but they are characterized by a low stability in the presence of oxygen and at high temperatures. At 180 °C, the IR spectra showed only the bands typical for nitrate species. Hadjiivanov et al. [11] studied the stability of the nitrates in the presence of water, propane or NO. Once formed, nitrates were only slightly affected by water and NO under their experimental conditions. However, they were able to oxidize propane at 180 °C.

2.1.2 Adsorption and desorption of NO_x on NO_x storage catalysts

In recent years, the mechanism of adsorption of nitrogen oxides on NSR catalysts has intensively been investigated. A typical NSR catalyst consists of (i) a supporting oxide with a high surface area, usually γ -Al₂O₃, (ii) noble metals like platinum and rhodium, and (iii) a NO_x storage component with basic properties, e.g. barium oxide.

The nitrogen oxides emitted by diesel engines consist to more than 90 % of NO. The first reaction step in the adsorption mechanism of NO is its oxidation to NO₂, which is the species that can be adsorbed. Figure 2-3 depicts the mechanism of NO_x storage proposed by Toyota [12]. First, NO is oxidized on platinum and then NO₂ reacts with the NO_x storage component to form nitrates.

Mahzoul et al. [13] studied the adsorption of nitrogen oxides over powder samples of commercial NO_x storage catalysts. They performed a series of adsorption tests in a feed gas containing 500 ppm NO, 7 % O₂ and balance N₂ (space velocity = 30 000 h⁻¹). They observed a maximum of NO_x storage at 350 °C. The adsorption of NO (500 ppm) at 300 °C was not depending on the concentration of oxygen above 3 % O₂. Additionally, they made some tests with NO₂. The presence of NO₂ enhanced the storage capacity. The storage of NO₂ was significant even if no oxygen was present in the gas phase. Accordingly, the rate of nitrate formation was depending on the gas composition, while the rate of nitrate decomposition increased with the amount of nitrate stored.

The effect of additional species contained in the exhaust has been studied in recent years. Lietti et al [14] showed that water (1 %) promotes the adsorption of NO on Pt/BaO/Al₂O₃ at low temperatures. Conversely, CO₂ depressed the NO_x adsorption. The simultaneous presence of both CO₂ and H₂O resulted also in a reduced adsorption.

Mechanism of adsorption

Mahzoul et al. [13] interpreted their experimental data as follows.

- 1) The molecules of NO, NO₂ and O₂ first adsorb on platinum sites close to barium oxide crystallites. Dioxygen adsorbs dissociatively.
- 2) These adsorbed species react with BaO to form barium nitrate according to the following reactions:

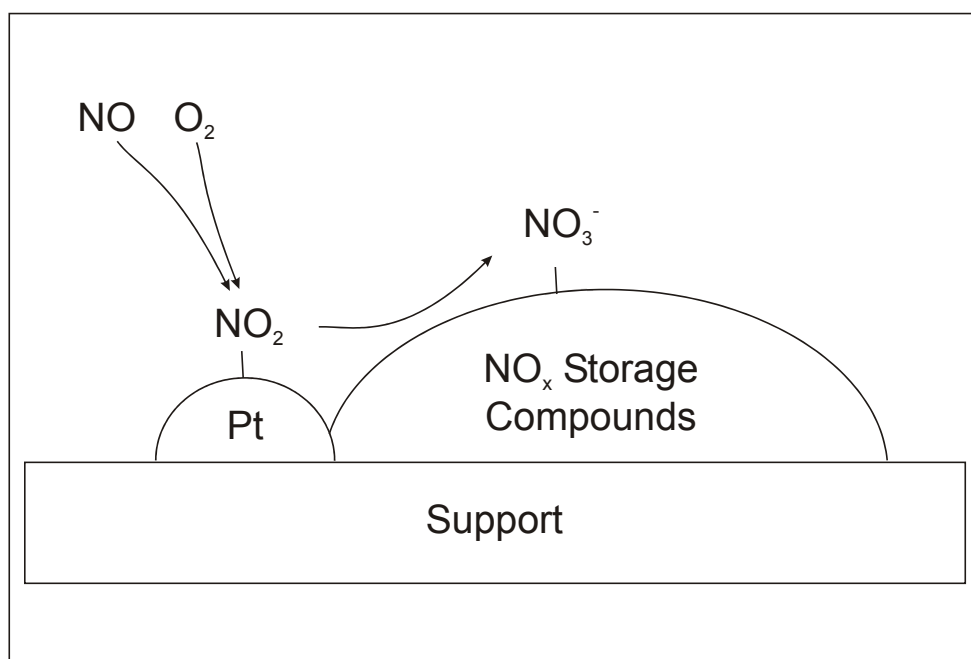


Figure 2-3: NO_x storage mechanism of NSR catalysts. Reprint from [12].

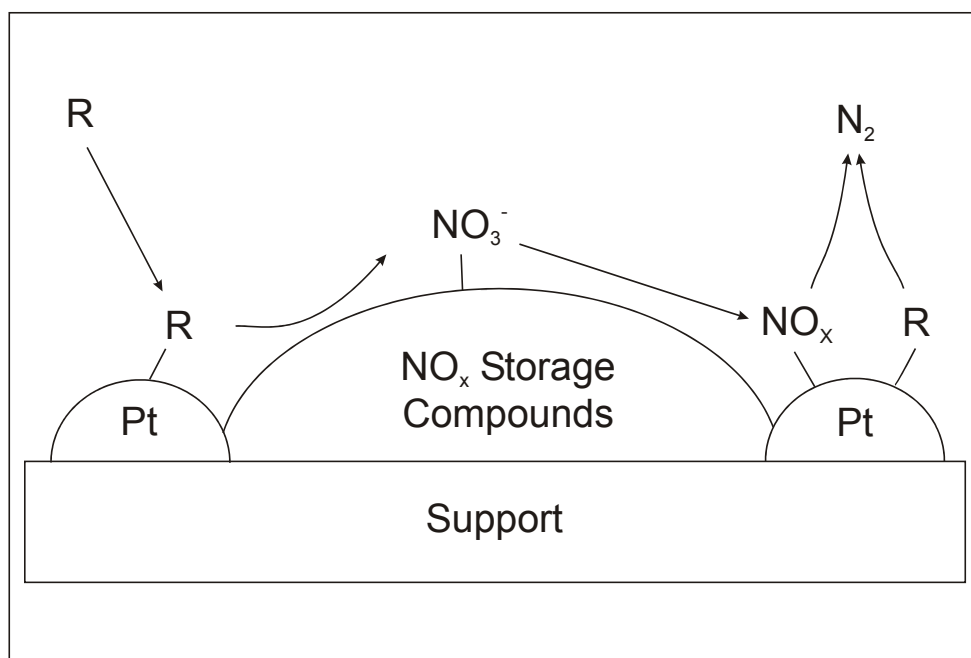
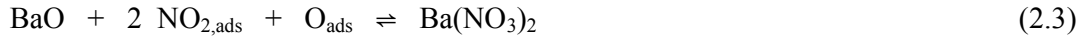
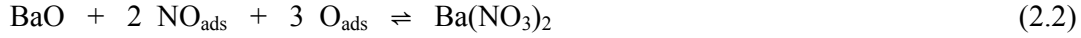
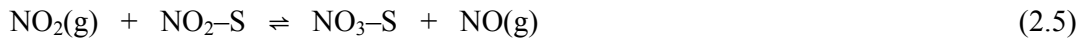


Figure 2-4: NO_x reduction mechanism of NSR catalysts. Reprint from [12].

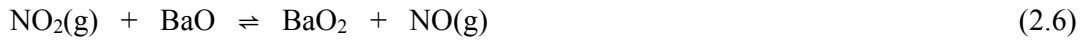


Fridell et al. [15] investigated the adsorption of NO_2 on a model catalyst containing $\text{Pt}/\text{BaO}/\text{Al}_2\text{O}_3$. They proposed the same overall reaction (2.3) for the interaction of NO_2 with the NO_x storage component. However, they do not specify if NO_2 or O_2 first adsorb prior to the reaction with BaO .

Later, Fridell et al. [16,17] observed the formation of NO during the adsorption of NO_2 . This formation was attributed to the oxidation of an intermediate nitrite species to nitrate by NO_2 as follows, where S represents an adsorption site:



They also suggested the oxidation of BaO to barium peroxide by NO_2 , followed by the adsorption of NO_2 :

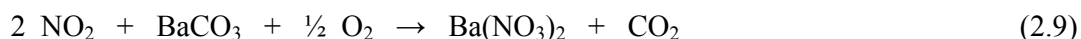


According to Fridell and coworkers, the mechanism via the oxidation of nitrite species seems more plausible. It relies on the fact that the formation of nitrite species before the formation of nitrate species was observed [17].

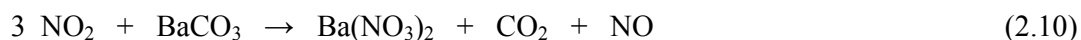
Recently, Cant and Patterson [18] studied the storage of NO_2 at 400°C on Al_2O_3 and $\text{BaO}/\text{Al}_2\text{O}_3$. They observed a stoichiometry 3 : 1 between the NO_2 adsorbed and the NO released. They proposed the following reaction:



It has also been claimed that the NO_x storage component in the NO_x traps is not in the form of barium oxide under real exhaust gas conditions, but more probably in the form of barium carbonate. The base metal compound would undergo a carbonate/nitrate conversion. The overall reaction for the adsorption of NO_2 becomes [19]:



Cant and Patterson [18] proposed an equation analogous to equation (2.8):



Mechanism of desorption

Figure 2-4 shows the mechanism of desorption and reduction proposed by Toyota [12]. First, the reducing agent (R) adsorbs on platinum, then reacts with the nitrate species, thus promoting the desorption of NO_x . After desorption, nitrogen oxides are reduced to nitrogen on the platinum catalyst.

Mahzoul et al. [13] proposed the following reaction for the desorption of nitrogen oxides. The rate of reaction (2.11) increases with the amount of nitrates formed.

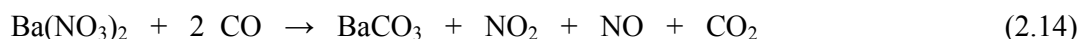


Fridell et al. [15] investigated the NO_x desorption mechanism from an NSR catalyst. They observed significant desorption peaks, mainly of NO, immediately after the switch from lean to rich conditions. They suggest that the decomposition of barium nitrate during the rich phase involves the following reactions:



The presence of NO during the rich phase prevents the regeneration of the NO_x storage catalyst to a large extent. They suggest that the platinum sites needed for the decomposition of the barium nitrate are occupied by NO. They also suggest that barium remains in an activated state, thus enabling the continuous formation of nitrates.

Different groups have claimed that CO_2 promotes the desorption of NO_x [20-22]. Balcon et al. [20] could even desorb stored NO_x completely at 350°C in a feed containing 10 % CO_2 in He in the absence of a reducing agent. Conversely, Li et al [19] proposed that the release of nitrogen oxides during the rich phase occurs by the reaction of the reducing agent, in their case carbon monoxide, with the nitrate species:



2.2 Oxidation of NO to NO₂

The oxidation of nitric oxide is of particular importance for many aftertreatment techniques. In the previous section, it was explained that the adsorption of NO on NO_x storage catalyst first requires its oxidation. It has been mentioned in chapter 1 that the presence of NO₂ is useful for the continuous regeneration of particulate filters (CRT), or for the SCR process with ammonia where NO₂ enables the fast SCR. The gas-phase oxidation of NO has been carefully investigated in the early years of industrial inorganic chemistry, since it is a necessary first step in the production of nitric acid. However, for aftertreatment techniques, the enrichment in NO₂ of the exhaust gases requires a catalyst for the following reaction:



2.2.1 Gas phase equilibrium

Figure 2-5 shows the thermodynamic stability of NO₂ as a function of temperature for partial pressures of oxygen between 0.01 and 0.3 bar. These ratios NO₂/NO_x are displayed for small concentrations of NO_x compared to O₂ (NO_x in the order of a few hundreds of ppm). NO₂ is stable at low temperatures. At temperatures above 200°C, the ratio NO₂/NO_x decreases due to the dissociation of NO₂ into NO and O₂. However, high partial pressures of oxygen increase the stability of NO₂ in the gas phase. At high temperatures, NO is more stable than NO₂.

2.2.2 Gas phase oxidation of NO

The gas-phase oxidation of NO was investigated at the beginning of the last century. Bodenstein [23,24] studied the kinetics of the reaction and proposed a third-order kinetics. The reaction rate of the production of NO was best described by the equation (2.16) with a second order respective to NO and a first order respective to O₂. The value of the reaction rate constant *k* determined by Bodenstein was 1.49·10⁴ l²/(mol²·s). The activation energy of the reaction was – 8.4 kJ/mol.

$$r = k \cdot (p_{\text{NO}})^2 \cdot (p_{\text{O}_2}) \quad (2.16)$$

England and Corcoran [25] studied the oxidation reaction at low concentrations of nitric oxide (below 40 ppm) and in the absence and in the presence of water. They found that water vapor had no specific catalytic effect in the gas-phase as long as the reaction was investigated in a glass reactor and in the absence of adsorbed water on the reactor surface.

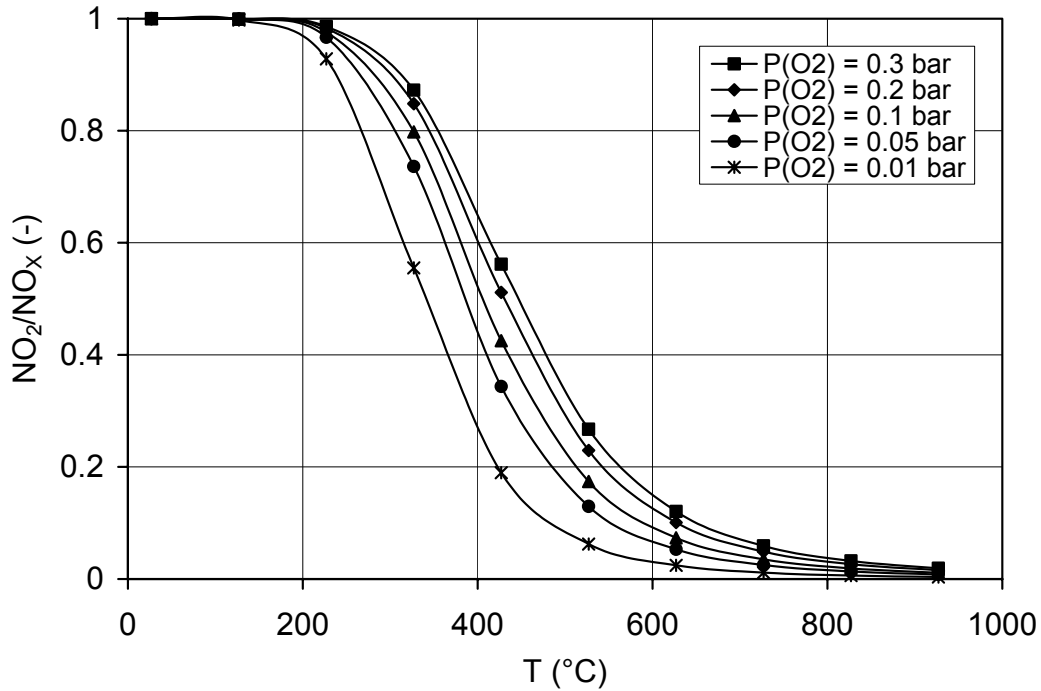


Figure 2-5: The ratio NO_2/NO_x according to the thermodynamic equilibrium for various partial pressures of oxygen as a function of temperature.

2.2.3 Catalytic oxidation of NO over supported platinum catalysts

Many materials have been investigated for the catalytic oxidation of NO, among them zeolites [26,27] or supported metal oxides such as MnO_2 , Cr_2O_3 or CuO [28-30]. However, noble metals like platinum or palladium are usually used as oxidation catalysts due to their better activity. Bourges et al. [31] investigated the oxidation of NO over supported noble metal catalysts in feeds simulating the exhaust gases. Platinum catalysts supported on γ -alumina showed the highest activity.

Influence of the support

Xue et al. [32] investigated the role of the support and of the platinum loading on the oxidation of NO in the presence of sulfur dioxide. Table 2-1 summarizes the results of activity measured over various supports. Platinum supported on SiO₂ exhibited a higher activity than Pt/Al₂O₃ and Pt/ZrO₂ with the same platinum loading. In order to explain the influence of the support, they proposed the influence of the following factors:

- 1) acidic and basic properties of the support, leading to the passivity of SiO₂ towards NO and NO₂, and to the strong interaction of NO and NO₂ with γ -Al₂O₃ and ZrO₂,
- 2) sulfation of the support, which can alter the catalytic properties of the sample,
- 3) difference in the population of surface OH⁻ groups on the supports,
- 4) nature of the adsorption of oxygen on the platinum.

Xue et al. [33] studied the oxidation of NO over a standard Pt/SiO₂ catalyst referred to as EuroPt-1 (6.3 w.-% Pt on SiO₂) in the same conditions as described previously. They observed a deactivation of the sample. A partial recovery of the activity could be observed after reduction of the used sample in hydrogen at 400°C. On the basis of a XPS study, they assume the formation of strongly adsorbed species (SO_x, NO_x) on the surface of the catalyst.

Influence of the platinum particle size

Xue and coworkers [32] have also investigated the influence of the particle size of platinum catalyst supported on SiO₂, γ -Al₂O₃ and ZrO₂. They showed that the reaction was strongly size-dependent for Pt/SiO₂. A faster oxidation rate was observed over the larger platinum particles. The structure sensitivity of the reaction was less prominent for Pt/ZrO₂. On the other hand, they did not evidence any influence of the platinum particle size for Pt/Al₂O₃.

Denton et al. [34] observed a similar trend over samples of Pt/SiO₂ used for the selective reduction of NO by C₃H₆ under lean-burn conditions. The intrinsic activity (mmol NO converted to NO₂ per hour and per m²) clearly increased with decreasing dispersion.

Table 2-1: Conversion of NO over various catalysts prepared from $\text{Pt}(\text{NH}_3)_4\text{Cl}_2$ and calcined at 500 °C for 2 h. Catalyst weight = 0.5 g, volume flow rate = 24 $\text{L}_\text{N}/\text{h}$, feed composition = 10 % O_2 , 500 ppm NO, 50 ppm SO_2 in N_2 [32].

Catalyst	d_{Pt} (nm) ^{a)}	D_{Pt} (%) ^{b)}	Conversion (%)			
			250 °C	300 °C	350 °C	400 °C
0.4 % Pt/SiO ₂	9.0	9	23	50	66	50
2.0 % Pt/SiO ₂	3.7	22	33	70	71	50
0.4 % Pt/Al ₂ O ₃	0.8	100	4	8	16	26
2.0 % Pt/Al ₂ O ₃	6.3	13	27	52	67	50
0.4 % Pt/ZrO ₂	2.9	28	0	2	6	12
2.0 % Pt/ZrO ₂	2.0	41	6	16	26	38

^{a)} platinum particle size, determined by hydrogen chemisorption.

^{b)} platinum dispersion, calculated using $D_{\text{Pt}} = 0.821 \cdot (1/d_{\text{Pt}})$.

Oxidation of NO over bimetallic M-Pt catalysts with M = Sn, Mo or V

Recently, Corro et al. [35] investigated the oxidation of NO over Pt/ γ -Al₂O₃ and Pt-Sn/ γ -Al₂O₃. They observed that the addition of Sn enhanced the conversion of NO to NO₂. On the basis of oxygen chemisorption, they suggest that Sn increases the oxygen chemisorption on the platinum surface, thus speeding up the oxidation reaction.

Liu et al. [36] studied the effect of MoO₃ on the oxidation of NO over MoO₃-Pt/SiO₂ samples. The weight of sample was 0.5 g, and the volume flow rate was 30 $\text{L}_\text{N}/\text{h}$. The feed gas contained 1000 ppm NO, 10 % O_2 in N_2 . The presence of MoO₃ strongly inhibited the reaction. On MoO₃-Pt/SiO₂, the reaction started at 200 °C and was thermodynamically limited at temperatures above 370°C. Conversely, on Pt/SiO₂ the reaction started at a lower value of 150°C and was thermodynamically limited above 270°C.

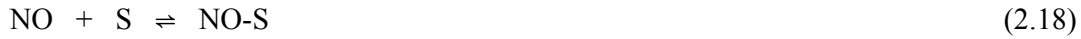
Proposed mechanism over platinum catalysts

Olsson et al. [37] combined laboratory tests and kinetic modeling to describe the oxidation of NO over Pt/Al₂O₃. The reaction mechanism used to describe the NO oxidation contains the following adsorption and desorption steps:

Dissociative adsorption and desorption of oxygen:



Adsorption and desorption of NO:



Adsorption and desorption of NO₂:



Oxidation of NO and dissociation of NO₂:



Olsson et al. [37] preferred an Eley-Rideal to a Langmuir-Hinshelwood mechanism described by reaction (2.21).



They did not find any experimental indications that the oxidation of NO is self-poisoned by a high coverage of oxygen. Also Burch et al. [38] postulated an Eley-Rideal mechanism.

The calculated activation energy (E_A) of the surface reaction of NO oxidation was equal to 40.8 kJ/mol. The activation energy of the dissociation reaction of NO₂ to NO and atomic oxygen (remaining on the surface) was 141.5 kJ/mol. The difference of activation energy for the two reactions was – 100.7 kJ/mol, a value in agreement with the one reported by Burch et al. The rate-determining step was found to be the oxidation of NO according to reaction (2.20) [37].

2.3 Surface reactions on platinum

2.3.1 Adsorption and desorption of oxygen on platinum

Model surfaces

Although the aim of the work was not a fundamental study of the oxidation of NO over model surfaces, the knowledge of the behavior of model surfaces is helpful for the understanding of real surfaces. The surface of a supported catalyst is heterogeneous in nature, with various sites where a reaction can take place. On a catalytic surface, in addition to well-defined arrangement of atoms such as terraces, there are steps, kinks and defects. The interaction of the molecules with metal atoms located at each of these sites is different, thus leading to a different reactivity of these sites. Therefore, studies with model surfaces simulating terraces or surfaces with steps can provide valuable informations that help to understand the catalytic reaction over supported metal catalysts.

Many fundamental researches in ultra high vacuum (UHV) have focused on the adsorption of O₂ on model platinum surface, e.g. Pt(111). Three states of oxygen have been evidenced: molecular oxygen (O₂), atomic oxygen O chemisorbed on the surface, and subsurface oxide [39-45].

Oxygen adsorbs molecularly on Pt(111) at temperatures below – 113 °C [39]. The adsorption of O₂ is followed by its fast dissociation into two oxygen atoms. Atomically chemisorbed oxygen on Pt(111) desorbs from 327 to 827 °C [40]. The temperature of maximum desorption decreases with the oxygen coverage [40]. The atomic oxygen state has a saturation coverage of 0.25 ML (monolayers) referenced to the Pt substrate. This coverage was obtained after saturation exposure of the crystal at a temperature below 27 °C in UHV.

It is interesting to note that higher coverages were obtained from exposure to NO₂ [41-43] or to ozone [44]. Segner et al. [41] reported a maximum coverage of 0.77 ML for a Pt(111) surface exposed to NO₂ at ≈ -127 °C. This high coverage is due to the decomposition of NO₂ to O_{ads} and NO released to the gas phase. Saliba et al. [44]

obtained oxygen coverages ranging from 0.03 to 0.95 ML after exposure of Pt(111) to ozone at 27 °C.

Subsurface oxide is more stable than chemisorbed oxygen. Its decomposition requires temperatures above 927 °C. Niehus and Comsa [45] produced an oxide layer by exposing the Pt(111) surface to O₂ at 827 °C. Saliba et al. [44] reported the formation of platinum oxide using ozone. They obtained surface coverages as high as 2.4 ML. They explained this very high coverage exceeding a monolayer by the formation of an oxide. At coverages between 1 and 2.4 ML, the temperature of maximum desorption increases with the oxygen coverage.

Supported platinum particles

The surface of a platinum crystallite can be described as an assembly of planes like Pt(111) forming steps and kinks at their intersection [46]. Therefore, in order to understand the reactions catalyzed by supported platinum particles, studies of model crystal surfaces are important.

The coordination of a platinum atom on a terrace or on a step is different. This leads to a different activity of terraces and steps. The concentration of steps and terraces is directly related to the size of the platinum particle. Large particles have a larger fraction of terraces. Contrary, smaller particles exhibit more kinks and step sites. Each of these sites has its own reactivity that explains the structure sensitivity of a reaction on crystallites. For example, oxygen is more strongly chemisorbed on a step site than on a surface [47].

2.3.2 Formation of platinum oxide

The work of McCabe et al. [48] considers the oxidation of platinum by examining the oxidation characteristics of both bulk Pt samples and supported platinum catalysts on alumina and silica. The authors showed that the oxidation of platinum was essentially limited to the surface layer of platinum atoms with the formation of a passivation layer. This explains why, in highly dispersed supported platinum catalysts, a higher fraction of Pt is present in the oxidized form. In their study, the oxidation of Pt was independent of both the platinum particle size and the type of support.

Wang and Ye [49] investigated the effects of the particle size on the oxidation of platinum on Al_2O_3 by oxygen. They observed the formation of a stable layer of platinum oxides at about 477 °C. The particle size had a profound effect on the oxidation. For particles smaller than 1.3 nm, the species was PtO_2 , while it was PtO for particles larger than 2 nm.

Additionally, Yoshida et al. [50] claimed a strong influence of the support on the oxidation state of platinum. Using XANES (X-ray absorption near edge structure), they showed that platinum supported on acidic support, e.g. $\text{Al}_2\text{O}_3\text{-SiO}_2$, was much more resistant to oxidation. On the other hand, the catalyst supported on basic supports e.g. MgO or La_2O_3 was fully in the oxidized form.

2.3.3 Adsorption of NO on platinum

The interaction of NO with platinum and other metals has received considerable attention [51-56]. The aim was to understand the mechanism of the dissociation of NO [52] or the mechanism of DeNOx reactions on three-way catalysts [53]. Campbell et al. [54] showed that NO adsorbs molecularly on Pt(111) at 11 °C. A maximum desorption rate was observed around 57 °C.

Morrow et al. [55] studied the adsorption of NO on highly and poorly dispersed platinum supported on SiO_2 by infrared spectroscopy. They observed linearly bound NO. They assigned other stretching bands to bent NO on steps or kinks sites. Due to the possible dissociation of NO to N_2 and O_{ads} , they also evidenced the adsorption of NO on oxidized platinum.

Co-adsorption of NO and oxygen on platinum

Campbell et al. [53] studied the adsorption of NO on a Pt(111) surface precovered with oxygen atoms. The study was performed at a saturation coverage of 0.25 ML. The adsorption of NO at 11 °C was not suppressed by the preadsorption of oxygen. However, the desorption of NO was observed at lower temperatures. The adsorption energy was estimated to be 33 kcal/mol on a clean surface compared to 17 kcal/mol on a surface precovered with oxygen. Oxygen on the surface causes a weakening of the bond between platinum and NO.

Bartram and coworkers [56] reported on the adsorption of NO on Pt(111) after exposure to oxygen and NO₂. The coverage of oxygen was 0.25 ML after the pretreatment with O₂ and 0.75 ML after pretreatment with NO₂. The high coverage of oxygen induced a change of the Pt–NO bond and prevented the formation of linear NO. Furthermore, the desorption of NO₂ was not observed during a TPD (up to 500 K) experiment with co-adsorbed NO and oxygen. The oxidation of NO surprisingly never took place. Bartram et al. showed that the energetic barrier of the oxidation of NO is larger than the desorption of NO at any coverage of oxygen. Therefore, during TPD, NO preferentially desorbs than reacts with O_{ads}.

2.4 Conclusions for the present thesis

The adsorption properties of zeolites will be used to adsorb nitrogen monoxide from synthetic exhaust gas. The adsorption of NO from dry and humid feeds will be studied at low temperatures, i.e. typically at 200 °C. Further, the adsorption of pure NO₂ and mixtures of NO₂ + NO has to be investigated.

Another goal of the thesis is to investigate the adsorption of nitrogen dioxide on supported barium oxide at low temperatures, typically at 200 °C. The aim of the work is to study the adsorption of NO₂ on a platinum-free NO_x storage catalyst based on BaO/TiO₂. Additionally, the adsorption of mixtures of NO₂ and NO will be performed to study the influence of NO on the adsorption of NO₂.

The practical application of platinum catalysts for the oxidation of NO in lean exhaust gases calls for active catalysts in the temperature range 150 - 300 °C. Considering the conversions values reported in the literature, the most active catalysts are based on Pt/SiO₂. Therefore, the oxidation of NO over Pt/SiO₂ will particularly be investigated. Attention will be paid to the influence of the concentrations of NO and O₂ in the feed to propose a mechanism for the oxidation reaction. Platinum supported on other oxides such as γ -Al₂O₃ or ZrO₂ is reported to be much less active. Therefore, a better understanding of the role of the supporting oxide is another goal of the present work.

2.5 References

- [1] W.M. Meier and D.H. Olson, *Atlas of zeolite structure types*, Butterworth-Heinemann, (1992)
- [2] M. Shelef, *Chem. Rev.* **95** (1995), 209
- [3] N.Y. Chen, *J. Phys. Chem.* **80** (1976), 60
- [4] T. Sano, K. Suzuki, H. Shoji, S. Ikai, K. Okabe, T. Murakami, S. Shin, H. Hagiwara and H. Takaya, *Chem. Lett.* (1987), 1421
- [5] R.A. Grinstead, H.W. Jen, C.N. Montreuil, M.J. Rokosz and M. Shelef, *Zeolites* **13** (1993), 602
- [6] M.J. Rokosz, A.V. Kucherov, H.W. Jen and M. Shelef, *Catal. Today* **35** (1997), 65
- [7] H. Arai and M. Machida, *Catal. Today* **22** (1994), 97
- [8] W.H. Zhang, H. Yahiro, N. Mizuno, J. Izumi and M. Iwamoto, *Langmuir* **9** (1993), 2337
- [9] [URL:www.iza-structure.org/databases](http://www.iza-structure.org/databases), date: 12.09.2002
- [10] B.J. Adelman, G.-D. Lei and W.M.H. Sachtler, *Catal. Lett.* **28** (1994), 119.
- [11] K. Hadjiivanov, D. Klissurski, G. Ramis and G. Busca, *Appl. Catal. B* **7** (1996), 251
- [12] N. Takahashi, H. Shinjoh, T. Iijima, T. Susuki, K. Yamazaki, K. Yokota, H. Suzuki, N. Miyoshi, S. Matsumoto, T. Tanizawa, T. Tanaka, S. Tateishi and K. Kasahara, *Catal. Today* **27** (1996), 63
- [13] H. Mahzoul, J.F. Brilhac and P. Gilot, *Appl. Catal. B: Environ.* **20** (1999), 47
- [14] L. Lietti, P. Forzatti, I. Nova and E. Tronconi, *J. Catal.* **204** (2001), 175
- [15] E. Fridell, M. Skoglundh, B. Westerberg, S. Johansson and G. Smedler, *J. Catal.* **183** (1999), 196
- [16] E. Fridell, H. Persson, B. Westerberg, L. Olsson and M. Skoglundh, *Catal. Lett.* **66** (2000), 71
- [17] E. Fridell, H. Persson, L. Olsson, B. Westerberg, A. Amberntsson and M. Skoglundh, *Top. Catal.* **16/17** (2001), 133
- [18] N.W. Cant and M.J. Patterson, *Catal. Today* **73** (2002), 271
- [19] Y. Li, S. Roth, J. Dettling and T. Beutel, *Top. Catal.* **16/17** (2001), 139

- [20] S. Balcon, C. Potvin, L. Salin, J.F. Tempère, G. Blanchard and G. Djéga-Mariadassou, *Catal. Lett.* **60** (1999), 39
- [21] F. Rodrigues, L. Juste, C. Potvin, J.F. Tempère, G. Blanchard and G. Djéga-Mariadassou, *Catal. Lett.* **72** (2001), 59
- [22] A. Amberntsson, H. Persson, P. Engström and B. Kasemo, *Appl. Catal. B: Environ.* **31** (2001), 27
- [23] M. Bodenstein, *Z. Elektrochem.* **24** (1918), 183
- [24] M. Bodenstein, *Z. Phys. Chem.* **100** (1922), 168
- [25] C. England and W.H. Corcoran, *Ind. Eng. Chem. Fund.* **14** (1975), 55
- [26] J. Seifert, *Untersuchung der heterogen katalysierten NO-Oxidation in einer rechnergesteuerten, echtzeitkontrollierten Versuchsanordnung*, Thesis, Erlangen (1989)
- [27] J.G.M. Brandin, L.H. Andersson and C.U.I. Odenbrand, *Acta Chem. Scand.* **44** (1991), 784
- [28] M. Misono, *Catalytic reduction of nitrogen oxides by bifunctional catalysts*, CATTECH (3), Baltzer Science Publishers, June 1998
- [29] M. Misono, Y. Hirao and C. Yokoyama, *Catal. Today* **38** (1997), 157
- [30] K. Shiba, H. Hinode and M. Wakihara, *React. Kinet. Catal. Lett.* **58** (1996), 133
- [31] P. Bourges, S. Lunati and G. Mabilon, *N₂O and NO₂ formation during NO reduction on precious metal catalysts*, 4th international congress on catalysis and automotive pollution control, Brussels, April 1997, volume 1, p. 81
- [32] E. Xue, K. Seshan and J.R.H. Ross, *Appl. Catal. B: Environ.* **11** (1996), 65
- [33] E. Xue, K. Seshan, J.G. Ommen and J.R.H. Ross, *Appl. Catal. B: Environ.* **2** (1993), 183
- [34] P. Denton, A. Giroir-Fendler, H. Praliaud and M. Primet, *J. Catal.* **189** (2000), 410
- [35] G. Corro, M.P. Elizalde and A. Velasco, *React. Kinet. Catal. Lett.* **76** (2002), 117
- [36] S. Liu, A. Obuchi, J. Oi-Uchisawa, T. Nanba and S. Kushiyaama, *Appl. Catal. B: Environ.* **30** (2001), 259
- [37] L. Olsson, B. Westerberg, H. Persson, E. Fridell, M. Skodlundh and B. Andersson, *J. Phys. Chem B* **103** (1999), 10433
- [38] R. Burch and T.C. Watling, *J. Catal.* **169** (1997), 45
- [39] T. Zambelli, J.V. Barth, J. Wintterlin and G. Ertl, *Nature* **390** (1997), 495
- [40] C.T. Campbell, G. Ertl, H. Kuipers and J. Segner, *Surf. Sci.* **107** (1981), 220

- [41] J. Segner, W. Vielhaber and G. Ertl, *Israel. J. Chem.* **22** (1982), 375
- [42] D.H. Parker, M.E. Bartram and B.E. Koel, *Surf. Sci.* **217** (1989), 489
- [43] D.H. Parker and B.E. Koel, *J. Vac. Sci. Technol. A* **8** (1990), 2585
- [44] N.A. Saliba, Y.L. Tsai, C. Panja and B.E. Koel, *Surf. Sci.* **419** (1999), 79
- [45] H. Niehus and G. Comsa, *Surf. Sci.* **93** (1980), L147
- [46] F.H. Ribeiro and G.A. Somorjai, in: G. Ertl, H. Knözinger and J. Weitkamp (Eds.), *Handbook of heterogeneous catalysis*, Vol. 2, Wiley-VCH, Weinheim (1997), pp. 771-786
- [47] H. Wang, R.G. Tobin, G.B. Fisher, C.L. DiMaggio and D.K. Lambert, *Surf. Sci.* **440** (1999), 429
- [48] R.W. McCabe, C. Wong and H.S. Woo, *J. Catal.* **114** (1988), 354
- [49] C.B. Wang and C.T. Yeh, *J. Catal.* **178** (1998), 450
- [50] H. Yoshida, Y. Yazawa, N. Takagi, A. Satsuma, T. Tanaka, S. Yoshida and T. Hattori, *J. Synchrotron Rad.* **6** (1999), 471
- [51] W.A. Brown and D.A. King, *J. Phys. Chem. B* **104** (2000), 2578
- [52] T. Furusawa and K.I. Aika, *Bull. Chem. Soc. Jpn.* **73** (2000), 795
- [53] C.T. Campbell, G. Ertl and J. Segner, *Surf. Sci.* **115** (1982), 309
- [54] B.A. Morrow, J.P. Chevrier and L.E. Moran, *J. Catal.* **91** (1985), 208
- [55] R.F. van Slooten and B.E. Nieuwenhuys, *J. Catal.* **122** (1990), 429
- [56] M.E. Bartram, B.E. Koel and E.A. Carter, *Surf. Sci.* **219** (1989), 467

Characterization methods and experimental setup

3.1 Physico-chemical characterization

The catalysts prepared for the study were characterized by nitrogen physisorption (BET), X-ray diffraction (XRD), X-ray photoelectron spectroscopy (XPS), and transmission electron microscopy (TEM). Introductions to the various characterization methods of solid catalysts are given e.g. in references [1-5]. XRD and XPS techniques will briefly be described in the following.

The size of platinum particles can be measured by chemical and physical methods. Chemical methods are based on the measurement of the quantity of a gas (H_2 , CO ,...) adsorbed selectively on the metal. Although these methods are widely used, they suffer from limitations. For example, H atoms can spillover from the metal to the support, leading to a higher H_2 uptake. Furthermore, the adsorption of gases can be hindered by contaminants (e.g. chlorine) on the metal surface. Chemisorption can also be hindered by decoration of the particle by the support in case of strong metal support interaction. This pertains primarily to smaller particle sizes [1].

In view of the drawbacks of chemical methods, the determination of the platinum particle size was carried out by analyzing the XRD pattern and the XPS intensities of supported platinum crystallites, as well as by transmission electron microscopy (TEM).

The models used to calculate the size from XRD line broadening and from XPS intensities are described in Annex 1. Transmission electron microscopy studies were also performed on samples Pt/SiO₂. However, the platinum particles for the samples Pt/ZrO₂ were not detectable due to the high dispersion of the platinum.

3.1.1 X-ray diffraction (XRD)

Principle of the technique

X-ray diffraction patterns of powders are obtained by irradiating the sample with a monochromatic X-ray beam of wavelength λ and measuring the angles of the diffracted X-rays. The X-ray sources are commonly Cu K α or Fe K α with wavelengths of 1.541 and 1.936 Å respectively. The X-rays are scattered by atoms in a periodic lattice. The distance between lattice planes is derived from the Bragg equation:

$$n \cdot \lambda = 2 \cdot d \cdot \sin \theta \quad (3.1)$$

with	n	the order of the reflection ($n = 1, 2, \dots$)
	λ	the wavelength of the X-ray radiation (Å)
	d	the distance between two lattice planes (Å)
	θ	the angle between the incoming X-ray and the normal to the reflecting lattice plane (°)

The major use of X-ray diffraction is the identification of bulk crystalline phases that are present in a sample. The pattern of the sample is compared with the diffraction patterns of single-phase powders. The main source for XRD patterns of reference compounds is the international center for diffraction data (ICDD, previously JCPDS). Additionally, XRD analysis provides information on the crystallinity of the sample (for example of zeolites) and on the size of supported metal crystallites (see Annex 1) [2].

Apparatus

X-ray analysis was performed on a Philips X-Pert – MPD diffractometer using the Fe or Cu K α radiations at 1.936 Å and 1.541 Å respectively. The scans were recorded continuously in the range of 2θ between 10 ° and 80 °, with a step width of 0.05 ° and a dwell time of 5 seconds.

3.1.2 X-ray photoelectron spectroscopy (XPS)

Principle of the technique

Surface analysis by XPS is accomplished by irradiating a sample with X-ray photons and measuring the kinetic energy of the emitted electrons. The X-ray photons are commonly Mg K α or Al K α with energies of 1253.6 and 1486.6 eV respectively. Their interaction with atoms in the surface region (1 – 10 μ m) leads to the emission of photoelectrons. However, only the electrons emitted by the upper atom layers are detected. The emitted electrons have a kinetic energy (E_k) given by the relation:

$$E_k = h\nu - BE - \Phi_s \quad (3.2)$$

with	$h\nu$	X-ray photon energy
	BE	the binding energy of the atomic orbital from which the electron originates
	Φ_s	the spectrometer work function

XPS spectra display the number of electrons as a function of binding energies, which are calculated using equation (3.2). However, the binding energies have to be corrected in the case of insulators. The BE values must be corrected for the electrostatic charging of the specimen. This charging reduces the kinetic energy of the emitted electrons, leading to a shift of the binding energy values towards higher values.

From the XPS spectra, information on the chemical state of atoms on the surface of a specimen can be obtained. Some tables summarize the BE values of elements of the periodic table in their various oxidation states. Table 3-1 gives the values of binding energies of the platinum 4f core-level for platinum and for the platinum oxides [6]. Concentrations of elements, or the size of particles in the case of supported catalysts, can be determined from the peak intensities (see Annex 1).

Apparatus

XPS spectra were recorded with an ESCALAB 220i XL (Thermo VGScientific), using non-monochromatic Mg K α radiation at 300 W. XPS spectra were recorded in the constant analyzer energy (CAE) mode with an analyzer pass energy of 50 eV for the survey scan and 20 eV for the detail scans of C 1s, O 1s, Pt 4f, Si 2p and Zr 3d. In order

to correct for the sample charging, binding energies were referred to Zr 3d at 182.2 eV or Si 2p at 103.5 eV. The composition of the samples was determined by quantitative analysis using the cross sections given by Scofield [7].

Table 3-1: Binding energies of the Pt 4f core-level for different platinum compounds from [6].

Compounds	Binding energies (eV)	
	4f _{7/2}	4f _{5/2}
Pt	71.2	74.6
PtO	72.3	75.6
PtO ₂	73.6	76.8

3.2 Experimental setup

The experimental setup for the catalytic testing is shown in Figure 3-1. It consists of three main components: the gas dosing system, the reactor, and the gas analyzer. Due to the possible presence of water in the feed gas, all gas lines were heated to 150-170 °C.

3.2.1 Gas dosing system

The feed gas was prepared by mixing gases of higher concentrations purchased from Carbogas (Table 3-2). The flow rate of each component was adjusted by a mass flow controller (MFC Brooks 5850S). Water was dosed by means of a liquid mass flow controller (MFC Brooks 5881), injecting it through a micro-capillary into an evaporator heated electrically to about 150 °C. All six mass flow controllers were controlled from a computer, by which the total flow rate and the final concentrations of NO, NO₂, CO, water and oxygen were set. Nitrogen was used as a balance gas and was automatically adjusted to make up the total flow rate. The total flow rate could be varied between 150 and 550 L_N/h.

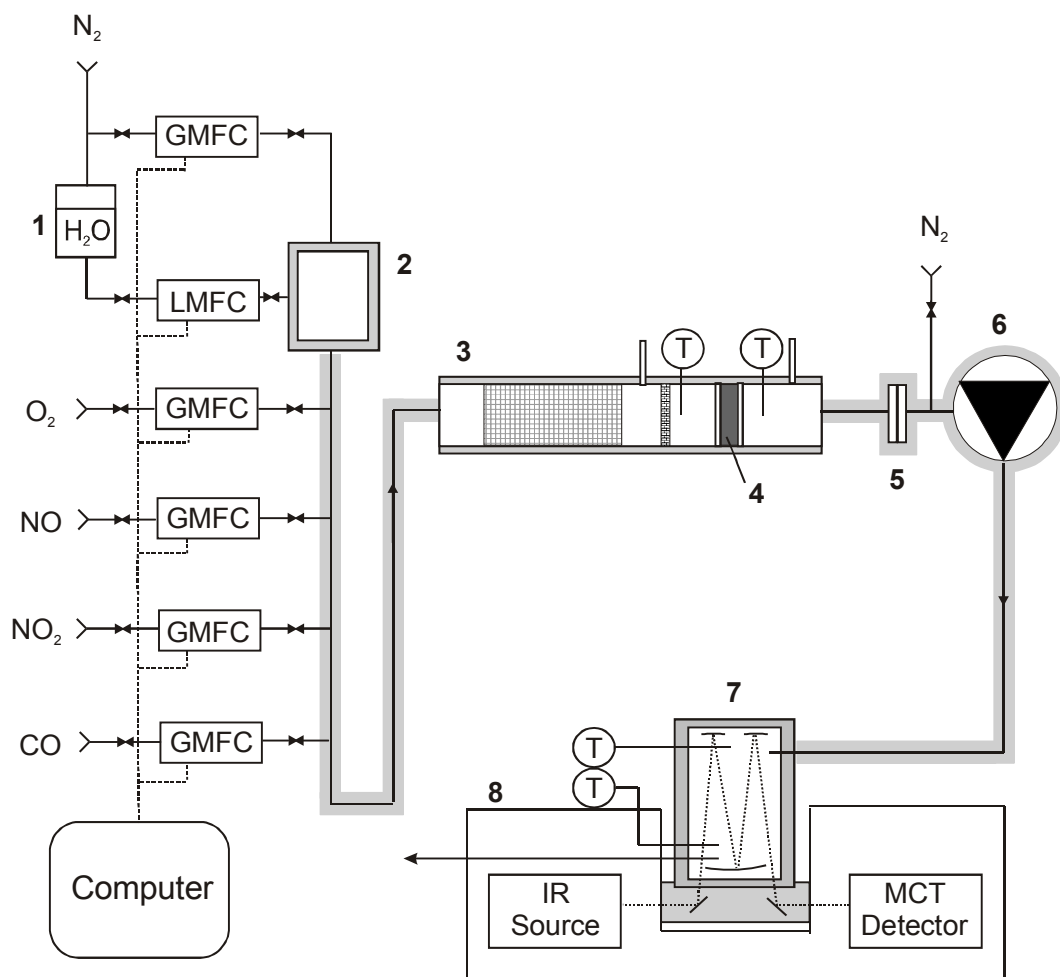


Figure 3-1: Experimental setup: (GMFC) gas mass flow controller, (LMFC) liquid mass flow controller, (T) thermocouple, (1) water reservoir, (2) water evaporator, (3) reactor, (4) catalyst sample, (5) filter, (6) diaphragm pump, (7) reflection gas cell, and (8) FTIR spectrometer.

Table 3-2: Gas mixtures from Carbagas used in the preparation of the feed gas.

Species	Concentration	Purity
N ₂	100 %	99.999 %
O ₂	100 %	99.5 %
NO	5 % in N ₂	99.9 %
NO ₂	1 % in N ₂	99 %
CO	5 % in N ₂	99.997 %

3.2.2 Reactors

Reactor for adsorption experiments

The reactor used for the adsorption experiments was a Pyrex glass tube of 28 mm internal diameter consisting of a pre-heating section filled with steatite pellets and a second section containing the catalyst sample (Figure 3-1). The powder sample was held between two quartz wool plugs. The two sections could be heated independently by two separate heating coils. The reactor temperature was controlled by two thermocouples fixed in front of and behind the catalyst.

Reactor for the oxidation of NO

The reactor used for oxidation experiments consisted of stainless steel and had an internal diameter of 16 mm. Figure 3-2 displays a schematic representation of the reactor. The catalyst sample of typically 0.8 g was held between two quartz wool plugs. A pre-heating section consisted of a stainless steel tube (2 mm internal diameter, 70 cm length) in spiral configuration. The reactor was placed inside a stainless steel cylinder heated by a heating coil connected to a temperature controller. The corresponding thermocouple was inserted in the quartz wool plug behind the catalyst via the gas line.

The reactor was equipped with a bypass to check the concentrations of reactants entering the reactor. The blank oxidation of NO to NO₂ due to the reactor surface was determined without catalyst in the reactor. Below 300 °C, it was negligible. Between 350 °C and 450 °C, the conversion of NO in a feed containing 10 % O₂ in N₂ was less than 4 %.

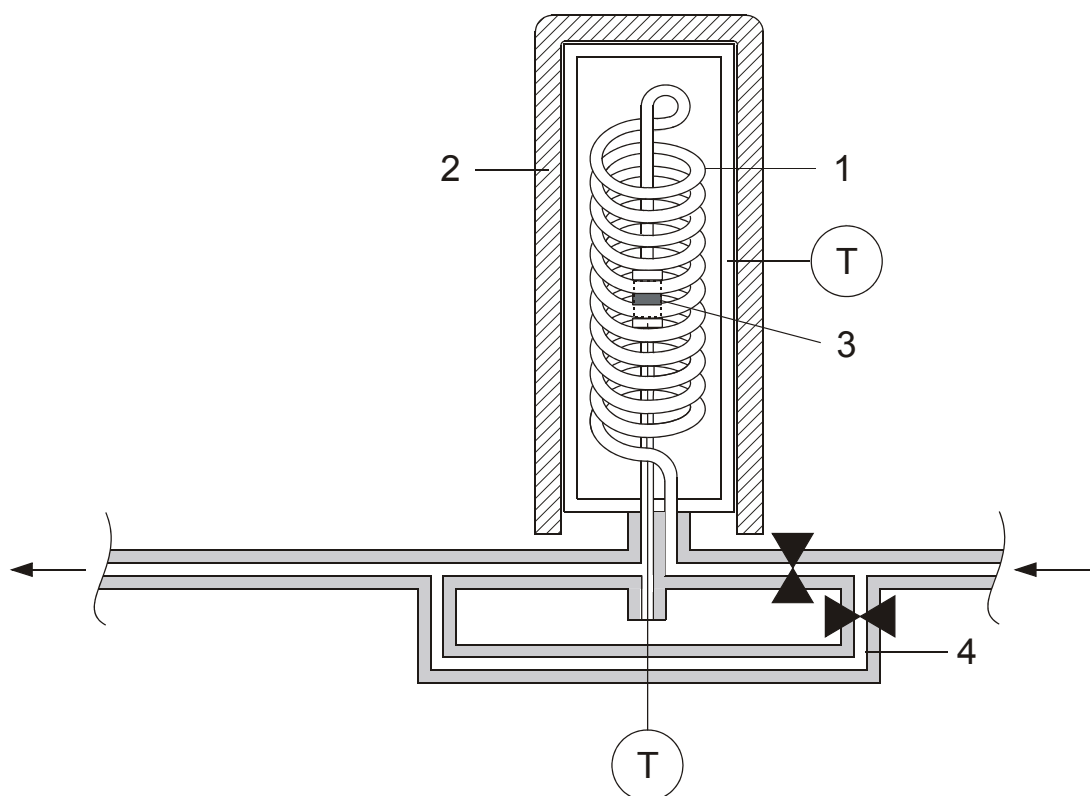


Figure 3-2: Schematic representation of the reactor for the oxidation tests.

(T) thermocouple, (1) pre-heating section, (2) heating coil, (3) powder sample and (4) bypass, from [9].

3.2.3 Gas analyzer

Apparatus

Analysis of the gases at the reactor outlet was performed by means of Fourier transform infrared (FTIR) spectroscopy. The apparatus is a Nicolet Magna IR 560 spectrometer equipped with a liquid nitrogen cooled MCT detector. A partial stream of the gases leaving the reactor was taken by the membrane pump and passed through the heated multiple pass gas cell (Graseby Specac G-2-4-BA-AU, 2 m path length, volume of 275 cm³, gold mirrors). The gas cell was heated to a temperature between 175 °C and 180 °C, thus preventing water condensation. The cell was equipped with special sandwich-type windows in order to avoid the formation of nitrates by NO₂ contained in the test gas. They consisted of a thin sheet (0.5 mm) of AgCl on the sample side on KBr (4 mm).

A background spectrum was taken in a flow of nitrogen by accumulation of 128 scans. For the measurements, 8 scans were accumulated in 8 seconds. However, for transient experiments, the number of scans could be decreased to 4, thus shortening the time between two measurements to 4 seconds. All spectra were recorded with a resolution of 0.5 cm^{-1} and a wavelength range between 400 and 4000 cm^{-1} .

Method of quantification

The concentrations of nitrogen monoxide, nitrogen dioxide, nitric acid and water were quantified by a method developed in-house using the OMNIC[®] Quantpad software. This software is based on the classical least-squares (CLS) quantitative analysis algorithm for quantifying sample mixtures in which there is little or no interaction between molecules. It allows correction for nonlinear absorbance versus concentration behavior. The method assumes that the concentration of each component is directly proportional to its absorbance at each wavelength of the IR region. However this is not true for all components. Therefore, the program provides means for correcting such effects. For example, the correction for nonlinear absorbance versus concentration behavior must be applied for the quantification of NO. Furthermore, the program enables the correction for physical interactions between molecules in the gas phase shifting the characteristic absorption bands. In our case, water interacts both with NO and NO₂. This requires standard calibration spectra of gas mixtures containing varying concentrations of the two interacting molecules. The software then calculates the correction factors for the interferences. The use of CLS algorithms and the corrections for nonlinearity and for gas phase interferences enables measuring the concentration of HNO₃, NO_x and water with fairly good detection limits. Table 3-3 shows the IR regions where the quantifications were performed, as well as the corresponding detection limits in dry and humid test gas.

Table 3-3: IR regions used for the quantification of various components and resulting detection limits in dry and humid feeds.

Species	IR regions	Detections limits (ppm)	
		without water	with 5 % vol. water
NO	1850-1940	3	5
NO ₂	1580-1634	1	3
HNO ₃	836-917	10	10
H ₂ O	2985-3073	300	-

3.3 Evaluation of the adsorption and the oxidation tests

The experimental conditions used in the various tests are given in the experimental part of the corresponding chapters.

3.3.1 Gas hourly space velocity

The gas hourly space velocity (GHSV) is defined as the ratio of the overall gas flow rate to the volume of catalyst sample.

$$\text{GHSV} = \frac{V^*}{V_{\text{cat}}} \quad (3.3)$$

with GHSV gas hourly space velocity at standard conditions [1/h],
 V^* gas flow rate at standard conditions [$\text{m}^3_{\text{N}}/\text{h}$],
 V_{cat} volume of catalyst [m^3].

3.3.2 Adsorption tests

Procedure

The interaction of nitrogen oxides from lean exhaust gases with the adsorbing materials was studied by combined adsorption and temperature programmed desorption (TPD). The gas feed used in the test typically contained 10 % O₂, 0 – 5 % H₂O with balance N₂. The adsorption-desorption tests included the following steps:

- 1) adsorption of NO, NO₂ or mixtures of NO and NO₂ for 1 hour.
- 2) equilibration at the temperature of adsorption in order to remove the weakly adsorbed species,
- 3) temperature programmed desorption from the temperature of adsorption to 450°C (8 °C/min).

Determination of the amount of NO_x adsorbed

The amounts of NO₂ stored on zeolites or on supported barium oxide during the adsorption was calculated according to:

$$\text{NO}_2 \text{ adsorbed} = \frac{V^*}{V_N \cdot m_{\text{cat}}} \int_{t_0}^t (c_{\text{NO}_2, \text{in}} - c_{\text{NO}_2, \text{out}}) dt \quad (3.4)$$

with	V^*	gas flow rate at standard conditions (m ³ _N /h)
	V_N	molar gas volume at standard conditions = 22 400 cm ³ _N
	m_{cat}	weight of catalyst (g)
	$c_{\text{NO}_2, \text{in}}$	concentration of NO ₂ entering the reactor (cm ³ _N /m ³ _N)
	$c_{\text{NO}_2, \text{out}}$	concentration of NO ₂ leaving the reactor (cm ³ _N /m ³ _N)

The amounts of NO_x desorbed during temperature programmed desorption (TPD) were calculated using the following equation:

$$\text{NO}_x \text{ desorbed} = \frac{V^*}{V_N \cdot m_{\text{cat}}} \int_{t_0}^t c_{\text{NO}_x, \text{out}} dt \quad (3.5)$$

with	$c_{\text{NO}_x, \text{out}}$	the concentration of NO or NO ₂ measured at time t.
------	-------------------------------	--

3.3.3 Oxidation tests

Procedure

The oxidation tests were performed in the stainless steel reactor with 800 mg of powdered sample. The particle size of the powder was between 160 and 200 μm to avoid mass transfer limitations. The oxidation of NO was investigated in the temperature range between 150 and 450 $^{\circ}\text{C}$. The overall flow rate was 150 l_N/h. The synthetic gas composition is given in Table 3-4.

Table 3-4: Synthetic gas composition.

Species	Concentrations
O ₂	0.1 – 30 %
H ₂ O	0 – 5 %
NO	100 – 1500 ppm
NO ₂	0 – 500 ppm
N ₂	Balance

Conversion of NO to NO₂

The conversion of NO to NO₂ over platinum catalysts is calculated as follows:

$$\text{Conversion (\%)} = \frac{c_{\text{NO}_2, \text{out}}}{c_{\text{NO}, \text{in}}} \cdot 100 \quad (3.6)$$

3.4 References

- [1] K.S.W. Sing, J. Rouquerol, P. Gallezot and G. Bergeret, in: G. Ertl, H. Knözinger and J. Weitkamp (Eds.), *Handbook of heterogeneous catalysis*, Vol. 2, Wiley-VCH, Weinheim (1997), pp. 427-475
- [2] J.W. Niemantsverdriet, in: *Spectroscopy in catalysis, an introduction*, VCH, Weinheim (1995)

- [3] A. Baiker, *Chimia* **35** (1981), 440
- [4] J.F. Watts, *Vacuum* **45** (1994), 653
- [5] *Handbook of X-ray photoelectron spectroscopy*, Perkin-Elmer Corporation
- [6] V. Pitchon and A. Fritz, *J. Catal.* **186** (1999), 64
- [7] J.H. Scofield, *J. Electron. Spectrosc. Relat. Phenom.* **8** (1976), 129
- [8] F.P.J.M. Kerkhof and J.A. Moulijn, *J. Phys. Chem.* **83** (1979), 1612
- [9] M. Kleemann, *Beschichtung von Cordierit-Wabenkörpern für die selective katalytische Reduktion von Stickoxiden*, Thesis ETH Nr. 13401, ETH Zurich, (1999)

Adsorption and desorption of NO and NO₂ on Cu-ZSM-5

4.1 Introduction

The adsorption of nitrogen oxides from flue gases has attracted much interest, e.g. for the selective NO_x recirculation (SNR) process developed by Daimler Benz [1]. This process involves two parallel NO_x adsorbers, one adsorbing the nitrogen oxides from the exhaust gas and the other being in the phase of regeneration. The adsorbed NO_x-species are then desorbed by temperature swing desorption using hot air. The desorbed NO_x may be reinjected into the combustion chamber where it dissociates into N₂ and O₂.

Arai and Machida [2] have discussed various materials for removing NO_x by sorption-desorption cycles, in particular metal oxides and zeolites. We have also investigated the adsorption of NO on various metal oxides in preliminary experiments. The tested oxides were ZrO₂, γ-Al₂O₃, TiO₂, WO₃-doped TiO₂, WO₃ or SiO₂. However, in the temperature range between 150 and 250 °C, the amount of adsorbed NO was much too low (0 – 50 μmol/g). Further, the adsorption of NO on these materials was completely suppressed if water was added to the feed.

The adsorption of NO on heteropoly acids, such as tungstophosphoric acid, has also been claimed in the literature [3,4]. These acids could adsorb NO at flue gas temperatures. However, adsorption tests performed in our group with unsupported and Al_2O_3 -supported $\text{H}_3\text{PW}_{12}\text{O}_{40} \cdot 6 \text{ H}_2\text{O}$ did not show any storage of NO in dry and humid oxidizing feeds.

Zeolites are widely used as a sorbent material. They are also used as catalysts in petrochemical reactions or in the aftertreatment of exhaust gases. They serve as a catalyst for DeNO_x using hydrocarbons or ammonia, e.g. Cu-ZSM-5 [5]. They can also be added to the composition of an oxidation catalyst in order to improve the oxidation of hydrocarbons [6]. Their adsorption properties can be utilized to adsorb nitrogen oxides from flue gases as well [7,8]. The adsorption of nitrogen oxides on zeolites has also been studied at low temperatures using spectroscopic methods [9-11]. Experimental works were performed to test their reliability to adsorb NO and mixture of NO + NO_2 .

Preliminary experiments about the adsorption of NO and NO_2 on Na- and H-ZSM-5 had led us to the following conclusions:

- a) Small amounts of NO may be stored at low temperatures (e.g. at 150 °C) in the absence of water. After saturation of the adsorption sites, a small fraction of NO is oxidized to NO_2 .
- b) If the feed contains water (typically 5 %), the storage and oxidation of NO is completely suppressed.
- c) However, NO_2 can still be adsorbed on these materials in the presence of water.

Unfortunately, NO_x in flue gas typically consists of more than 90 % NO. Therefore, in order to achieve the storage of NO, it must previously be oxidized to NO_2 . Thus, an ideal storage material should possess both capabilities of oxidizing NO to NO_2 and of storing the formed NO_2 . Cu-ZSM-5 has been reported to be highly effective for oxidizing NO in the absence of water [12]. This prompted us to test Cu-ZSM-5 for the selective adsorption of NO. The present chapter reports on adsorption experiments of NO and NO_2 in the absence and presence of water with a copper exchanged ZSM-5. The influence of NO on the stability of the adsorbed species is also investigated.

4.2 Experimental

4.2.1 Catalyst preparation

Cu-ZSM-5 was prepared by ion-exchange of Na-ZSM-5 (Zeocat PZ2-40, $\text{SiO}_2\text{:Al}_2\text{O}_3 = 40$, Chemie Uetikon AG). 6 g of the zeolite were suspended in 400 ml deionized water. 100 ml of a copper(II) acetate solution (25 mmol/l) were then added slowly and the suspension stirred for 24 hours keeping the temperature at 80 °C. After ion exchange, the sample was filtered and dried at 120 °C overnight. The exchange procedure was repeated three times to achieve a complete exchange of sodium by copper. Finally, the sample was calcined in static air at 550 °C for 5 hours.

4.2.2 Characterization

Copper content

The copper content was determined by inductively coupled plasma - atomic emission spectroscopy (ICP-AES). The copper loading was 3.3 wt.% Cu, corresponding to an exchange level of 134 % based on one Cu^{2+} ion per two aluminum cations. Such highly exchanged zeolites are commonly referred to as over-exchanged zeolites.

BET measurements

The specific surface areas (S_{BET}) of Na-ZSM-5 and Cu-ZSM-5 were determined by nitrogen physisorption at 77 K using a Micromeritics ASAP 2001 apparatus. Prior to the measurement, the samples were degassed at 250 °C. S_{BET} were calculated in a relative pressure range 0.05-0.2 assuming a cross-sectional area of 0.162 nm² for the nitrogen molecule. The specific surface areas of both samples were approximately 360 m²/g: no substantial loss of surface area occurred due to ion exchange and calcination at 550 °C.

X-ray diffraction (XRD)

X-ray analysis was performed on a Philips X'Pert - MPD diffractometer (Fe $\text{K}\alpha$ radiation). The apparatus has been described in chapter 3. The tested samples were Cu-ZSM-5 after the calcination step ("fresh sample") and Cu-ZSM-5 after the NO_x adsorption experiments ("used sample"). The XRD patterns are shown in Figure 4-1.

No peaks characteristic of crystalline copper oxide can be seen. The samples even did not lose their crystallinity after testing them in the presence of H_2O at $450\text{ }^\circ\text{C}$.

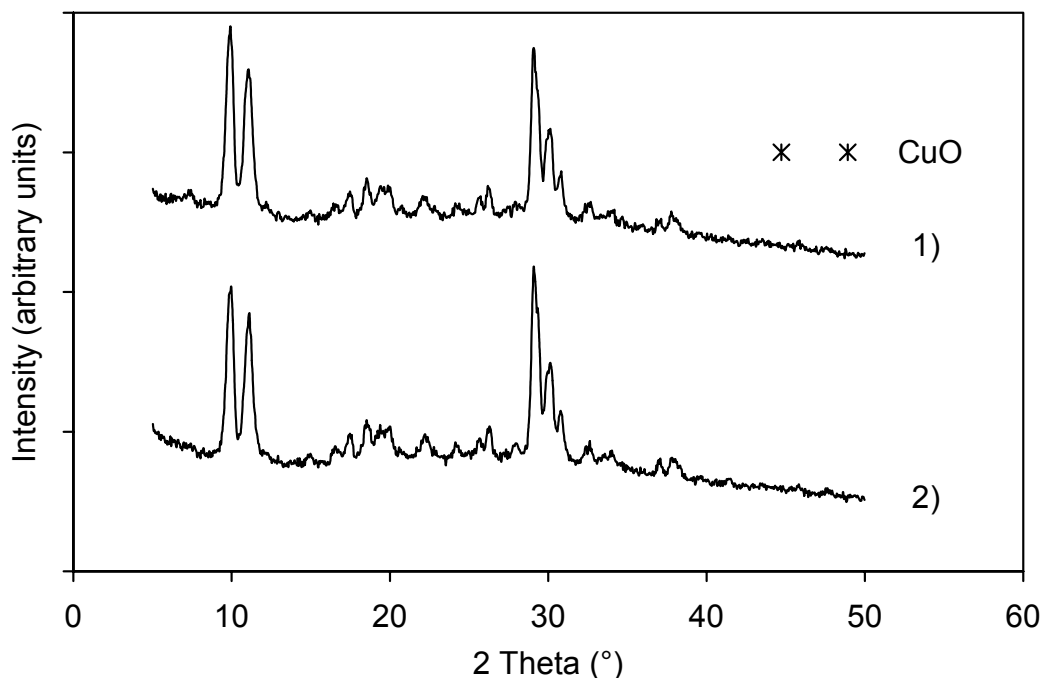


Figure 4-1. XRD patterns of Cu-ZSM-5: 1) after calcination at $550\text{ }^\circ\text{C}$ (fresh sample), 2) after NO_x adsorption experiments (used sample). The asterisk denotes the positions where CuO reflections would be expected.

4.2.3 Adsorption tests

Adsorption tests

The experimental setup used for these tests has been described in details in chapter 3. Adsorption tests were performed with 3 g Cu-ZSM-5 (particle size 0.2 - 2 mm) held between two quartz wool plugs in a tubular reactor (inner diameter 28 mm). The overall gas flow rate was $300\text{ l}_\text{N}/\text{h}$, yielding a space velocity of $50\text{ }000\text{ h}^{-1}$. Two different base feeds were used, referred to as “dry base feed” and “humid base feed”. The “dry base feed” contained 10 % O_2 with balance N_2 . The “humid base feed” contained 5 % H_2O and 10 % O_2 with balance N_2 . Prior to each NO_x adsorption test, the sample was

pretreated at 450 °C for ten minutes in the base feed. The sample was then cooled to the starting temperature of the adsorption experiment.

Tests procedures

The combined adsorption-desorption tests included the following steps:

- 1) adsorption of NO_x with various concentrations of NO and NO₂ in the appropriate base feed for an hour,
- 2) equilibration in the base feed at the temperature of adsorption during 20 minutes in order to remove the weakly adsorbed species,
- 3) temperature programmed desorption starting at the adsorption temperature and heating up at a rate of 8 °C/min to 450 °C.

Experiments with NO present during the desorption included the following steps:

- 1) adsorption of 500 ppm NO₂ in the humid base feed for 1 hour,
- 2) equilibration at the temperature of adsorption without NO₂ in the feed during five minutes,
- 3) desorption in the presence of 500 ppm NO at the temperature of adsorption for 15 minutes, and finally
- 4) temperature programmed desorption from the temperature of adsorption up to 450 °C (8 °C/min) with 500 ppm NO permanently present in the feed.

4.3 Results

4.3.1 Adsorption and oxidation of NO in dry and humid base feeds

In a first experiment, the adsorption of NO on Cu-ZSM-5 has been investigated in the absence of water. Figure 4-2 shows the adsorption of 1000 ppm NO at 200 °C in the dry base feed, followed by temperature programmed desorption. At the beginning of the adsorption period, the concentration of NO behind catalyst increased slowly reaching a steady state after 10 minutes. When the feed of NO had been stopped, no desorption of weakly bound species could be detected. During the subsequent TPD, only NO₂ could be detected at the reactor outlet with a maximum of desorption at 380 °C. A small peak of NO was observed at high temperatures, between 370 °C and 410 °C.

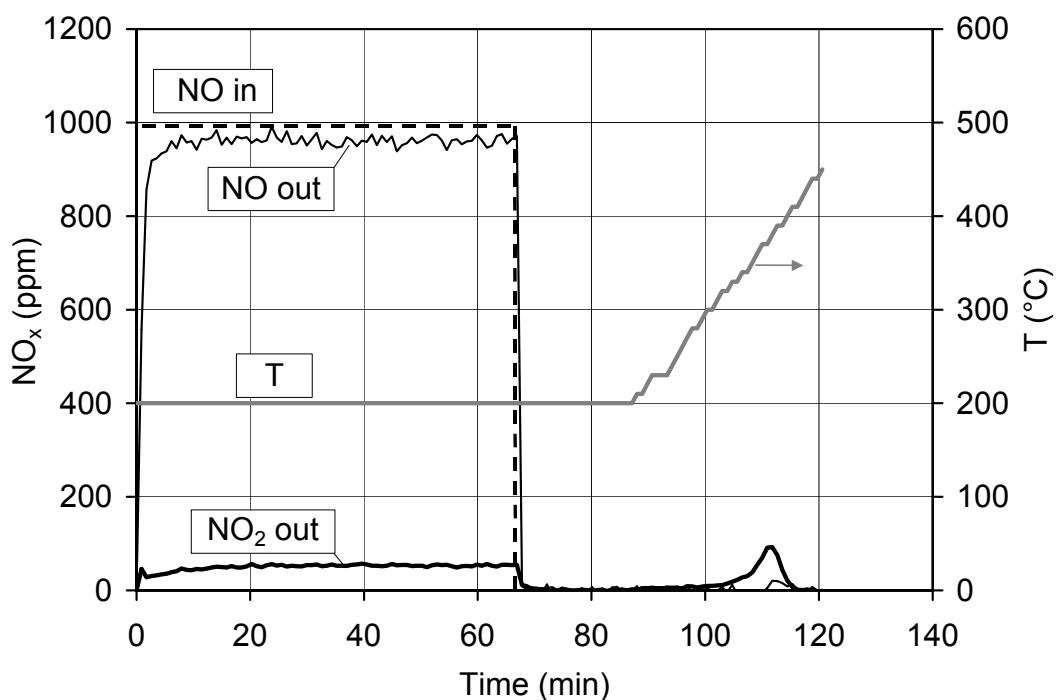


Figure 4-2: Adsorption of NO (1000 ppm) on Cu-ZSM-5 at 200 °C in a dry feed, followed by TPD. Space velocity: 50 000 h⁻¹. Base feed: 10 % O₂, and balance N₂.

This experiment has been repeated with the humid feed, i.e. in the presence of 5 % H_2O . During the TPD, no release of NO or NO_2 could be measured. This suggests that NO was not adsorbed in the presence of H_2O .

It is discernible from Figure 4-2 that the catalyst Cu-ZSM-5 was capable to oxidize NO to NO_2 during the adsorption of NO at 200 °C in the dry base feed. The conversion was about 5 % at steady state. The influence of temperature and water on the conversion of 1000 ppm NO was investigated in the temperature range 200-450 °C (Figure 4-3). The conversion reached a maximum value at 375 °C in both dry and humid conditions. However, water strongly inhibited the oxidation of NO. At temperatures below 250 °C, the conversion in the presence of H_2O became negligible. Additional experiments (not reported in this paper) proved that the inhibiting effect by water was reversible.

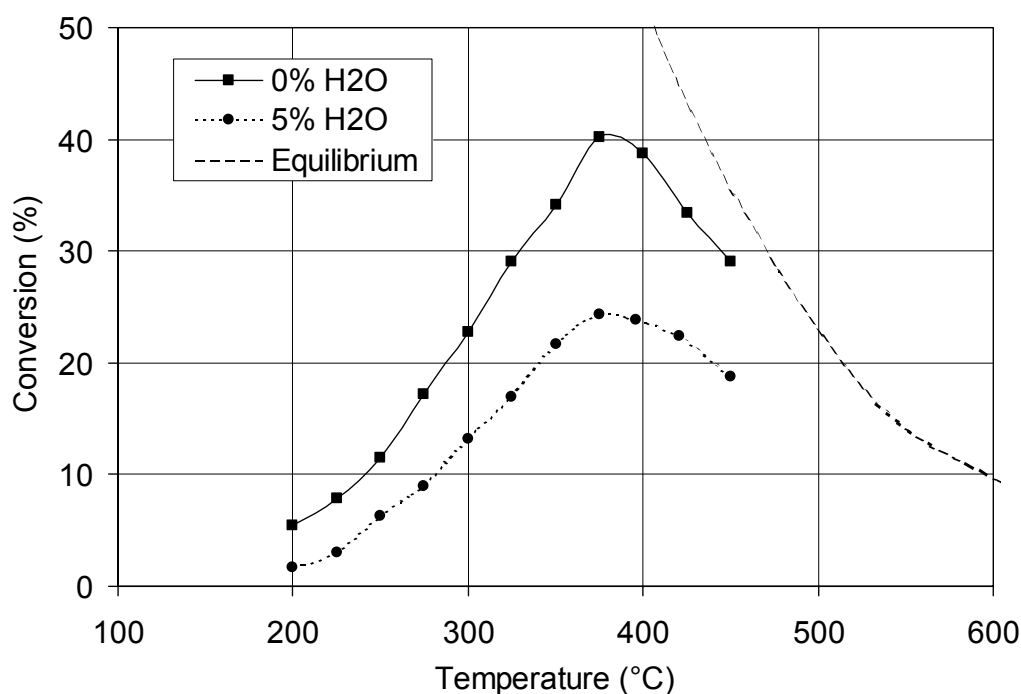


Figure 4-3: Influence of H_2O on the oxidation of 1000 ppm NO over Cu-ZSM-5. Space velocity: 50 000 h^{-1} . Base feed: 10 % O_2 , 0 - 5 % H_2O , and balance N_2 .

4.3.2 Adsorption of NO₂ in dry and humid base feeds

The adsorption capacity of Cu-ZSM-5 was investigated with NO₂ in the two base feeds. Figure 4-4 shows the adsorption of 500 ppm NO₂ in the dry base feed at 200 °C, followed by temperature programmed desorption. During the first twenty minutes of adsorption, the concentration of NO₂ behind the catalyst increased slowly accompanied with the simultaneous release of NO, which was obviously formed during the adsorption of NO₂. The quantitative determination of NO₂ adsorbed and NO released during the adsorption yields a ratio of 1.31 mole NO produced per 3 moles NO₂ adsorbed (Table 4-1, test 1). During the TPD, only NO₂ could be detected with a maximum desorption rate at 380 °C. Above 400 °C, a small peak of NO was observed due to its higher thermodynamic stability in this temperature regime. Table 4-1 gives the amount of NO_x released during the temperature programmed desorption (test 1). The NO₂ storage capacity corresponds to the total molar amount of NO and NO₂ desorbed during TPD.

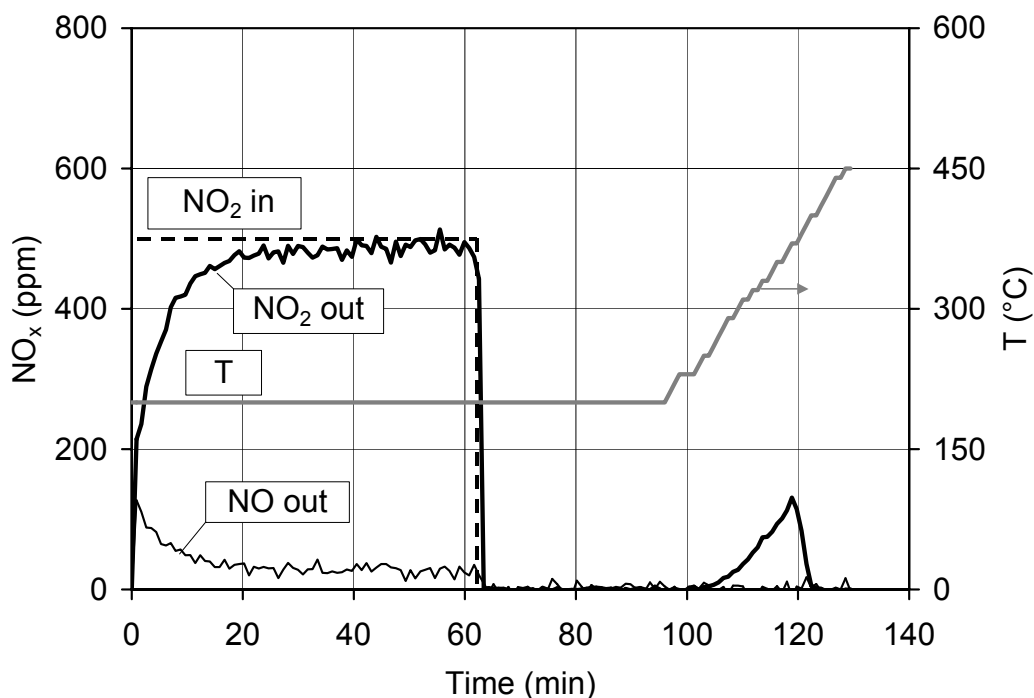


Figure 4-4: Adsorption of NO₂ (500 ppm) on Cu-ZSM-5 at 200 °C in a dry feed, followed by TPD. Space velocity: 50 000 h⁻¹. Base feed: 10 % O₂, and balance N₂.

The adsorption of 500 ppm NO₂ was repeated in the humid base feed (Table 4-1, test 2). The adsorption behavior of NO₂ is similar to that in the dry base feed. NO was also released during the adsorption of NO₂, the molar ratio NO₂:NO amounting to 3 : 1.12. In the presence of 5 % H₂O, the NO₂ adsorption capacity amounted to 78 µmol NO_x per gram Cu-ZSM-5 (test 2), compared to 116 µmol/g in the absence of H₂O (test 1). Therefore, water has an inhibiting effect on the adsorption of NO₂.

Table 4-1: Influence of H₂O and NO on the adsorption of NO₂ at 200 °C on Cu-ZSM-5. Sample weight = 3.0 g. Space velocity: 50 000 h⁻¹. Base feed: 10 % O₂, and balance N₂. Desorption by TPD from 200 to 450 °C.

Test No.	Adsorption						TPD	
	NO _{in} (ppm)	NO _{2,in} (ppm)	H ₂ O (%)	NO _{2,adsorbed} (µmol/g _{cat.})	NO _{produced} (µmol/g _{cat.})	NO _{2,adsorbed} : NO _{produced}	NO _{x,desorbed} (µmol/g _{cat.})	NO _{2,adsorbed} : NO _{x,desorbed}
1	-	500	-	165	72	3 : 1.31	116	3 : 2.11
2	-	500	5	139	52	3 : 1.12	78	3 : 1.68
3	500	500	-	102	27	3 : 0.79	86	3 : 2.53
4	500	500	5	84	31	3 : 1.10	56	3 : 2.00
5	1000	500	5	71	25	3 : 1.06	43	3 : 1.81

4.3.3 Influence of NO on the adsorption of NO₂

In order to get a better understanding of the adsorption of NO₂, the influence of NO on the adsorption process was investigated. These experiments have been carried out at 200 °C. The first test was performed using the dry base feed with 500 ppm each of NO₂ and NO. Test 3 in Table 4-1 shows the amount of NO_x released during the subsequent temperature programmed desorption. Comparing this amount with test 1 suggests that the presence of NO lowered the adsorption of NO₂ significantly.

Test 4 in Table 4-1 shows the analogous test result for the humid base feed. The amount of NO₂ released during the TPD was smaller if water was present in the feed. The influence of a higher concentration of NO, i.e. 1000 ppm NO, in the humid base

feed was also investigated and is given by test 5. The higher NO concentration resulted in a further decrease of the NO₂ adsorption. Summarizing, both H₂O and NO inhibit the adsorption of NO₂.

All experiments exhibited an increase in the NO outlet concentration during the first minutes of the NO₂ adsorption period. The NO production corresponded, on average, roughly to a ratio of one mole NO for 3 moles of NO₂ adsorbed.

4.3.4 Effect of temperature on the adsorption of an equimolar mixture of NO and NO₂

The effect of temperature on the adsorption of the equimolar mixture (500 ppm each of NO and NO₂) in the humid base feed was investigated. Figure 4-5 shows the amount of NO_x (mainly NO₂) desorbed during the TPD after adsorption at various temperatures. As expected, increasing adsorption temperatures yield decreasing adsorption capacities. Adsorbed NO_x-species on Cu-ZSM-5 were thermally stable up to 380 °C in the humid base feed. Above T > 400 °C, the adsorption of NO₂ is no longer possible.

Another type of experiment to study the influence of temperature on NO₂ adsorption is reported in Figure 4-6. First, the humid base feed was fed to the catalyst sample at 100 °C. Subsequently, 500 ppm NO and 500 ppm NO₂ were added and simultaneously, the sample was heated at a rate of 8 °C/min to a final temperature of 450 °C.

Between 100 °C and 225 °C, the adsorption of NO₂ may be observed accompanied with the simultaneous release of NO (roughly 1 additional mole of NO released per 3 moles of NO₂ adsorbed). Therefore, the efflux concentrations of NO were clearly higher than 500 ppm NO.

Between 225 °C and 400 °C, the concentrations of NO₂ clearly exceed the input concentration of 500 ppm, suggesting the decomposition of adsorbed NO_x-species or the oxidation of NO. However, due to the fact that the NO_x concentration also exceeds the input concentration (1000 ppm) in a similar way, the peak of NO₂ must be attributed to the decomposition of adsorbed NO_x-species.

The maximum concentration of NO_2 was observed at 310 °C, a definitely lower temperature compared to the temperature of desorption in the absence of NO (380 °C). At temperatures above 400 °C the sum of the concentrations of NO + NO_2 corresponds again to the total input concentration of NO_x (1000 ppm). The increasing NO fraction at these high temperatures is due to the increasing thermodynamic stability of NO at high temperatures.

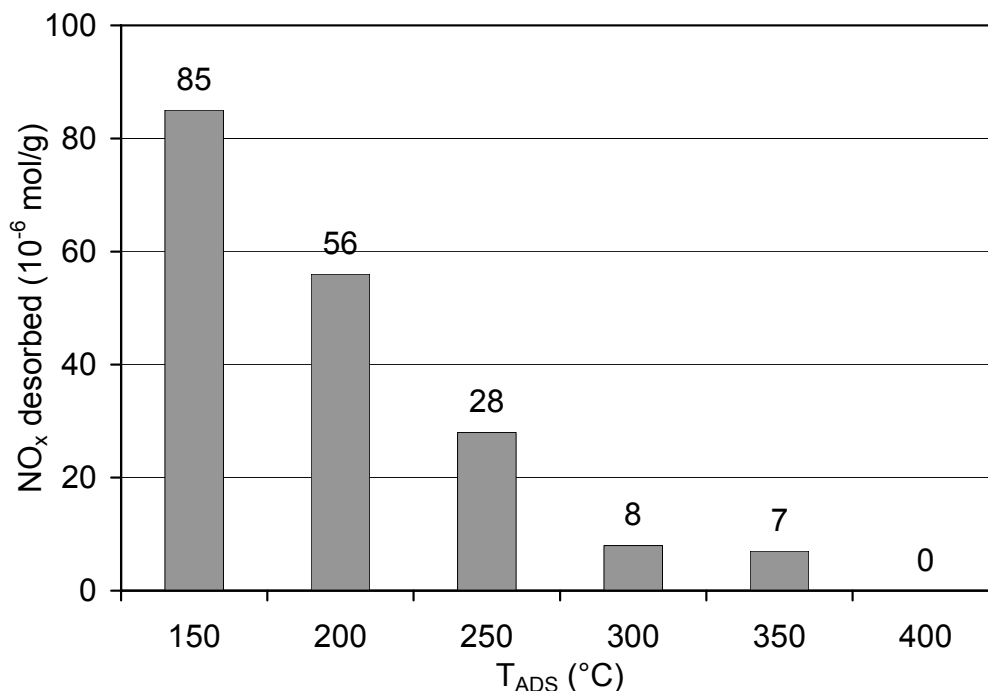


Figure 4-5: Influence of temperature on the adsorption of an equimolar mixture of NO and NO_2 on Cu-ZSM-5. Space velocity: 50 000 h^{-1} . During adsorption, $\text{NO}_{2\text{ in}} = \text{NO}_{\text{in}} = 500$ ppm. Base feed: 10 % O_2 , 5 % H_2O , and balance N_2 .

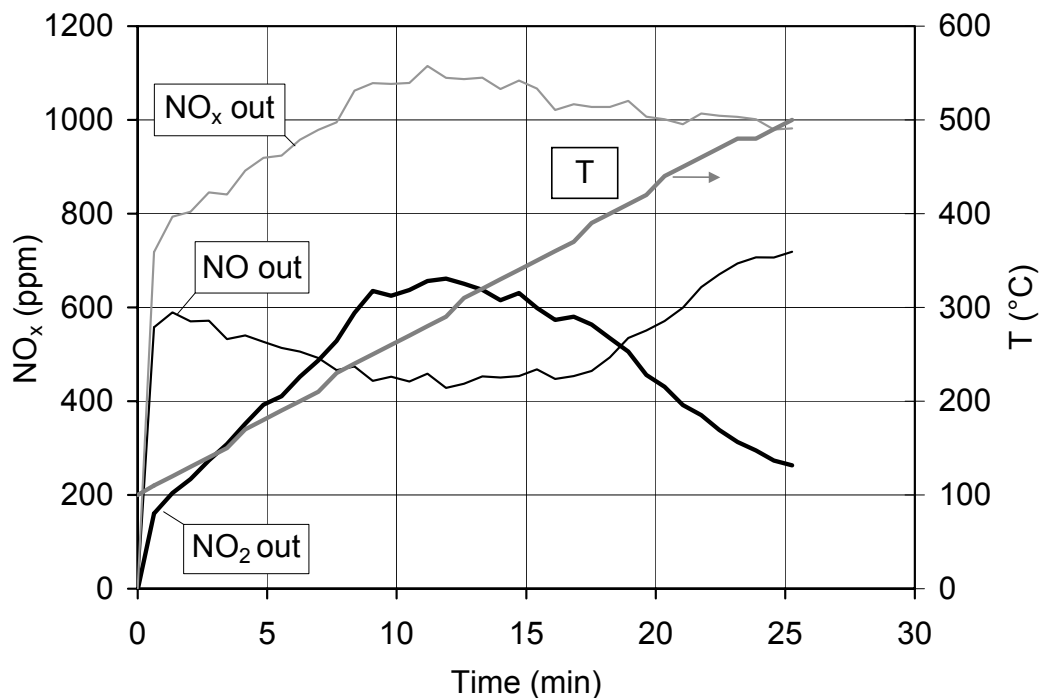


Figure 4-6: Temperature programmed adsorption of NO_x on Cu-ZSM-5. Space velocity: $50\,000\text{ h}^{-1}$. Heating rate: $8\text{ }^\circ\text{C/min}$. Feed: $\text{NO}_2\text{ in} = \text{NO in} = 500\text{ ppm}$, $10\text{ }\%$ O_2 , $5\text{ }\%$ H_2O , and balance N_2 .

4.3.5 Influence of NO on the desorption of adsorbed NO_x -species

The effect of NO on the adsorbed species was further investigated at $150\text{ }^\circ\text{C}$ and $200\text{ }^\circ\text{C}$. In this experiment, Cu-ZSM-5 was first loaded at $150\text{ }^\circ\text{C}$ with 500 ppm NO_2 in the humid base feed for one hour. After the adsorption, the sample was stabilized in the humid base feed for 20 minutes. Subsequently, 500 ppm NO were added to the feed keeping the temperature at $150\text{ }^\circ\text{C}$. Figure 4-7 shows that considerable amounts of NO_2 are already desorbed without heating, while a decrease of NO is observed. The temperature of the sample was kept at $150\text{ }^\circ\text{C}$ until a constant low concentration of NO_2 was observed ($\approx 20\text{ ppm NO}_2$). Finally, the temperature was raised, and another production peak of NO_2 and a consumption peak of NO were observed. However, these amounts were about equal. The experiment was repeated at a higher adsorption temperature of $200\text{ }^\circ\text{C}$, and showed analogous results.

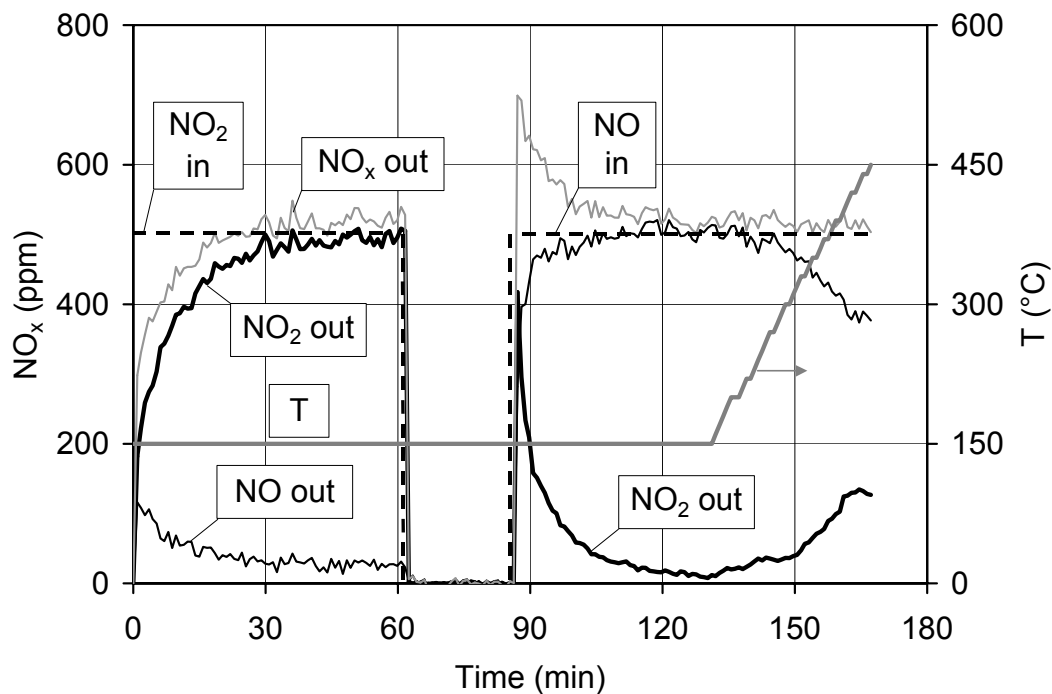


Figure 4-7: Adsorption of NO_2 (500 ppm) on Cu-ZSM-5 at 150 °C in a humid feed, followed by TPD in the presence of 500 ppm NO. Space velocity: 50 000 h^{-1} . Base feed: 5 % H_2O , 10 % O_2 , and balance N_2 .

In conclusion, NO reacts with adsorbed NO_x -species under formation of NO_2 . At a temperature of 150 °C, the reaction of NO with the adsorbed species was completed in 35 minutes. At 200 °C, the reaction was faster and required only 20 minutes. The molar ratio between NO reacted and NO_2 released is approximately 1 : 3. During the subsequent temperature programmed desorption in the presence of NO, the total NO_x concentration at the outlet remained constant, suggesting that practically no further desorption occurred during this TPD. Therefore, the formation of NO_2 observed during the subsequent TPD must be attributed to the oxidation of NO to NO_2 over Cu-ZSM-5, similar to the experiment reported in section 3.1.

4.4 Discussion

4.4.1 Adsorption of NO on Cu-ZSM-5

At 200 °C, an adsorption of NO on Cu-ZSM-5 from dry or humid feeds could not be observed. On the other hand, NO₂ may be adsorbed over a wide temperature range from both dry and humid feeds. Therefore, in order to obtain adsorption of NO, it must first be oxidized to NO₂. This reaction is sufficiently fast with a dry feed on Cu-ZSM-5 at temperatures above 200 °C, but is inhibited by water in the feed (Figure 4-3). Therefore, water in the feed also impedes the storage of NO on these catalysts.

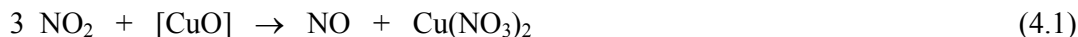
The results suggest that the sites for NO oxidation and for H₂O adsorption are probably competing with each other. Wang et al. [13] have described a similar effect for the adsorption of NO on H-type mordenite. The catalyst used in our study was an over-exchanged zeolite. Under oxidizing conditions, such catalysts tend to form species containing extra-lattice oxygen. Nevertheless, these species do not represent crystalline copper oxide as evidenced by X-ray diffraction. These findings are supported by Yan et al. [14] who reported the formation of [Cu-O-Cu]²⁺ species and by Pârvulescu et al. [15] who suggested the formation of asymmetric dimers [Cu⁺-O-Cu²⁺] on the basis of XPS measurements. The formation of such bridging oxygen between two Fe³⁺ in iron-exchanged zeolites has also been claimed by Boudart et al. [16]. Oxygen bound in this manner could be used to oxidize CO according to Fu et al. [17]. Therefore, we assume that this extra-lattice oxygen is also involved in the oxidation of NO.

4.4.2 Adsorption of NO₂ on Cu-ZSM-5 and desorption of the adsorbed species

Mechanism of adsorption

The adsorption experiments show the simultaneous formation of NO during the adsorption of NO₂, as may be seen e.g. in Figure 4-4. The molar ratio NO_{2,adsorbed} : NO_{produced} during the adsorption implies the disproportionation of NO₂ into gaseous NO and adsorbed NO_x-species. An infrared study of the adsorbed species showed the formation of nitrate species above 180 °C [11]. The formation of nitrates has also been reported for the adsorption of NO₂ on barium exchanged Y zeolites [8]. Therefore, it is

very likely that the adsorbed species formed during adsorption are nitrates bound to copper cations, and we propose the following reaction for the adsorption reaction:



The species $[\text{CuO}]$ would represent half of the dimer species involved in the over-exchanged zeolites.

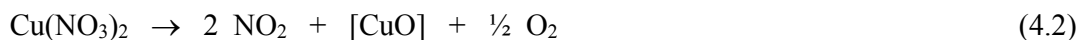
Influence of water on the adsorption of NO_2

The presence of 5 % water in the feed decreases the amount of NO_2 adsorbed on Cu-ZSM-5 considerably (Table 4-1). The influence of water is reversible as it is in the oxidation of NO. An inhibiting effect of water on the catalytic activity of Cu-ZSM-5 was also observed in the reduction of NO to N_2 with hydrocarbons (e.g. [18]).

In order to investigate the adsorption of water on Cu-ZSM-5, Ganemi et al. [19] carried out thermogravimetric experiments, which revealed the loss of two molecules of water per copper ion in the temperature range 100-300 °C. The reversible deactivation of the sample by water suggests a weak adsorption of the water molecules, probably by the formation of hydrogen bonds with the copper cluster and the zeolite framework. This weakly adsorbed water may block a part of the adsorption sites for NO_2 , thus lowering the amount of NO_2 adsorbed on Cu-ZSM-5.

Mechanism of desorption

The temperature programmed desorption allowed the complete desorption of the adsorbed NO_x -species by heating up to 450 °C. Among the possible nitrogen-containing molecules, only NO_2 could be observed in the exhaust gas, except above 400 °C when NO becomes thermodynamically more stable. Combining this result with the findings of the infrared investigations of the nitrates on the Cu-ZSM-5 surface, the following overall reaction is proposed for the desorption process:



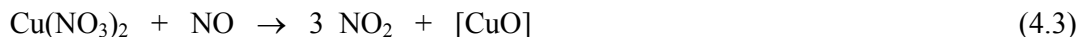
The decomposition of the nitrate species occurs at high temperatures. Under the conditions used in our experiments, the maximum desorption was observed at 380 °C,

suggesting a high thermal stability of the adsorbed species. This high stability enables the adsorption of NO₂ under isothermal conditions up to 350 °C. The decomposition of the adsorbed species by heating permits the complete restoration of the adsorption sites. This behavior was observed whatever the water content of the feed gas (dry or humid feeds).

The formation of oxygen during desorption could not be shown directly in our experiments due to basic analytical limitations. However, the TPD experiments up to 450 °C demonstrated the complete regeneration of the adsorption sites, which we assume to be [CuO]. Thus, oxygen must have been produced in parallel with NO₂.

Influence of NO on the desorption

As shown in Figure 4-7, the desorption of NO₂ is accompanied with a consumption of NO, the molar ratio amounting to 3:1. Therefore, the decomposition of the nitrates in the presence of NO can be best described by the following equation:



This equation corresponds to the back reaction of the disproportionation reaction (4.1). In reaction (4.3), the adsorbed nitrate species play the role of the oxidizer, and NO the role of the reducing agent. As a result, the high reactivity of NO with nitrates at low temperatures has a strong influence on the stability of the nitrates formed during the adsorption of NO₂. If the feed contains both NO and NO₂ during the adsorption (tests 3, 4 and 5), NO₂ will adsorb on Cu-ZSM-5 and form nitrates, but at the same time NO will react with them. Therefore, a steady state between the formation of nitrates and their reaction with NO will be established thus limiting the amount of adsorbed NO₂. The reduced stability of the nitrates in the presence of NO is also reflected by the lower temperature, at which the maximum decomposition rate is observed during the temperature programmed adsorption experiment (Figure 4-6). This temperature was ≈380°C in the absence of NO (Figure 4-2), but ≈310°C in the presence of NO (Figure 4-6).

4.5 Conclusions

NO cannot be adsorbed on Cu-ZSM-5 at 200 °C. However, after its oxidation to NO₂, an adsorption becomes possible. Due to the fact that water in the exhaust gas inhibits the oxidation reaction, water hinders the interaction of NO with Cu-ZSM-5.

Nitrogen dioxide can be adsorbed over a wide temperature range from both dry and humid feeds. This adsorption involves a disproportionation reaction yielding two adsorbed nitrate species and one molecule of NO released to the gas phase. Water as well as NO lowers the adsorption of NO₂ on Cu-ZSM-5 significantly. The negative effect of NO is due to its reaction with the adsorbed nitrates, a comproportionation reaction shifting the equilibrium back to NO₂. The presence of NO allows the complete desorption of the nitrates at temperatures as low as 150 °C instead of 300-400 °C. This effect may be used to desorb adsorbed nitrates at a much lower temperature than their normal decomposition temperature.

4.6 References

- [1] B. Krutzsch, G. Wenninger, M. Weibel, P. Stapf, A. Funk, D.E. Webster, E. Chaize, B. Kasemo, J. Martens, A. Kiennemann, SAE paper 982592 (1998)
- [2] H. Arai and M. Machida, *Catal. Today* **22** (1994), 97
- [3] R. Bélanger and J.B. Moffat, *J. Catal.* **152** (1995), 179
- [4] N. Chen and R.T. Yang, *J. Catal.* **157** (1995), 76
- [5] Y. Traa, B. Burger and J. Weitkamp, *Microp. Mesop. Mater.* **30** (1999), 3
- [6] L. Musmann, D. Lindner, R. van Yperen, E. Lox and T. Kreuzer, U.S. Patent 6,080,375 (2000), Assignee: Degussa Aktiengesellschaft
- [7] E. Chaize, D.E. Webster, B. Krutzsch, G. Wenninger, M. Weibel, Sh. Hodjati, C. Petit, V. Pitchon, A. Kiennemann, R. Loenders, O. Monticelli, P.A. Jacobs, J.A. Martens and B. Kasemo, SAE paper 982593 (1998)
- [8] O. Monticelli, R. Loenders, P.A. Jacobs and J.A. Martens, *Appl. Catal. B* **21** (1999), 215
- [9] J.R. Pearce, D.E. Sherwood, M.B. Hall and J.H. Lunsford, *J. Phys. Chem.* **84** (1980), 3215

- [10] L.M. Aparicio, W.K. Hall, S.M. Fang, M.A. Ulla, W.S. Millman and J.A. Dumesic, *J. Catal.* **108** (1987), 233
- [11] K. Hadjiivanov, D. Klissurski, G. Ramis and G. Busca, *Appl. Catal. B* **7** (1996), 251
- [12] C. Yokoyama and M. Misono, *J. Catal.* **150** (1994), 9
- [13] Z.M. Wang, T. Arai and M. Kumagai, *Ind. Eng. Chem. Res.* **40** (2001), 1864
- [14] J.Y. Yan, W.M.H. Sachtler and H.H. Kung, *Catal. Today* **33** (1997), 279
- [15] V.I. Pârvulescu, P. Oelker, P. Grange and B. Delmon, *Appl. Catal. B* **16** (1998), 1
- [16] M. Boudart, R.L. Garten and W.N. Delgass, *J. Phys. Chem.* **73** (1969), 2970
- [17] C.M. Fu, M. Deeba and W.K. Hall, *Ind. Eng. Chem. Prod. Res. Dev.* **19** (1980), 299
- [18] X. Feng and W.K. Hall, *J. Catal.* **166** (1997), 368
- [19] B. Ganemi, E. Björnbom, B. Demirel and J. Paul, *Micropor. Mesopor. Mater.* **38** (2000), 287

Adsorption and desorption of NO and NO₂ on BaO/TiO₂

5.1 Introduction

Since the pioneering work of Takahashi et al. [1] reporting on a novel NO_x storage catalyst, many investigations have been performed to understand the mechanism of adsorption and desorption of nitrogen oxides on supported barium oxide. The mechanisms proposed in the literature have been summarized in chapter 2.

It has been shown in chapter 4 that the adsorption of nitrogen dioxide on Cu-ZSM-5 involves a disproportionation reaction of NO₂ into adsorbed nitrate species and NO released to the gas phase. The aim of this study is to investigate the behavior of supported BaO during the adsorption of NO₂.

Furthermore, whereas the influence of CO₂ on the adsorption and desorption processes is quite well understood, little is known about the influence of NO. In chapter 4, we have shown that nitrogen monoxide can react with nitrate species formed on Cu-ZSM-5 at low temperatures, i.e. in the temperature range between 150 °C and 200 °C [2]. Due to the fact that NO can be present in the gas phase, the present study considers also the effect of NO on nitrate species formed on a model NO_x storage catalyst consisting of BaO/TiO₂. The adsorption of NO_x was studied at 200 °C with either pure NO₂ or a mixture of NO₂ + NO. The desorption of the adsorbed species was investi-

gated by temperature programmed desorption in various feeds. On the basis of these experimental results, a model is proposed to describe the adsorption and desorption processes occurring on NO_x storage catalysts.

5.2 Experimental

5.2.1 Sample preparation

BaO/TiO₂ (BaO loading: 11 wt.-%) was prepared by wet impregnation. 3.5 mL of deionized water was added under stirring to 4.5 g of the supporting oxide (DT51, Rhone-Poulenc, anatase modification, 90 m²/g). 10 mL of an aqueous solution containing 0.96 g of barium nitrate (Ba(NO₃)₂, Fluka, puriss. p.a.), was mixed with the paste and stirred for two hours at room temperature. After evaporating the solvent at \approx 100 °C, the sample was dried at 120 °C overnight, and finally calcined in air at 600 °C for one hour. A fraction with particle sizes between 0.2 and 2 mm was obtained by crushing and sieving.

The sample consisting of pure TiO₂ was prepared by suspending DT51 in deionized water. The resulting paste was dried at 120 °C overnight. After crushing, a fraction between 0.2 and 2 mm was again obtained by sieving. The material was finally calcined at 600 °C for one hour.

5.2.2 Sorption experiments

The experimental setup has been described in details in chapter 3. The experiments were performed using 3.0 g of the sample consisting of either BaO/TiO₂ or TiO₂, held between quartz wool plugs. The gas flow rate was 300 L_N/h, corresponding to an approximate gas hourly space velocity of 50 000 h⁻¹. All experiments were carried out in a humid gas feed with 5 % H₂O. The adsorption of NO₂ or of the mixture NO-NO₂ was performed at 200 °C, using a feed containing 10 % O₂, 5 % H₂O, and balance N₂ (referred to in the following as "base feed"). The desorption of adsorbed NO_x species was subsequently studied by TPD from 200 °C to 530 °C at a heating rate of 8 °C/min.

Various feeds were applied during the desorption experiments and these are summarized in Table 5-1.

5.2.3 X-ray diffraction analysis

The samples were characterized by means of powder X-ray diffraction on a Philips X'Pert - MPD diffractometer using Cu K α radiation at 1.54056 nm. The scans were recorded continuously in the range of 2θ between 10° and 80° , with a step width of 0.05° and a measuring time of 5 seconds per step.

5.3 Results

5.3.1 Adsorption

Adsorption of pure NO₂ (test 1):

The results for test 1 on BaO/TiO₂ with 500 ppm NO₂ in the base feed are shown in Figure 5-1. It is evident that the adsorption of NO₂ is accompanied by a simultaneous formation of NO. The amounts of NO₂ adsorbed and NO formed during adsorption, as well as the amount of NO_x desorbed during TPD have been quantified. The molar ratio NO_{2,adsorbed} : NO_{produced} was equal to 3 : 1.11, and the ratio NO_{2,adsorbed} : NO_{x,produced} was 3 : 2.22.

Figure 5-2 shows the XRD patterns of the sample BaO/TiO₂ as prepared, and the sample after NO₂ adsorption. The peaks of TiO₂ (anatase phase) could be identified on both samples. On both XRD patterns, peaks at 2θ of 45.075° and 56.125° were found, which were attributed to barium titanium oxide BaTiO₃. This phase was probably formed during the calcination at 600 °C. A new crystalline phase appeared after adsorption of NO₂ at 200 °C. The peak at a 2θ of 18.925° allowed the identification of the new phase as barium nitrate on the basis of JCPDS data.

Table 5-1: Adsorption/desorption experiments. GHSV = 50 000 h⁻¹. Adsorption base feed: 10 % O₂, 500 ppm NO₂, 5 % H₂O, and balance N₂. Temperature during adsorption = 200 °C. TPD base feed: 5 % H₂O, and balance N₂. Temperature during TPD = 200 - 530 °C at 8 °C/min.

Test No.	Sample	Adsorption				TPD								
		NO _{in} (ppm)	NO _{2,adsorbed} (μmol/g _{cat})	NO _{produced} (μmol/g _{cat})	NO _{2,adsorbed} : NO _{produced}	O _{2,in} (%)	NO _{in} (ppm)	CO _{in} (ppm)	NO _{consumed} (μmol/g _{cat})	NO _{produced} (μmol/g _{cat})	NO _{2, produced} (μmol/g _{cat})	NO _{x, produced} (μmol/g _{cat})	NO _{2,produced} : NO _{consumed}	NO _{2,adsorbed} : NO _{x,produced}
1	BaO/TiO ₂	-	401	148	3 : 1.11	10	-	-		60 (20 %)	229 (80 %)	289		3 : 2.22
1a	TiO ₂	-	190	73	3 : 1.15									
2	BaO/TiO ₂	500	309	87	3 : 0.84	10	-	-		45 (21 %)	176 (79 %)	222		3 : 2.15
3	BaO/TiO ₂	-	421	144	3 : 1.03	-	-	-		80 (25 %)	227 (75 %)	307		3 : 2.19
4	BaO/TiO ₂	-	382	154	3 : 1.21	-	-	500		117 (40%)	183 (60 %)	300		3 : 2.36
5	BaO/TiO ₂	-	395	150	3 : 1.14	-	500	-	143	^{a)}	406	406	3 : 1.06	3 : 3.08
5a	TiO ₂	-	205	77	3 : 1.13	-	500	-	106	^{a)}	217	217	3 : 1.47	3 : 3.18

^{a)} not determined.

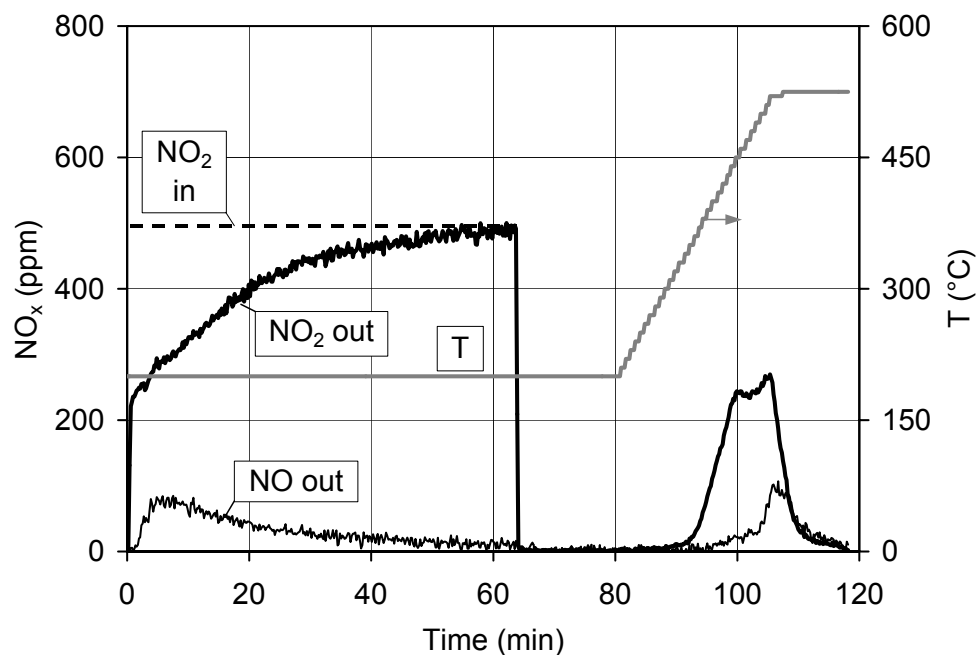


Figure 5-1: Test 1. Adsorption of NO_2 (500 ppm) on BaO/TiO_2 at 200 °C, followed by TPD. Base feed: 10 % O_2 , 5 % H_2O , and balance N_2 .

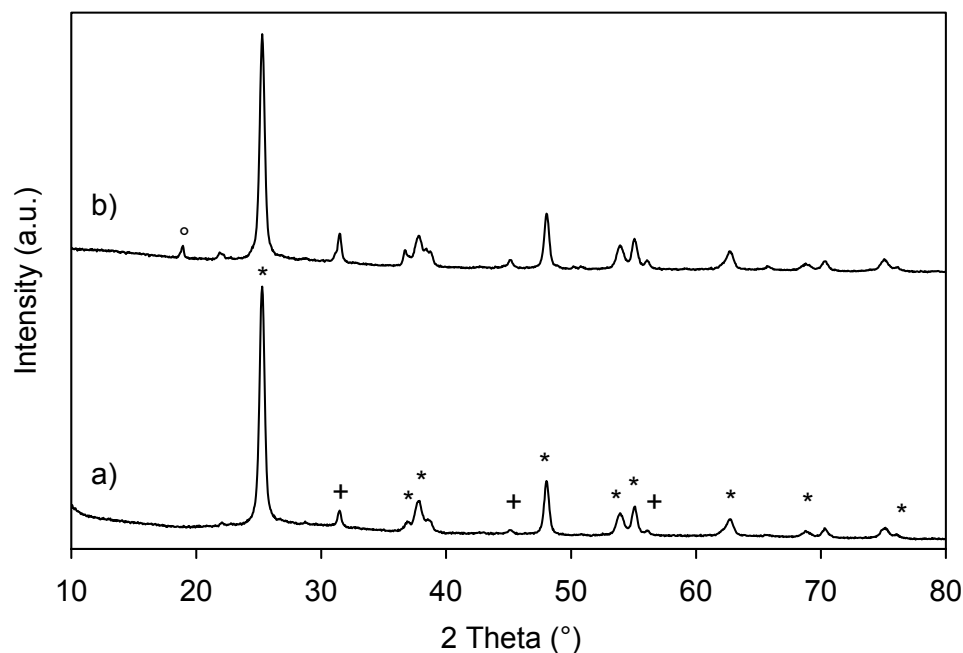


Figure 5-2: XRD patterns of BaO/TiO_2 a) after calcination at 600 °C (sample as prepared), and b) after NO_2 adsorption at 200 °C. (*) TiO_2 anatase, (+) BaTiO_3 and (°) $\text{Ba}(\text{NO}_3)_2$.

The experiment was repeated with the sample consisting of pure TiO_2 (test 1a) and the results are shown in Figure 5-3. The formation of NO was again observed during the adsorption of NO_2 , the molar ratio $\text{NO}_{2,\text{adsorbed}} : \text{NO}_{\text{produced}}$ being 3 : 1.15. The TPD yielded not only NO_2 , but also nitric acid. Their sum amounts to $117 \mu\text{mol/g}_{\text{cat}}$, which corresponds to $\approx 2/3$ of the NO_2 adsorbed.

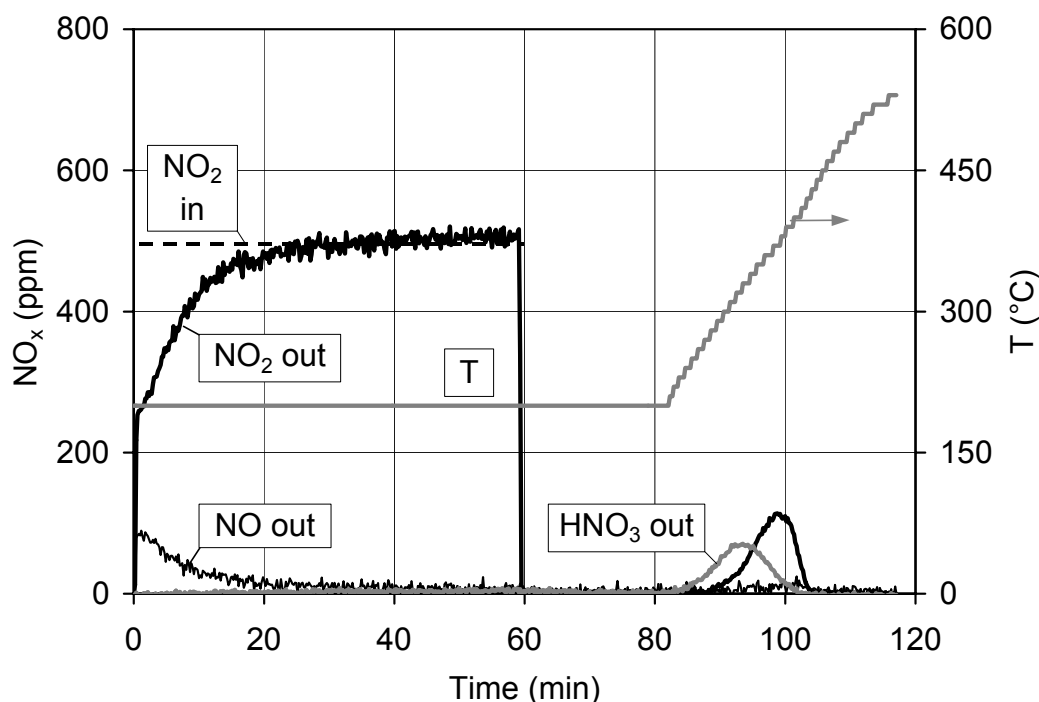


Figure 5-3: Test 1a. Adsorption of NO_2 (500 ppm) on TiO_2 at 200°C , followed by TPD. Base feed: 10 % O_2 , 5 % H_2O , and balance N_2 .

Adsorption of equimolar NO + NO₂ (test 2):

An experiment was made with 500 ppm each of NO_2 and NO using BaO/TiO_2 as the sorbent (test 2). Figure 5-4 shows the concentrations of NO and NO_2 during adsorption and desorption. Due to the fact that the NO concentration behind catalyst is higher than the feed concentration of 500 ppm, the adsorption of NO_2 is again accompanied by the formation of NO. However, the presence of NO lowers the amounts of NO_2 adsorbed and NO formed. These amounts were 401 and $148 \mu\text{mol/g}_{\text{cat}}$ for test 1, but only 309 and $87 \mu\text{mol/g}_{\text{cat}}$ in test 2.

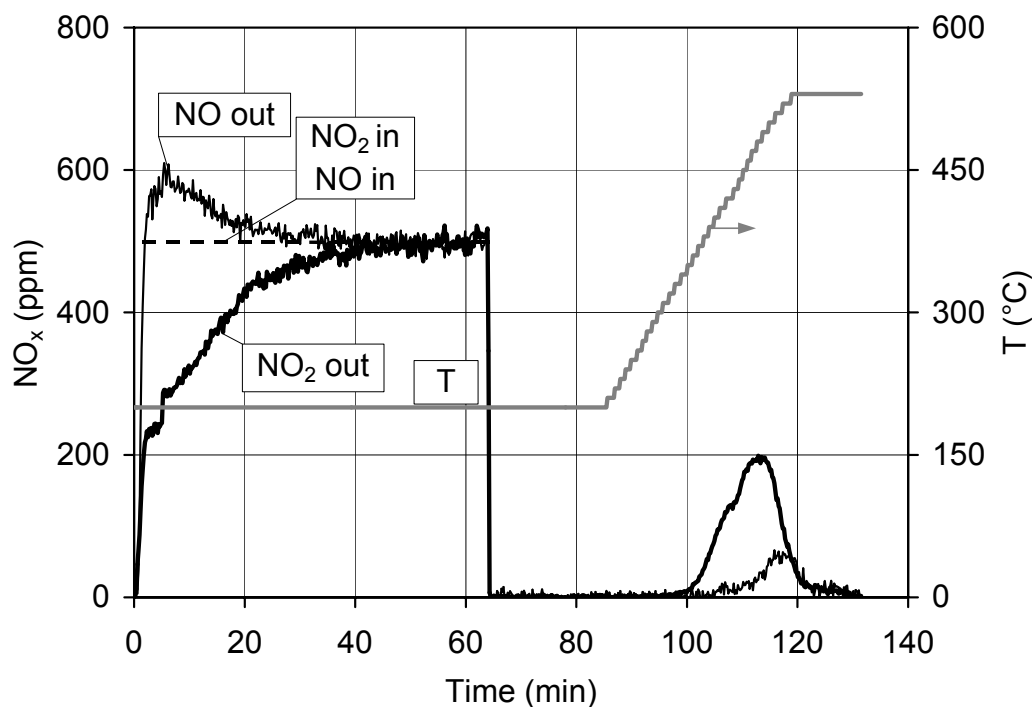


Figure 5-4: Test 2. Adsorption of a mixture of NO_x (500 ppm each of NO and NO_2) on BaO/TiO_2 at 200 °C, followed by TPD. Base feed: 10 % O_2 , 5 % H_2O , and balance N_2 .

5.3.2 Desorption

The influence of various gases on the thermal desorption of stored NO_x has been studied. All these tests have been performed with the sample BaO/TiO_2 , which was loaded at 200 °C with a feed containing 500 ppm NO_2 , 10 % O_2 , 5 % H_2O , and balance N_2 . The temperature programmed desorption was then run from 200 °C to 530 °C.

Desorption in the presence of 10 % O_2 (test 1):

According to Figure 5-1, the main product of desorption is NO_2 , which is observed between 250 °C and 530 °C with two maximums at 450 °C and 520 °C. The desorption of NO is observed in the temperature range 370 °C to 530 °C with one maximum at 520 °C. As mentioned previously, the ratio of $\text{NO}_{2,\text{adsorbed}} : \text{NO}_{x,\text{produced}}$ was 3 : 2.22.

Desorption in the absence of O₂ (test 3):

The feed of oxygen was interrupted two minutes prior to starting the TPD. Figure 5-5 compares the temporal evolution of NO and NO₂ during TPD for test 1 (with O₂) and test 3 (without O₂). No significant change of the temporal evolution profile of both NO and NO₂ due to the absence of oxygen was observed. With both feeds, the desorption of NO₂ takes place in the temperature range 250 – 530 °C. Two desorption peaks are discernible, one centered at 450 °C and the other one at 520 °C. NO is observed at higher temperatures, i.e. between 370 °C and 530 °C, with a flat maximum in the range 500 – 530 °C. This maximum is at about the same temperature as the second peak of NO₂. Table 5-1 reports the amounts of NO and NO₂ desorbed. The relative amount of NO corresponds to 20 % and 25 % of the total NO_x in the presence and absence of oxygen, respectively.

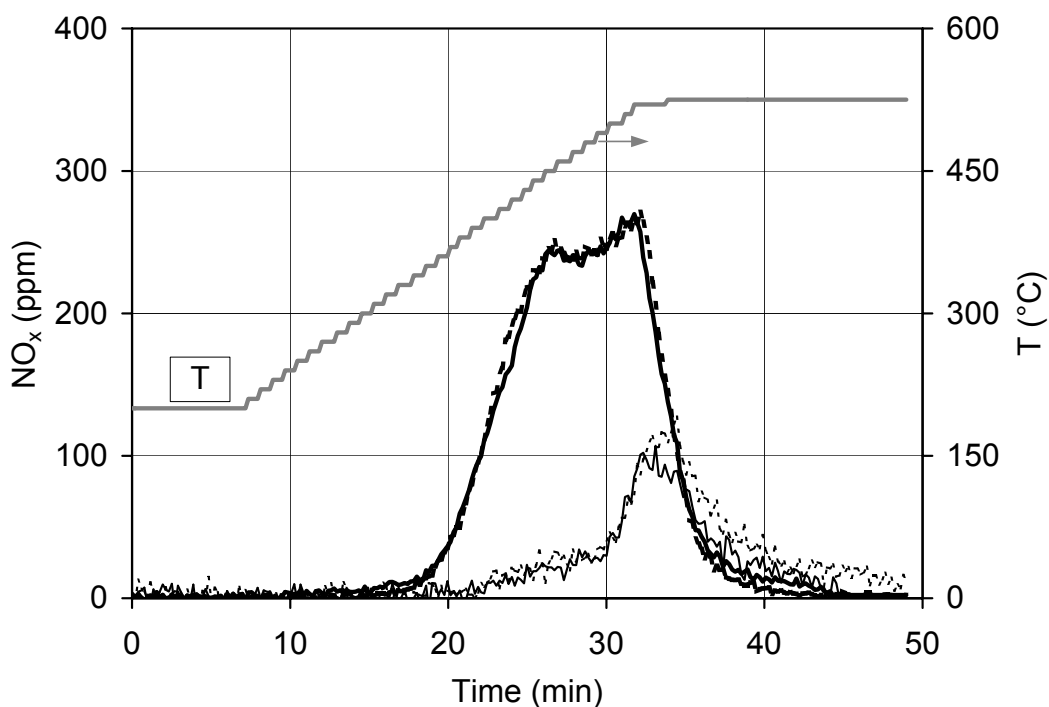


Figure 5-5: Tests 1 and 3. Desorption of NO_x from sample BaO/TiO₂ during TPD with or without O₂, after adsorption of NO₂ (500 ppm) at 200 °C. Base feed: 5 % H₂O, and balance N₂. NO₂ with O₂ (—), NO with O₂ (—), NO₂ without O₂ (---), NO without O₂ (-----).

Desorption in the presence of CO (test 4):

The feed of oxygen was again interrupted two minutes before starting the TPD, and 500 ppm CO added to the humid gas stream. Figure 5-6 shows the release of both NO and NO₂ in the temperature range 320 – 530 °C. Contrary to the previous tests, only a single peak of NO₂ is observed, with a maximum at 460 °C. Two shoulders at 420 °C and 500 °C are discernible. The maximum desorption of NO occurs at 520 °C. Above 520 °C, the release of NO exceeds the release of NO₂. The amounts of NO and NO₂ formed in test 4 are also reported in Table 5-1. Compared to test 3 (absence of CO) the relative amount of NO has increased from 25 to 40 % of the total NO_x. On the other hand, the amount of total NO_x is about equal in both tests.

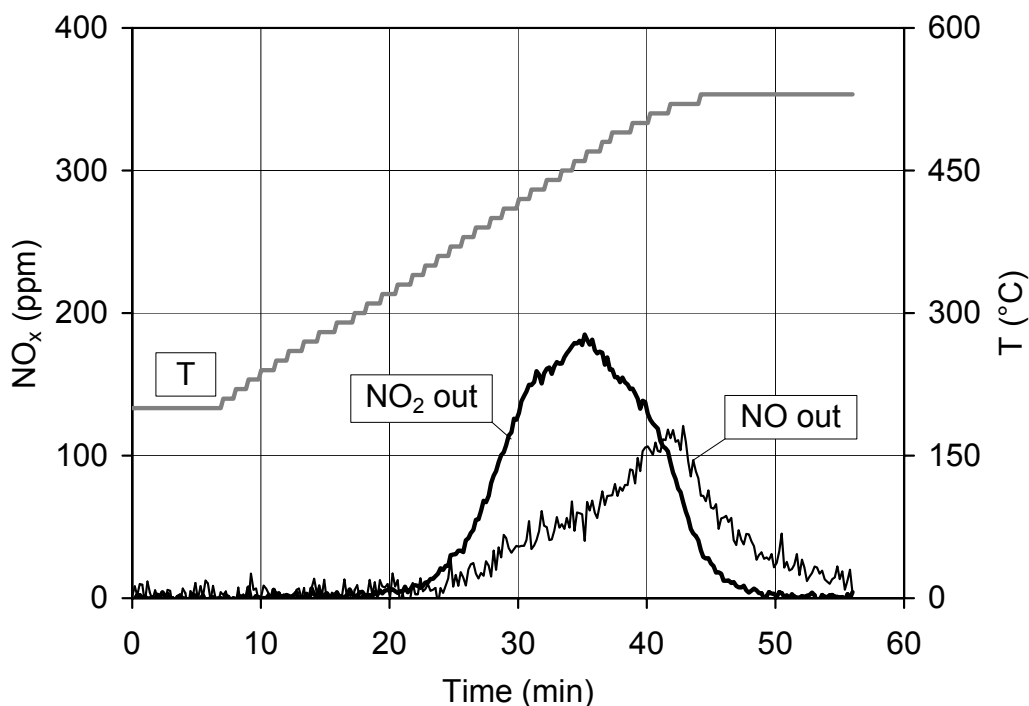


Figure 5-6: Test 4. Desorption of NO_x from sample BaO/TiO₂ during TPD with CO, after adsorption of NO₂ (500 ppm) at 200 °C. Feed during TPD: 500 ppm CO, 5 % H₂O, and balance N₂.

Desorption in the presence of NO (test 5):

The influence of NO on the desorption was investigated on both samples BaO/TiO₂ and TiO₂. In these experiments, the gas feed during TPD consisted of 500 ppm NO and 5 % H₂O in N₂. Figure 5-7 shows the concentrations of NO and NO₂ during TPD on BaO/TiO₂. In contrast to the previous experiments, the desorption of NO₂ starts already at 200 °C and continues up to 530 °C. Three maximums of NO₂ desorption are discernible, the first one occurring immediately after adding NO to the feed, i.e. at 200 °C. The second maximum is seen at 280 °C. A last broad NO₂ peak is observed at the highest temperatures with a maximum of desorption at 520 °C. On the other hand, the NO concentration remains below the input NO concentration of 500 ppm up to the highest temperatures, indicating a consumption of NO.

The quantity of NO₂ desorbed during TPD amounts to 406 µmol/g_{cat}. This is equal to the amount of NO₂ taken up during the adsorption (395 µmol/g_{cat}). The consumption of NO amounts to 143 µmol/g_{cat}, which yields a ratio 3 : 1.06 for NO_{2,produced} : NO_{consumed}.

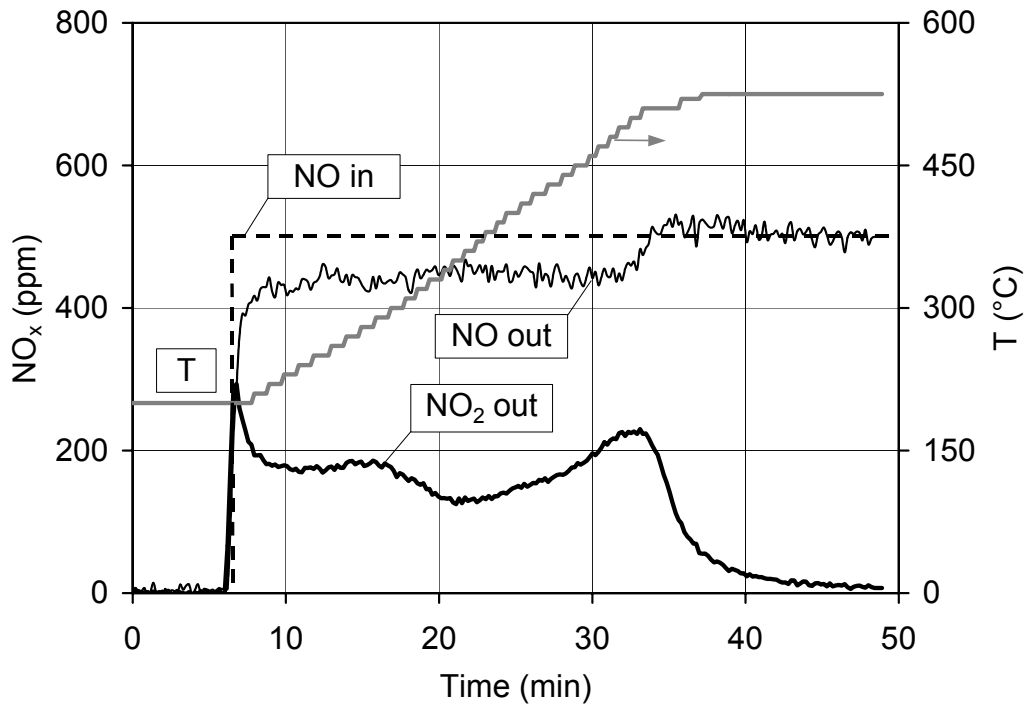


Figure 5-7: Test 5. Desorption of NO_x from sample BaO/TiO₂ during TPD with NO, after adsorption of NO₂ (500 ppm) at 200 °C. Feed during TPD: 500 ppm NO, 5 % H₂O, and balance N₂.

Figure 5-8 shows the results for the same experiment with a sample of pure TiO_2 (test 5a). Again, desorption of NO_2 started at 200 °C, but, in contrast to BaO/TiO_2 , it was complete at 350 °C. At 200 °C, a vigorous production of NO_2 was observed, whose maximum was about two times higher than for BaO/TiO_2 . This sharp peak runs into a broad shoulder with a second maximum at 230 °C. The NO concentration at the reactor outlet was substantially lower than the NO input as long as NO_2 was desorbed. The shape of the NO concentration curve was the mirrored shape of the NO_2 desorption curve. However the amount of $\text{NO}_{\text{consumed}}$ was substantially lower than the amount of $\text{NO}_{2,\text{produced}}$. The ratio of $\text{NO}_{2,\text{produced}} : \text{NO}_{\text{consumed}}$ was 3 : 1.47.

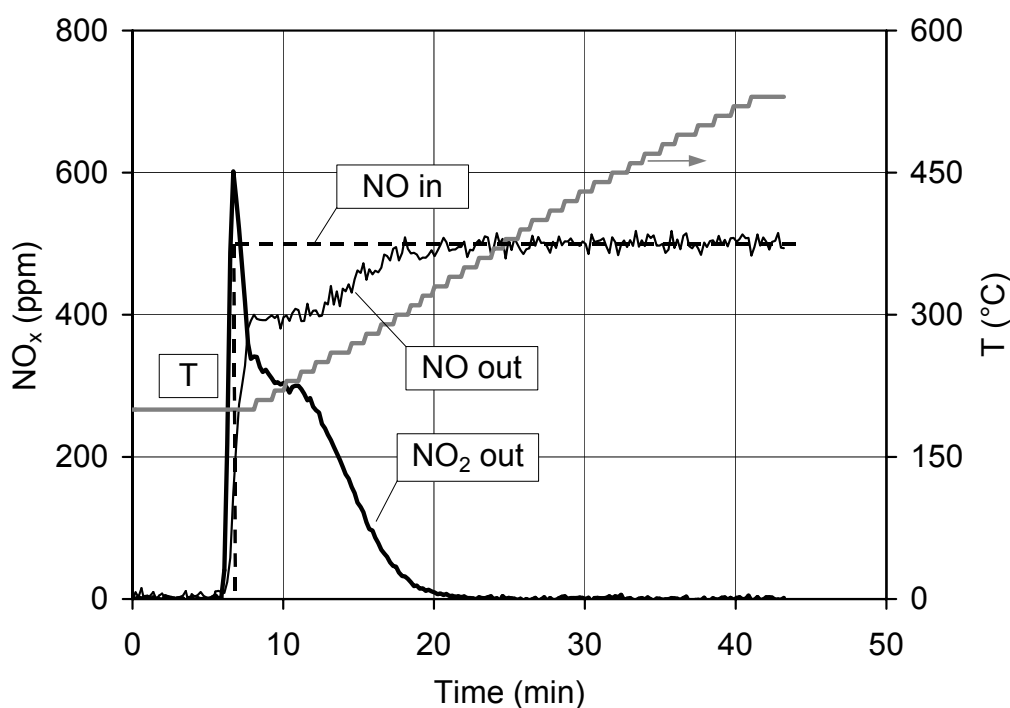


Figure 5-8: Test 5a. Desorption of NO_x from sample TiO_2 during TPD with NO , after adsorption of NO_2 (500 ppm) at 200 °C. Feed during TPD: 500 ppm NO , 5 % H_2O , and balance N_2 .

5.4 Discussion

5.4.1 Adsorption and desorption of NO₂ in the absence of NO and CO

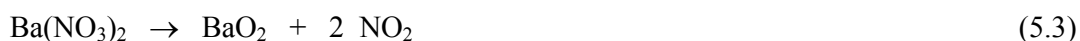
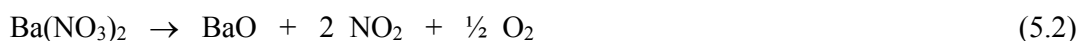
Adsorption:

The adsorption of pure NO₂ (500 ppm) in the base feed on BaO/TiO₂ is accompanied by the formation of NO (test 1, Figure 5-1), with a ratio of about 3 : 1 between NO_{2,adsorbed} and NO_{produced}. The quantitative evaluation of the results evidences the disproportionation of NO₂ over BaO/TiO₂ according to the following reaction:



Desorption:

The TPD yields the same results for a feed with or without oxygen (Figure 5-5). Both NO and NO₂ are detectable at the reactor outlet as products of the thermal decomposition of the nitrate species. The major species is NO₂, NO being only observed at the highest temperatures. Two reactions may be proposed for the thermal decomposition of nitrates:



Reaction (5.2) assumes the direct decomposition of barium nitrate with formation of oxygen. However, thermodynamic calculations suggest that barium peroxide formed in the alternate decomposition reaction (5.3) is thermodynamically stable up to about 600 °C, at higher temperatures splitting into BaO and oxygen. The reality is probably best described by considering the formation of BaO₂ as a possible intermediate which then decomposes further into barium oxide and oxygen thereby restoring the adsorption site.

The two peaks of NO₂ observed during the TPD are due to various nitrate species on barium oxide (Figure 5-5). The formation of surface nitrates and bulk nitrates has already been reported by Fridell and coworkers [3-5]. The first peak of NO₂ desorption at 460 °C should then be attributed to the decomposition of less stable surface nitrates

on barium oxide. Due to the fact that NO_2 adsorbs also on TiO_2 (Figure 5-3), the first desorption peak likely also includes a contribution from the decomposition of surface nitrates adsorbed on TiO_2 .

The second peak at 530 °C results from the decomposition of more stable nitrate species. Our XRD analysis revealed the formation of small amounts of bulk nitrates during the adsorption of NO_2 (Figure 5-2). We are envisioning these nitrates as a layer around the core of the crystallites. Therefore, we can attribute the second desorption peak of NO_2 at 530 °C to the decomposition of bulk barium nitrate. A peak of NO is also seen at this temperature. The simultaneous occurrence of NO must be explained by its higher thermodynamic stability at higher temperatures:



5.4.2 Influence of CO and NO

Carbon monoxide:

Carbon monoxide has been used as a typical reducing agent to test the effect of reducing conditions on the desorption. The desorption in test 4 was performed in a feed containing 500 ppm CO, and 5% H_2O in N_2 . Comparing Figure 5-6 with Figure 5-5 shows that the presence of CO has no influence on the temperature of decomposition of the nitrate species and on the total amount of NO_x desorbed. In contrast to Figure 5-5, only one peak of NO_2 desorption is present at 460 °C, and the ratio of $\text{NO}_{\text{produced}} : \text{NO}_{x,\text{produced}}$ has increased by a factor of about two (Table 5-1). These results confirm the findings of Balcon et al. [6] who showed that the presence of a reducing agent is not required for the desorption process. The higher amount of NO measured in the presence of CO must be attributed to a partial reduction of NO_2 by CO according to reaction (5.5). The oxidation of CO by NO_2 has also been claimed by Erkfeldt et al. [7].



Nitric oxide:

The presence of NO has a very strong effect on the desorption of the nitrate species. As may be seen from Figure 5-7, the release of NO₂ is extended over the entire temperature range from 200 °C to 530 °C. The desorption of NO₂ is accompanied by a consumption of NO, thus showing that NO reacts with the adsorbed species. The ratio of NO_{2,produced} : NO_{consumed} amounts to roughly 3 : 1 suggesting the reverse reaction of reaction (5.1). This is the comproportionation between NO and nitrate species under the formation of NO₂ and BaO. In this reaction, the adsorbed nitrate species play the role of the oxidizer, and NO the role of the reducing agent:



Figure 5-8 supports the storage of considerable amounts of NO₂ in form of nitrates not only on BaO but also on the TiO₂ support. The NO₂ concentration curve exhibited a similar pattern as for BaO/TiO₂, but the desorption was more vigorous and complete at lower temperatures. This might be explained by the presence of weakly bound nitrates at the TiO₂ surface and the lack of bulk nitrates, which are hard to desorb. The desorption of surface nitrates from TiO₂ can be described by a reaction scheme similar to reaction (5.6). It is probable that the deviation found in the ratio of NO_{2,produced} : NO_{consumed} = 3 : 1.47 from 3 : 1 arises from a measuring error of the amount of NO_{consumed}.

The desorption curve for BaO/TiO₂ in Figure 5-7 can be interpreted as a superposition of the NO₂ desorption curve of pure TiO₂ and BaO. Three peaks in the desorption of NO₂ are discernible, although less pronounced than in test 1. The first, immediately after starting the addition of NO to the feed at 200 °C, may be attributed to the reaction of NO with nitrates adsorbed on titania. The second peak at 280 °C is attributed to the reaction of NO with surface nitrates formed on barium oxide. The third peak at 510 °C is at about the same temperature than for test 1 and is attributed to bulk barium nitrate.

The high reactivity of NO with the adsorbed species also explains the reduced amount of NO₂ adsorbed in the presence of NO (test 2). Due to this high reactivity, reactions (5.1) and (5.6) should better be considered as a single reaction whose equilibrium is attained at least partially under our experimental conditions. Therefore, high concentrations of NO will shift the equilibrium of reaction (5.6) to the right side

(decomposition of barium nitrate), and high concentrations of NO_2 will shift it to the left side (formation of barium nitrate).

5.5 Proposed mechanism for the NO_x adsorption-desorption process on NO_x storage catalysts

On the basis of our experimental study, we propose a mechanism for the NO_x adsorption during the lean phase and the NO_x desorption during the rich phase, on a catalyst consisting of Pt/BaO/TiO₂. Due to the fact that in practice a NSR catalyst is operated in the adsorption mode for less than a few minutes it is unlikely that bulk barium nitrate forms. Therefore, the present model will not take into account its formation.

Figure 5-9 proposes a scheme for the surface reactions taking place during the lean phase. In a first step, NO is oxidized to NO_2 over platinum. Subsequently, NO_2 reacts with barium oxide and TiO₂ according to the disproportionation reaction (5.1) leading to the formation of nitrates on TiO₂ and barium oxide and NO. Due to the fact that NO shifts the equilibrium of reaction (5.1) backwards, its fast reoxidation on platinum is favorable for the adsorption process [8].

The proposed surface reactions occurring during the rich phase are shown in Figure 5-10. When the engine is turned to rich conditions, the oxygen concentration in the exhaust decreases considerably. As a consequence, the oxidation of NO to NO_2 over platinum is no longer possible resulting in a high concentration of NO in the gas phase. NO can then react fast with the nitrates adsorbed on the support and on barium oxide, as shown for BaO in reaction (5.6). This fast oxidation of NO by nitrates could explain the breakthrough peak of NO_x observed when switching the engine from lean to rich conditions [9]. In the last step, NO_2 is reduced to N_2 by CO or other reducing agents on the platinum particles.

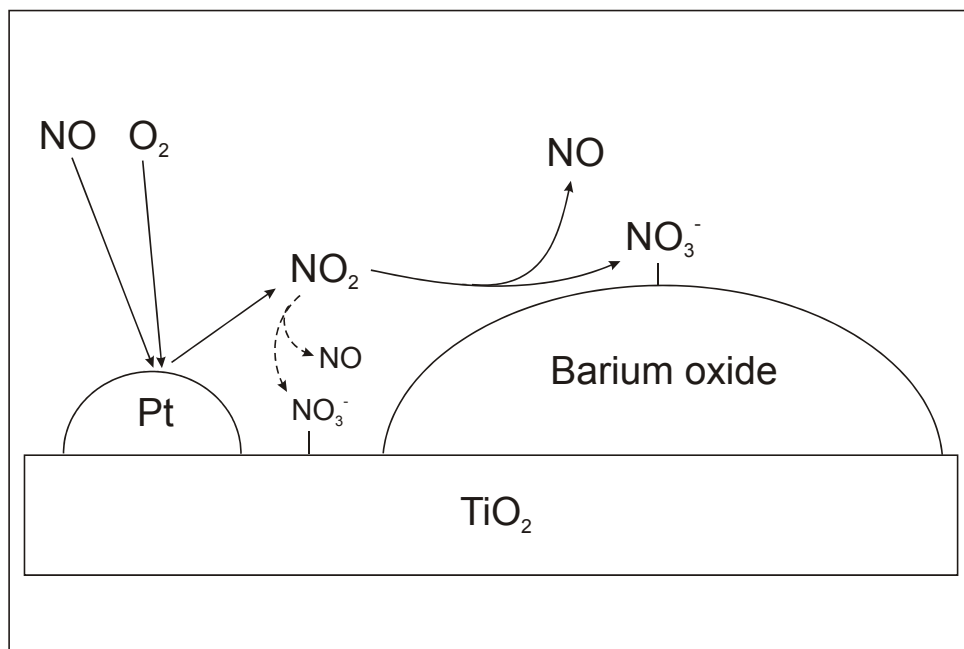


Figure 5-9: Proposed reaction scheme for the NO_x adsorption process.

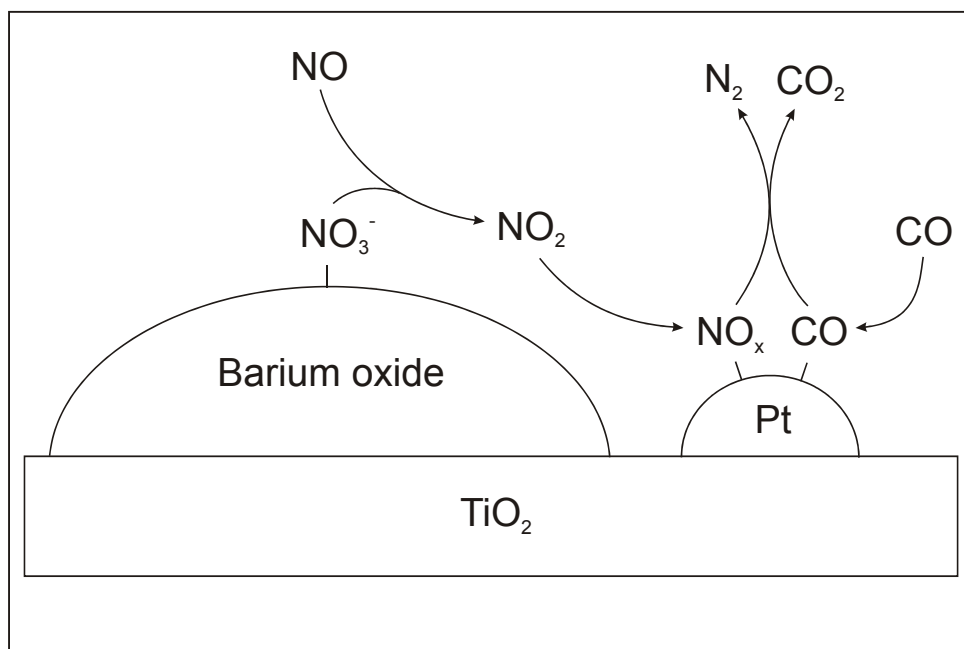


Figure 5-10: Proposed reaction scheme for the NO_x desorption and reduction process.

5.6 Conclusions

The adsorption of NO_2 at 200 °C on BaO/TiO_2 under lean conditions involves the disproportionation of NO_2 to nitrate species and nitrogen monoxide released to the gas phase. Three different nitrate species form on the catalyst: surface nitrates on the support TiO_2 , surface nitrates on BaO , and bulk barium nitrate. During TPD in lean conditions, surface nitrates on TiO_2 decompose at 370 °C and at 450 °C on barium oxide. Bulk barium nitrate is more stable and its decomposition to NO_2 and NO occurs at 530 °C. Temperature programmed desorption showed that the temperatures of decomposition are not influenced by oxygen. The presence of CO in the feed only increased the share of NO due to the gas-phase reduction of NO_2 by CO .

However, the presence of NO during TPD causes a drastic change of the temporal NO_x formation during TPD. Nitrogen monoxide reacts easily with the nitrates under formation of NO_2 . This is a comproportionation reaction occurring between 200 °C and 350 °C with nitrates adsorbed on titania, and below 330 °C with surface nitrates on barium oxide. Bulk barium nitrate is less reactive towards NO . These findings suggest that the regeneration of an NSR catalyst involves the reaction of NO with the nitrates prior to NO_x reduction.

5.7 References

- [1] N. Takahashi, H. Shinjoh, T. Iijima, T. Susuki, K. Yamazaki, K. Yokota, H. Suzuki, N. Miyoshi, S. Matsumoto, T. Tanizawa, T. Tanaka, S. Tateishi and K. Kasahara, *Catal. Today* **27** (1996), 63
- [2] J. Despres, M. Koebel, O. Kröcher, M. Elsener and A. Wokaun, to be published
- [3] E. Fridell, H. Persson, L. Olsson, B. Westerberg, A. Amberntsson and M. Skoglundh, *Top. Catal.* **16/17** (2001), 133
- [4] E. Fridell, M. Skoglundh, B. Westerberg and S. Johansson, G. Smedler, *J. Catal.* **183** (1999), 196
- [5] B. Westerberg and E. Fridell, *J. Mol. Catal. A: Chem.* **165** (2001), 249

- [6] S. Balcon, C. Potvin, L. Salin, J.F. Tempère, G. Blanchard and G. Djéga-Mariadassou, *Catal. Lett.* **60** (1999), 39
- [7] S. Erkfeldt, E. Jobson and M. Larsson, *Top. Catal.* **16/17** (2001), 127
- [8] H. Mahzoul, J.F. Brilhac and P. Gilot, *Appl. Catal. B: Environ.* **20** (1999), 47
- [9] W. Bögner, M. Krämer, B. Krutzsch, S. Pischinger, D. Voigtländer, G. Wenninger, F. Wirbeleit, M.S. Brogan, R.J. Brisley and D.E. Webster, *Appl. Catal. B: Environ.* **7** (1995), 153

Screening of supported platinum catalysts for the oxidation of NO

6.1 Introduction

It has been demonstrated in chapters 4 and 5 that the oxidation of NO to NO₂ is a necessary first reaction if NO is to be adsorbed, e.g. on NO_x storage catalysts. Also other aftertreatment processes, like the selective catalytic reduction of nitrogen oxides at low temperatures over vanadium-based catalyst with ammonia or urea, and the regeneration of soot filters, profit of a feed enriched in NO₂. This is most easily accomplished by adding a platinum-based oxidation catalyst upstream of the DeNO_x catalyst or of the filter [1,2]. The oxidation catalyst oxidizes NO in the exhaust to NO₂. In order to obtain high conversions of NO and soot, the oxidation catalyst should be active already at low temperatures.

The catalytic activity of a platinum catalyst is strongly depending on the preparation conditions, on the platinum precursor, on the support and on the reaction considered [3,4]. In this chapter, we report on the oxidation of NO to NO₂ over supported platinum catalysts prepared with various precursors and various supporting oxides. Additionally, the influence of calcination and reduction temperatures was investigated.

6.2 Experimental

6.2.1 Sample preparation

Various commercially available oxides in powder or pellet form (cylinders of about 2 to 3 mm) have been used as supports in the present study. Supports in the form of pellets (SiO_2 and ZrO_2) were crushed and sieved to get the fraction between 160 and 200 μm . TiO_2 and $\text{Al}_2\text{O}_3\text{-SiO}_2$ were in the form of powders with particle sizes below 100 μm . Therefore, they were first agglomerated using a method developed in house [5]. For the agglomeration, the powder was suspended in deionized water. Then, a binder was added to the suspension. After mixing, the suspension was poured on a watch glass and the resulting film was successively dried at 120 $^\circ\text{C}$. The dried layer was then scraped off the watch glass. A fraction with sizes between 160 and 200 μm was obtained by crushing and sieving. The material was finally calcined at 550 $^\circ\text{C}$ for 3 h. γ -alumina was obtained as a powder with particle sizes between 100 and 500 μm . The fraction with particle sizes between 160 and 200 μm was obtained again by sieving.

All platinum catalysts were prepared by incipient wetness impregnation. In this technique, a volume V of solution containing the metal precursor is put into contact with a dried support of pore volume V . The solution penetrates inside the pores by capillary forces and the water is subsequently evaporated.

Samples 2.5 % Pt/ Al_2O_3 (P1 to P10)

Samples **P1** to **P7**. 7.0 g of $\gamma\text{-Al}_2\text{O}_3$ (Puralox Nwa-155, Condea, 155 m^2/g) were added to 7.5 mL of an aqueous solution containing 0.472 g of $\text{H}_2\text{PtCl}_6\cdot\text{aq}$ (Fluka, 38 w.% Pt). After 1 h of equilibration at RT, the paste was dried at 120 $^\circ\text{C}$ overnight. The sample then was divided into seven fractions of 1 g. The first four fractions were calcined at 250 (**P1**), 300 (**P2**), 350 (**P3**) or 400 $^\circ\text{C}$ (**P4**) for 2 h, and finally, the samples were reduced at 450 $^\circ\text{C}$ for 1 h in a flow of 5 % H_2/N_2 (8 $\text{L}_\text{N}/\text{h}$). The last three fractions were calcined at 300 $^\circ\text{C}$ for 2 h, prior to the reduction for 1 h at 350 (**P5**), 400 (**P6**), or 500 $^\circ\text{C}$ (**P7**).

Sample **P8**. 2.5 g of $\gamma\text{-Al}_2\text{O}_3$ were added to 2.7 mL of an aqueous solution containing 0.114 g of $\text{Pt}(\text{NH}_3)_4\text{Cl}_2\cdot\text{aq}$ (Alfa Aesar, Johnson Matthey, 56.4 w.% Pt). After 1 h of

equilibration at RT, the paste was dried at 120 °C overnight. The sample then was calcined at 300 °C for 2 h, and finally reduced at 450 °C for 1 h in a flow of 5 % H₂/N₂ (8 L_N/h).

Sample **P9**. The preparation of **P9** was analogous to the preparation of **P8**, except that an aqueous solution containing 0.127 g of Pt(NH₃)₄(NO₃)₂ (Aldrich, purity = 99.995 %) was used. After 1 h of equilibration at RT, the paste was dried at 120 °C overnight. The final calcination and reduction were performed in an analogous procedure as sample **P8**.

Sample **P10**. This sample was prepared by adding 2.5 g of γ-Al₂O₃ to 2.7 mL of an aqueous solution containing 0.675 g of Pt(NH₃)₄(OH)₂·aq (Johnson Matthey, ≈ 9.5 w.% Pt). After 1 h of equilibration at RT, the paste was dried at 120 °C overnight. The final calcination and reduction were performed in similar conditions as described for sample **P8**.

Samples 2.5 % Pt/SiO₂ (P11 to P14)

Sample **P11**. 2.5 g of SiO₂ (Aerosyl® 200, Degussa, 160 m²/g) were added to 2.7 mL of an aqueous solution containing 0.114 g of Pt(NH₃)₄Cl₂·aq (Alfa Aesar, Johnson Matthey, 56.4 w.% Pt). After 1 h of equilibration at RT, the paste was dried at 120 °C overnight. The sample then was calcined at 300 °C for 2 h, and finally reduced at 450 °C for 1 h in a flow of 5 % H₂/N₂ (8 L_N/h).

Sample **P12**. Into 2.7 mL of an aqueous solution containing 0.168 g of H₂PtCl₆·aq (Fluka, 38 w.% Pt) was added 2.5 g of SiO₂. Then, the preparation of **P12** was analogous to the preparation of sample **P11**.

Sample **P13**. Similarly to sample **P11**, the sample **P13** was prepared by adding 2.5 g of SiO₂ to 2.7 mL of an aqueous solution containing 0.127 g of Pt(NH₃)₄(NO₃)₂ (Aldrich, purity = 99.995 %). After 1 h of equilibration at RT, the paste was dried at 120 °C overnight. The final calcination and reduction were performed in an analogous procedure as sample **P11**.

Sample **P14**. The preparation of Pt/SiO₂ (referred to as **P14**) was analogous to the preparation of sample **P11**, except that 2.7 mL of an aqueous solution containing 0.675

g of $\text{Pt}(\text{NH}_3)_4(\text{OH})_2\cdot\text{aq}$ (Johnson Matthey, ≈ 9.5 w.% Pt) were used. After 1 h of equilibration at RT, the paste was dried at 120 °C overnight. Again, the sample was calcined in air at 300 °C for 2 h and reduced at 450 °C for 1 h.

Samples Pt/SiO₂ (P15 to P19)

For these samples, the platinum loading was varied between 0.2 and 10 w.%. Table 6-1 gives the platinum loading for each sample. All samples were prepared as described previously for sample **P11** (except the weight of platinum precursor). The samples were calcined at 300 °C for 2 h and finally reduced at 450 °C for 1 h in 5 % H₂/N₂.

Table 6-1: Platinum loading over samples Pt/SiO₂ referred to as **P15** to **P19**.

Sample	Platinum loading (w.%)
P15	0.2
P16	0.5
P17	1
P18	5
P19	10

Sample 2.5 % Pt/TiO₂ (P20) and sample 2.5 % Pt/ZrO₂ (P21)

Sample **P20**. 2.5 g of TiO₂ (DT51, Rhone-Poulenc, 90 m²/g) were added to 2.0 mL of an aqueous solution containing 0.114 g of $\text{Pt}(\text{NH}_3)_4\text{Cl}_2\cdot\text{aq}$ (Alfa Aesar, Johnson Matthey, 56.4 w.% Pt). After 1 h of equilibration at RT, the paste was dried at 120 °C overnight. The sample then was calcined at 300 °C for 2 h, and finally reduced at 450 °C for 1 h in a flow of 5 % H₂/N₂ (8 L_N/h).

Sample **P21**. 2.5 g of ZrO₂ (ECO100E, MEL Chemicals/MEI, 75 m²/g) were added to 1.8 mL of an aqueous solution containing 0.114 g of $\text{Pt}(\text{NH}_3)_4\text{Cl}_2\cdot\text{aq}$. After 1 h of equilibration at RT, the paste was dried at 120 °C overnight. The sample then was

calcined at 300 °C for 2 h, and finally reduced at 450 °C for 1 h in a flow of 5 % H₂/N₂ (8 L_N/h).

Samples 2.5 % Pt/Al₂O₃-SiO₂ (P22 to P24)

Sample **P22**. This sample was prepared by adding 2.5 g of Al₂O₃-SiO₂ (SIRAL 5, Condea, Al₂O₃(%):SiO₂(%) = 94.8 : 5.2, 280 m²/g) to 2.7 mL of an aqueous solution containing 0.114 g of Pt(NH₃)₄Cl₂·aq. After 1 h of equilibration at RT, the paste was dried at 120 °C overnight. The sample then was calcined at 300 °C for 2 h, and finally reduced at 450 °C for 1 h in a flow of 5 % H₂/N₂ (8 L_N/h).

Sample **P23**. 2.5 g of Al₂O₃-SiO₂ (SIRAL 10, Condea, Al₂O₃(%):SiO₂(%) = 90.5 : 9.5, 410 m²/g) were added to an aqueous solution (2.7 mL, 0.114 g of Pt(NH₃)₄Cl₂·aq.) After 1 h of equilibration at RT, the paste was dried at 120 °C overnight. The final calcination and reduction were performed in an analogous procedure as sample **P22**.

Sample **P24**. The preparation of sample **P24** was analogous to the preparation of sample **P22**, except that the supporting oxide was Al₂O₃-SiO₂ (SIRAL 20, Condea, Al₂O₃(%):SiO₂(%) = 78.1 : 21.9, 446 m²/g). The sample was again calcined at 300 °C and reduced at 450 °C in analogy to sample **P22**.

6.2.2 Catalytic tests

The experimental setup has been described in chapter 3. The catalytic tests were performed in the stainless steel reactor with 0.8 g of sample. Mass transfer limitations during the reaction were avoided due to the use of the fraction of particles between 160 and 200 µm.

All samples were tested after reduction. The gas flow rate V* was 150 L_N/h. The sample was heated to 450 °C in a gas feed consisting of 10 % O₂, 5 % H₂O and balance N₂, prior to the addition of 500 ppm NO. The catalytic test was performed between 150 and 450 °C. The concentrations of NO and NO₂ after the catalyst were measured at constant temperatures.

6.3 Results

6.3.1 Influence of calcination and reduction temperatures

The study was performed using samples of Pt/Al₂O₃ prepared with H₂PtCl₆. Table 6-2 gives the conversion of 500 ppm NO at 300 °C measured over the samples **P1** to **P7** calcined and reduced at various temperatures. The calcination temperature has only a weak influence on the conversion. Only the sample **P2** calcined at 300 °C exhibits a slightly higher activity.

The influence of the temperature of reduction was investigated on samples previously calcined at 300 °C for 2 h. The sample **P2** reduced at 450 °C is slightly more active than the other samples. It can be seen that the temperature of reduction does not strongly influence the activity of the samples.

Table 6-2: Influence of the temperature of calcination and reduction (calcination time: 2 h, reduction time: 1 h)

Sample ^{a)}	Calcination temperature (°C)	Reduction temperature (°C)	Conversion ^{b)} (%)
P1	250	450	14.8
P2	300	450	17.0
P3	350	450	13.8
P4	400	450	13.0
P5	300	350	14.0
P6	300	400	14.4
P2	300	450	17.0
P7	300	500	14.6

^{a)} platinum loading = 2.5 w.%, platinum precursor = H₂PtCl₆.

^{b)} catalyst weight = 0.8 g, V* = 150 L_N/h, T = 300 °C, feed = 500 ppm NO, 10 % O₂, 5 % H₂O, and balance N₂.

6.3.2 Influence of the platinum precursor

Sample Pt/Al₂O₃

Figure 6-1 shows the conversion over Pt/Al₂O₃ prepared with four different platinum precursors. It is observed that the conversion traces a parabolic path. Over sample **P8**, the maximum of conversion is reached at 350 °C, but only at 375 °C over sample **P9** and at ≈400 °C over samples **P2** and **P10**. The decreasing conversion at high temperatures is due to the thermodynamic equilibrium $\text{NO} + \frac{1}{2} \text{O}_2 \rightleftharpoons \text{NO}_2$.

In the temperature range between 200 and 325 °C, the sample **P8** prepared with Pt(NH₃)₄Cl₂ exhibits the highest conversion of NO to NO₂. Compared with **P8**, the sample **P10** prepared with Pt(NH₃)₄(OH)₂ was the less active. The samples **P9** and **P2** prepared with Pt(NH₃)₄(NO₃)₂ and H₂PtCl₆ respectively showed a moderate activity.

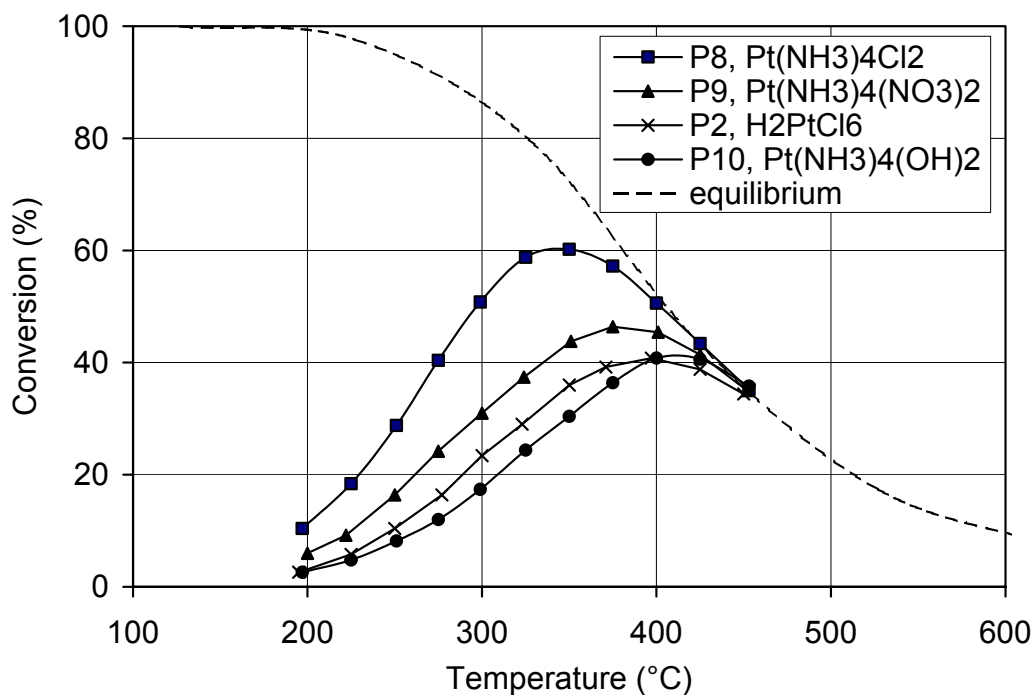


Figure 6-1: Conversion of NO as a function of temperature over samples of Pt/Al₂O₃ prepared with different precursors (Pt loading: 2.5 w.%). Sample weight = 0.8 g, V* = 150 L_N/h, feed: 500 ppm NO, 10 % O₂, 5 % H₂O, and balance N₂.

Samples Pt/SiO₂

The oxidation of 500 ppm NO over Pt/SiO₂ prepared with the four platinum precursors is shown in figure 6-2. Similarly to samples Pt/Al₂O₃, the conversion traces a parabolic path. The maximum of conversion is observed at 300 °C over sample **P11**, while it shifts to 325 °C over sample **P12** and to 375 °C for samples **P13** and **P14**. From Figure 6-2, it is obvious that the activity of the samples ranged in the following order:



The influence of the platinum precursor does not change drastically between Al₂O₃ and SiO₂, except for the sample prepared with H₂PtCl₆. Sample **P12** exhibits a higher activity than sample **P13** prepared with Pt(NH₃)₄(NO₃)₂. In order to get the best conversion at low temperatures, Pt(NH₃)₄Cl₂ is again the best precursor for the preparation of Pt/SiO₂.

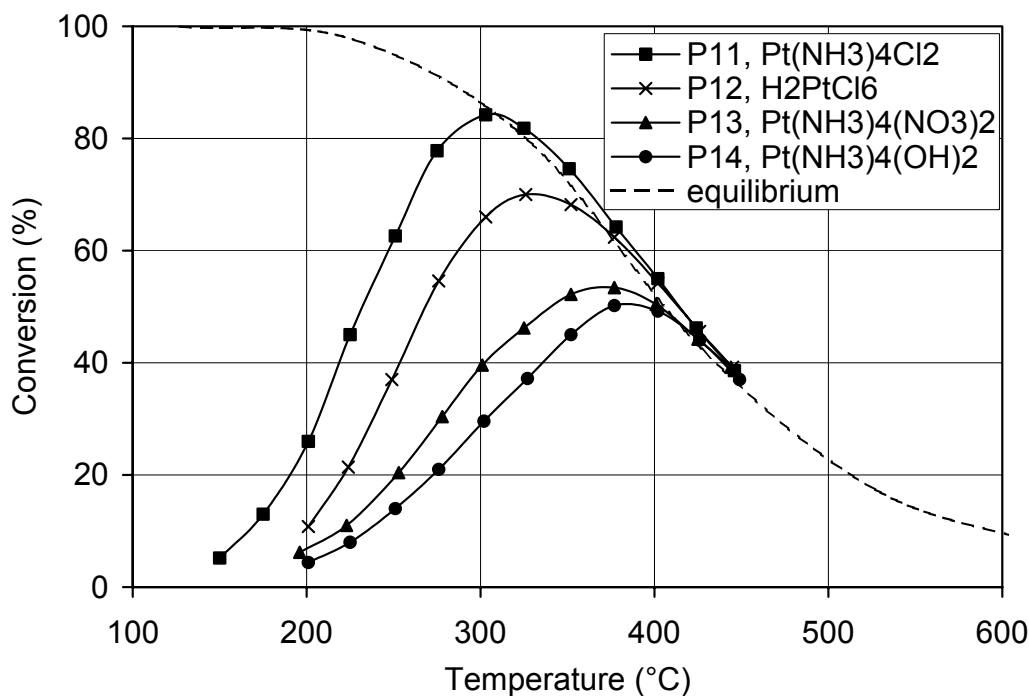


Figure 6-2: Conversion of NO as a function of temperature over samples of Pt/SiO₂ prepared with different precursors (Pt loading: 2.5 w.%). Sample weight = 0.8 g, V* = 150 L_N/h, feed: 500 ppm NO, 10 % O₂, 5 % H₂O, and balance N₂.

6.3.3 Influence of the platinum loading

Due to the fact that the platinum catalyst supported on SiO_2 prepared with $\text{Pt}(\text{NH}_3)_4\text{Cl}_2$ showed the highest conversion of NO to NO_2 , we investigated the effect of the platinum loading on the activity of Pt/ SiO_2 . Figure 6-5 shows the conversion of 500 ppm NO at 200, 225 and 250 °C as a function of the platinum loading in a feed consisting of 10 % O_2 , 5 % H_2O and balance N_2 . At these low temperatures, the conversion is not limited by the thermodynamic equilibrium.

From 0.2 w.% (P15) to 1 w.% (P17), a sharp increase of the conversion is observed at the three temperatures. On the other hand, from 2.5 w.% (P11) to 10 w.% (P19), the conversion increases much more slowly although the platinum loading of sample P19 is four times higher than sample P11.

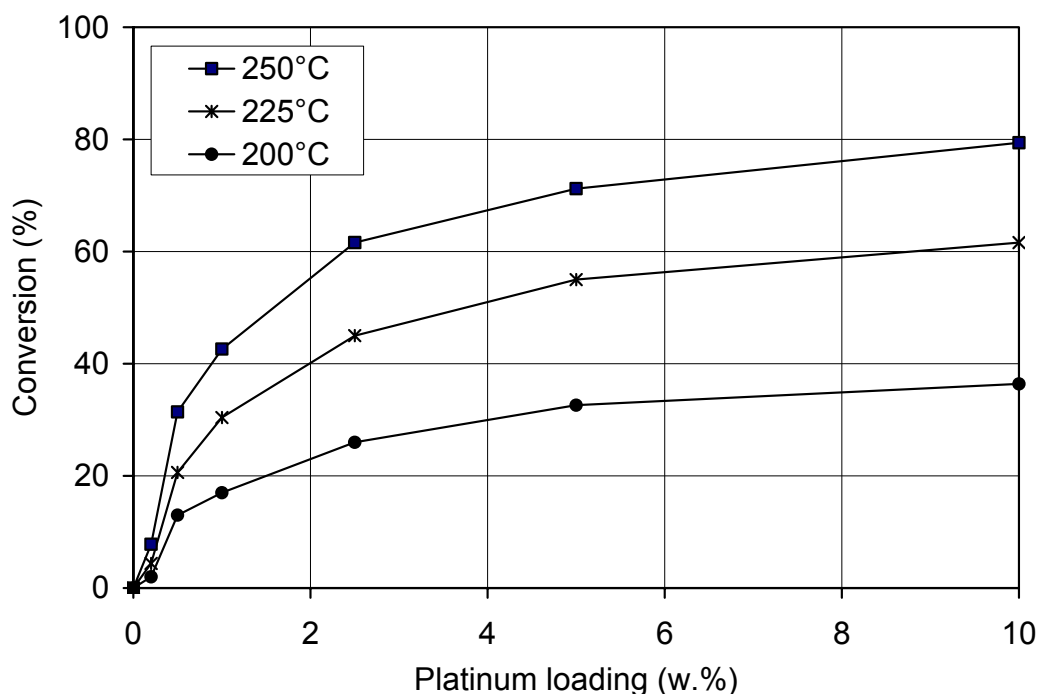


Figure 6-3: Conversion of NO as a function of the platinum loading over various samples of Pt/ SiO_2 . Sample weight = 0.8 g, $V^* = 150 \text{ L}_\text{N}/\text{h}$, feed: 500 ppm NO, 10 % O_2 , 5 % H_2O , and balance N_2 .

6.3.4 Activity of platinum catalysts supported on various supports

Oxidation of NO over Pt/Al₂O₃, Pt/SiO₂, Pt/TiO₂ and Pt/ZrO₂

In order to investigate the influence of the support on the oxidation of NO over supported platinum catalysts, various supporting oxides were impregnated with Pt(NH₃)₄(Cl)₂. Figure 6-4 shows the conversion observed over Pt/Al₂O₃, Pt/SiO₂, Pt/TiO₂ and Pt/ZrO₂. The platinum loading for all samples was 2.5 w.%. The activity ranged in the following order:

$$\text{Pt/SiO}_2 \text{ (P11)} > \text{Pt/Al}_2\text{O}_3 \text{ (P8)} \approx \text{Pt/TiO}_2 \text{ (P20)} > \text{Pt/ZrO}_2 \text{ (P21)}$$

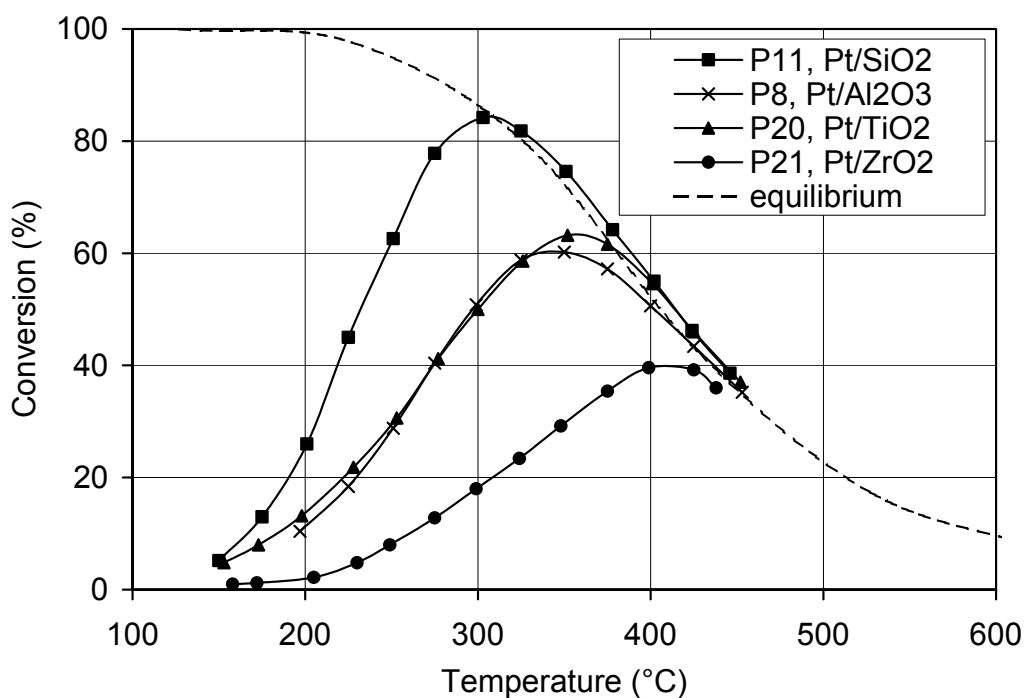


Figure 6-4: Conversion of NO as a function of temperature over platinum supported on various supporting oxides (Pt loading: 2.5 w.%, precursor: Pt(NH₃)₄Cl₂). Sample weight = 0.8 g, V* = 150 L_N/h, feed: 500 pm NO, 10 % O₂, 5 % H₂O, and balance N₂.

Oxidation of NO over Pt/Al₂O₃-SiO₂

The oxidation of NO was also studied over platinum supported on aluminosilicates with varying SiO₂ content. Table 6-3 gives the conversion at 200, 225 and 250 °C as a

function of the SiO₂ content. At all temperatures, the conversion increases with the silica content. The sample **P24** with 20 % of SiO₂ exhibited the same conversion as the pure silica sample **P11** consisting of Pt/SiO₂.

Table 6-3: Influence of the silica content on the conversion of NO to NO₂ at 200, 225 and 250 °C over various samples of Pt/Al₂O₃, Pt/Al₂O₃-SiO₂ and Pt/SiO₂.

Sample ^{a)}	SiO ₂ (%)	Conversion (%) ^{b)}		
		200 °C	225 °C	250 °C
P8	0	10.4	18.4	28.8
P22	5	14.2	22.0	32.6
P23	10	18.4	27.4	44.0
P24	20	29.0	43.8	62.4
P11	100	26.0	45.0	62.6

^{a)} platinum loading = 2.5 w.%, platinum precursor = Pt(NH₃)₄Cl₂.

^{b)} catalyst weight = 0.8 g, V* = 150 L_N/h, feed = 500 ppm NO, 10 % O₂, 5 % H₂O, and balance N₂.

6.4 Discussion

The influence of the calcination and reduction temperatures was studied with samples of Pt/Al₂O₃ (**P1** to **P7**) prepared with H₂PtCl₆. The sample **P2** calcined at 300 °C and reduced at 450 °C showed a slightly higher activity than the samples calcined and reduced at other temperatures (Table 6-2). Therefore, all the samples prepared during the study were calcined at 300 °C for 2 hours and reduced at 450 °C for 1 hour.

The sample consisting of Pt/Al₂O₃ prepared with Pt(NH₃)₄Cl₂ as a platinum precursor (**P8**) exhibited a better activity than samples prepared with other precursors (Figure 6-1). An analogous result was observed with the sample Pt/SiO₂ (**P11**) (Figure 6-2). The

low activity of the sample Pt/Al₂O₃ (**P2**) prepared with H₂PtCl₆ can be ascribed to the presence of residual chlorine at the surface of the platinum crystallites. A trace amount of chlorine could be evidenced by an EDX (energy dispersive X-ray) analysis. The temperatures of calcination and reduction were probably not sufficiently high to decompose completely the PtCl₆²⁺ ions. Poisoning of the platinum surfaces by chlorine has been described in the literature [6-8]. On the other hand, the higher activity of samples prepared with Pt(NH₃)₄Cl₂ could be explained by the absence of residual chlorine. The EDX analysis did not show any traces of chlorine on sample **P11**. Samples of Pt/Al₂O₃ and Pt/SiO₂ prepared with Pt(NH₃)₄(OH)₂ (**P10** and **P14** respectively) showed a surprisingly low activity. Due to its use in the preparation of diesel exhaust catalyst [3], such a result is quite unexpected.

The support of a catalyst has a strong influence on the activity of a catalyst. For the oxidation of NO, platinum supported on SiO₂ (**P11**) exhibits the best activity, compared to other samples with the same platinum loading (Figure 6-4). Xue et al. [9] and Oi-Ushisawa et al. [10] also obtained the highest activities with the silica support. For the supports consisting of alumino-silicate, the content of SiO₂ has also a strong influence on the activity of the samples (Table 6-3). The higher the content of SiO₂, the better the activity of the platinum catalyst (**P24**).

The results shown in Figure 6-3 indicate that the platinum content influences the activity of the samples consisting of Pt/SiO₂. The major boost in activity is observed in the range from 0.2 w.% (**P15**) to 2.5 w.% (**P11**) platinum. At higher loadings, the increase is less significant. Due to the high cost of the platinum precursors, a compromise between platinum loading and activity must be obtained. A platinum loading of 2.5 w.% is considered to be an optimum value.

6.5 Conclusions

The results of the catalytic tests have shown that both the platinum precursor and the support have a strong influence on the activity of supported platinum catalyst for the oxidation of NO. The comparison of catalysts prepared with different precursors shows that samples prepared with Pt(NH₃)₄Cl₂ reach the highest activity. A definitely lower

activity is observed over samples prepared with $\text{Pt}(\text{NH}_3)_4(\text{OH})_2$. Silica as a support improves the activity of the platinum catalyst at low temperatures. On the other hand, the sample consisting of Pt/ZrO_2 shows the lowest catalytic activity. Therefore, further characterization of the platinum surface may help to elucidate the effect of the support.

6.6 References

- [1] G. Madia, M. Koebel, M. Elsener and A. Wokaun, *Ind. Eng. Chem. Res.* **41** (2002), 3512
- [2] B.J. Cooper, H.J. Jung and E.J. Thoss, US Patent 4,902,487 (1990), Assignee: Johnson Matthey Inc.
- [3] J.A.A. van den Tillaart, J. Leyrer, S. Eckhoff and E.S. Lox, *Appl. Catal. B: Environ.* **10** (1996), 53
- [4] D. Schmitt, H. Fuess, H. Klein, U. Neuhausen and E.S. Lox, *Top. Catal.* **16** (2001), 355
- [5] G. Madia, *Measures to enhance the NO_x conversion in urea-SCR systems for automotive applications*, Thesis ETH Nr. 14595, ETH Zurich, (2002)
- [6] E. Marceau, M. Che, J. Saint Just and J.M. Tatibouet, *Catal. Today* **29** (1996), 415
- [7] M. Paulis, H. Peyrard and M. Montes, *J. Catal.* **199** (2001), 30
- [8] F.J. Gracia, J.T. Miller, A.J. Kroft and E.E. Wolf, *J. Catal.* **209** (2002), 341
- [9] E. Xue, K. Seshan and J.R.H. Ross, *Appl. Catal. B, Environ.* **11** (1996), 65
- [10] J. Oi-Ushisawa, A. Obuchi, R. Enomoto, S. Liu, T. Nanba and S. Kushiyama, *Appl. Catal. B: Environ.* **26** (2000), 17

The unexpected kinetic behavior of platinum catalysts for the oxidation of NO

7.1 Introduction

It has been shown in chapter 6 that the sample consisting of Pt/SiO₂ was the most active catalyst for the oxidation of NO to NO₂ at low temperatures. In the following, we investigate the influence of the concentrations of oxygen and of nitric oxide on the oxidation rate of NO to NO₂ over Pt/SiO₂. This kinetic study was performed in both dry and humid feeds. Additional catalytic tests were performed in a feed containing a constant NO concentration and various concentrations of NO₂.

7.2 Experimental

7.2.1 Sample preparation

The sample consists of Pt/SiO₂ with a platinum loading of 2.5 wt.%. Its preparation has been described in chapter 6, where it has been referred to as sample **P11**. It was prepared by incipient wetness impregnation of SiO₂ with an aqueous solution of

$\text{Pt}(\text{NH}_3)_4\text{Cl}_2$. After impregnation, the sample was calcined at 300 °C for 2h and finally reduced in 5 % H_2/N_2 for 1h.

7.2.2 Transmission electron microscopy (TEM) measurements

TEM measurements were performed on a JEOL 2010 microscope equipped with a LaB_6 cathode and with high-tilt objective lenses. The acceleration voltage was 200 kV.

7.2.3 X-ray diffraction (XRD) measurements

X-ray analysis was performed on a Philips X-Pert – MPD diffractometer using the Fe $K\alpha$ radiation at 1.936 Å. The scans were recorded continuously in the range of 2θ between 10 ° and 80 °, with a step width of 0.05 ° and a dwell time of 5 seconds.

7.2.4 Catalytic tests

The experimental setup has already been described in chapter 3. The oxidation tests were performed using 0.8 g of the powder sample Pt/SiO_2 at a flow rate of 150 $\text{L}_\text{N}/\text{h}$. The influence of the feed concentrations of oxygen, nitrogen monoxide, water and nitrogen dioxide was investigated using a single sample. The concentration of O_2 was varied between 0.1 and 30 %. The oxidation of NO in a concentration range between 100 and 1500 ppm was investigated in both dry and humid conditions. In the following, a feed consisting of 10 % O_2 , 5 % H_2O and balance N_2 is referred to as base feed. In addition, the oxidation of 500 ppm NO in the base feed with the addition of 100 - 500 ppm NO_2 was studied.

A first study with various concentrations of NO has shown us that the catalyst deactivated after successive oxidation tests. Therefore, in order to regenerate the catalyst, it was heated in an oven at 650 °C in static air for 1h prior to each oxidation test. This pretreatment proved to restore the initial activity of the sample.

7.2.5 Calculations

Conversion

The oxidation of NO was investigated in various feeds. In the calculation of the conversion, two cases must be distinguished:

1) if the feed consists of NO, O₂, with or without water, and balance N₂, the conversion is calculated according to reaction (7.1), given already in chapter 3:

$$\text{Conversion (\%)} = \frac{c_{\text{NO}_2, \text{out}}}{c_{\text{NO}, \text{in}}} \cdot 100 \quad (7.1)$$

2) if the feed contains also NO₂, the conversion is calculated as follows:

$$\text{Conversion (\%)} = \frac{(c_{\text{NO}_2, \text{out}} - c_{\text{NO}_2, \text{in}})}{c_{\text{NO}, \text{in}}} \cdot 100 \quad (7.2)$$

Reaction rate

In order to calculate the reaction rates, only conversions below about 30 % were taken into account. At these low conversions, the concentrations of reactants are assumed as constant along the catalyst bed. The small particle size of Pt/SiO₂ (between 160 and 200 μm) excludes mass transfer limitations.

The reaction rate was calculated using the following equations

$$r = \frac{\Delta \dot{n}_{\text{NO}_2}}{W} = \frac{\dot{n}_{\text{NO}_2, \text{out}} - \dot{n}_{\text{NO}_2, \text{in}}}{W} \quad (7.3)$$

$$r = \frac{V^*}{W} \cdot (c_{\text{NO}_2, \text{out}} - c_{\text{NO}_2, \text{in}}) \quad (7.4)$$

with	r	reaction rate (mol/(g·s))
	W	weight of sample (g)
	$\dot{n}_{\text{NO}_2, \text{out}}$	molar flux of NO ₂ behind the catalyst (mol/s)
	$\dot{n}_{\text{NO}_2, \text{in}}$	molar flux of NO ₂ before the catalyst bed (mol/s)

$c_{\text{NO}_2,\text{out}}$	concentration of NO_2 behind the catalyst (mol/L)
$c_{\text{NO}_2,\text{in}}$	concentration of NO_2 before the catalyst (mol/L)
V^*	volume flow rate (L/s)

The reaction order respective to O_2 and NO were calculated using the following power rate law, where k is the reaction rate constant:

$$r = k \cdot c_{\text{NO}}^{\alpha} \cdot c_{\text{O}_2}^{\beta} \quad (7.5)$$

7.3 Results

7.3.1 Determination of the platinum particle size

Transmission electron microscopy

Figure 7-1 shows a TEM micrograph of the freshly reduced sample Pt/SiO_2 . The small dark spots correspond to the platinum particles. The larger gray spheres, which are round in shape, correspond to the grains of silica. The platinum particle size was roughly determined from the size of 50 particles. The resulting average particle size is 12.7 nm.

XRD line broadening analysis

Figure 7-2 displays the XRD pattern of the freshly reduced sample. The XRD pattern of the silica support was subtracted from the pattern of the sample Pt/SiO_2 . The peaks observed at 2θ values of 50.7° and 59.4° are characteristic of platinum. On the basis of JCPDS data (Platinum, No. 04-0802), these peaks are attributed to $\text{Pt}(111)$ and $\text{Pt}(200)$.

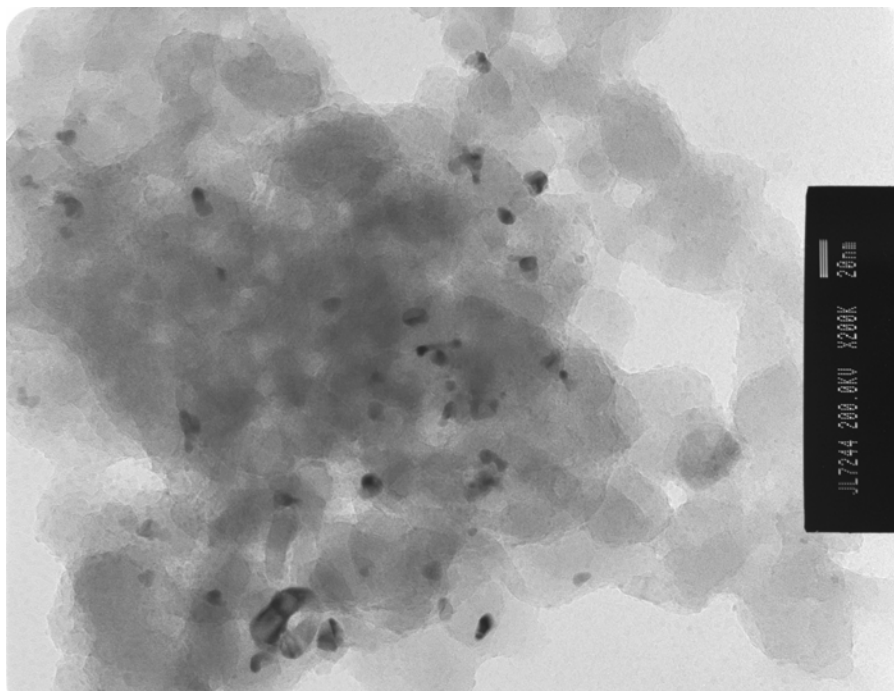


Figure 7-1: TEM micrograph of a freshly reduced sample Pt/SiO₂. The picture was taken at a magnification of 200,000. The white vertical bar in the legend corresponds to 20 nm.

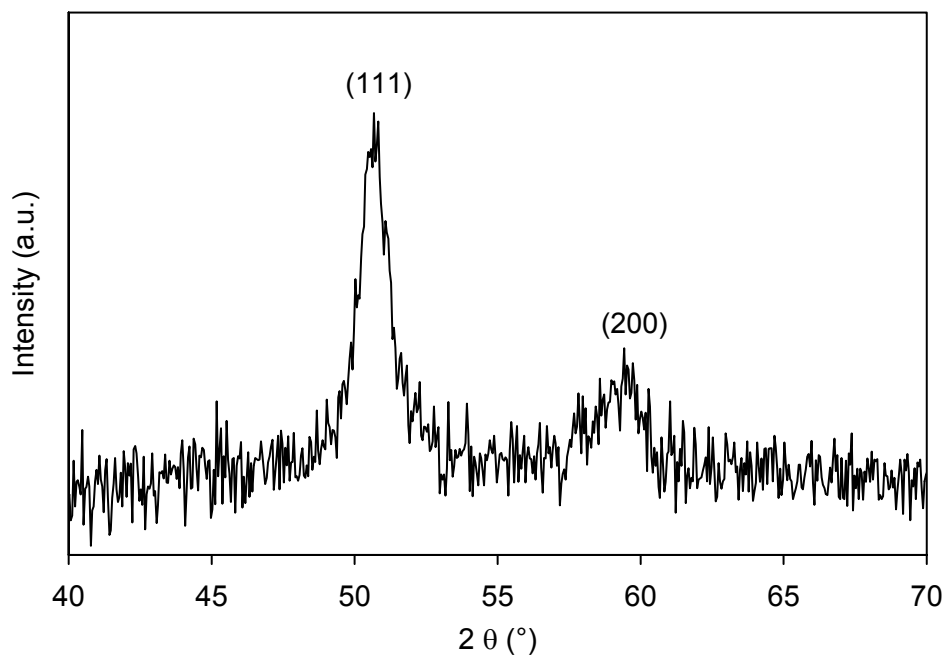


Figure 7-2: X-ray diffraction pattern of sample Pt/SiO₂. The pattern of SiO₂ has been subtracted.

The XRD line broadening analysis was performed with the Pt(111) peak at a 2θ value of 50.7° . The average Pt particle size was calculated using the Scherrer equation (given in Annex 1). The full width at half maximum (FWHM) was determined using the Profit software from Philips (version 1.0c, 1996).

The resulting average particle size of the freshly reduced sample is 10.1 nm. This value is in good agreement with the value of 12.7 nm determined by TEM analysis. The small difference between the sizes determined using XRD and TEM could be explained by the difference of the total number of platinum particles taken into account for the calculations. Using XRD line broadening analysis, the average Pt particle size is determined from a higher total number of particles than in the TEM study.

7.3.2 Influence of the oxygen concentration

Figure 7-3 reports the conversion of 500 ppm NO in various concentrations of O_2 as a function of temperature. At all O_2 concentrations, a maximum of conversion is observed at $\approx 300^\circ C$. Above $300^\circ C$, the conversion decreases due to the thermodynamic equilibrium. As may be observed in chapter 2, Figure 2-1, the ratios NO_2/NO_x given by the thermodynamic equilibrium are depending on the concentrations of O_2 in the gas phase. This explains the difference of conversion observed above $300^\circ C$ in the various O_2 feed concentrations.

In the temperature range between 150 and $250^\circ C$, the reaction is limited kinetically. At the highest O_2 concentrations, the conversion increases sharply with increasing temperatures. The increase in conversion with temperature is much slower at low O_2 concentrations.

Figure 7-4 shows the influence of the O_2 feed concentration on the oxidation rate at 150, 175 and $200^\circ C$. For O_2 concentrations below 10 %, the reaction rate increases with increasing concentrations of oxygen. Above 20 % O_2 in the feed, the reaction rate levels off. From the values of the oxygen concentrations in the feed and of the reaction rates, an apparent reaction order α for O_2 was found to be 0.51 at $150^\circ C$, and 0.36 at both temperatures of 175 and $200^\circ C$.

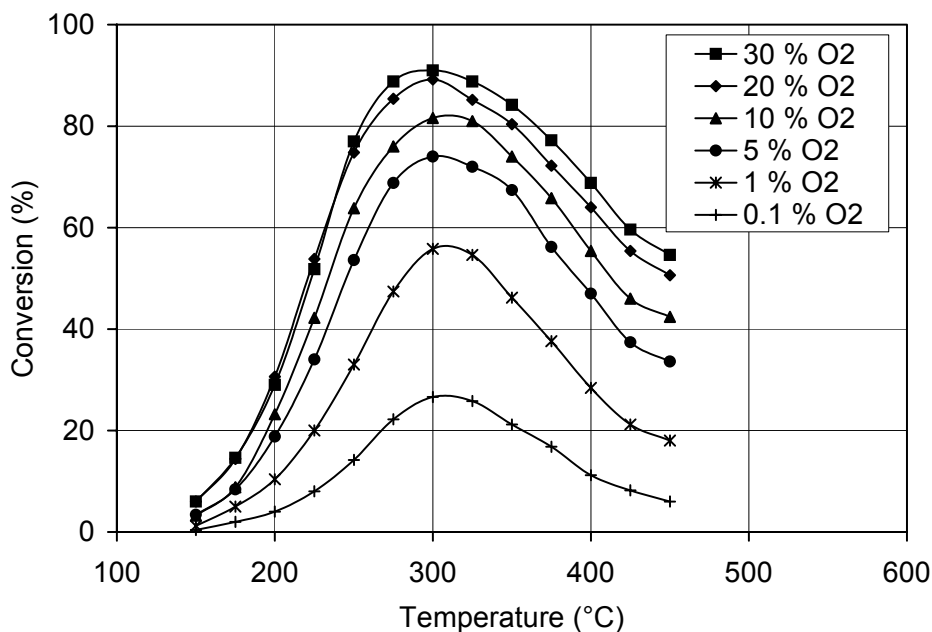


Figure 7-3: Influence of the concentration of O₂ on the conversion of NO on Pt/SiO₂ as a function of temperature. Sample weight = 0.8 g, V* = 150 L_N/h, feed: 500 ppm NO, 0.1 - 30 % O₂, 5 % H₂O, and balance N₂.

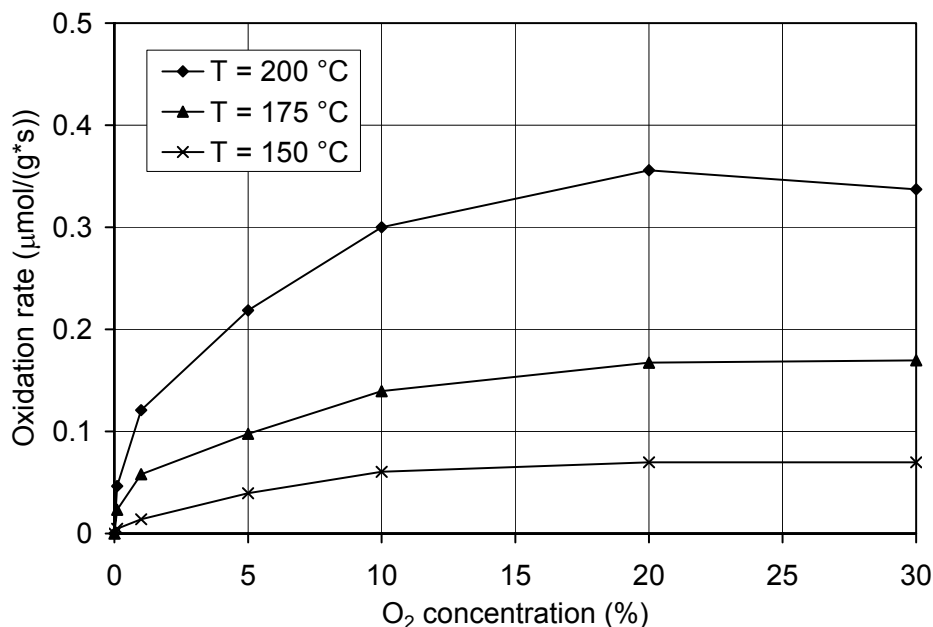


Figure 7-4: Influence of the oxygen concentration on the reaction rate of NO oxidation at 150, 175 and 200 °C. Sample weight = 0.8 g, V* = 150 L_N/h, feed: 500 ppm NO, 0.1 - 30 % O₂, 5 % H₂O, and balance N₂.

7.3.3 Influence of the NO concentration

Figure 7-5 shows the conversion at various NO concentrations as a function of temperature. In these catalytic tests, the O_2 feed concentration was 10 %. The conversion traces again a parabolic curve with the maximum of conversion depending on the NO concentration. For a concentration of 100 ppm NO, the maximum is observed at 275 °C. At higher concentrations of NO, the maximum of conversion is shifted to higher temperatures. Experimental values of conversion exceeding the theoretical equilibrium values may be attributed to experimental errors of the temperature measurement.

Between 150 and 300 °C, the conversion of NO to NO_2 decreases with increasing concentrations of NO. At 200 °C for example, the conversion at 100 ppm NO is 55 %, but only 12 % at 1000 ppm NO.

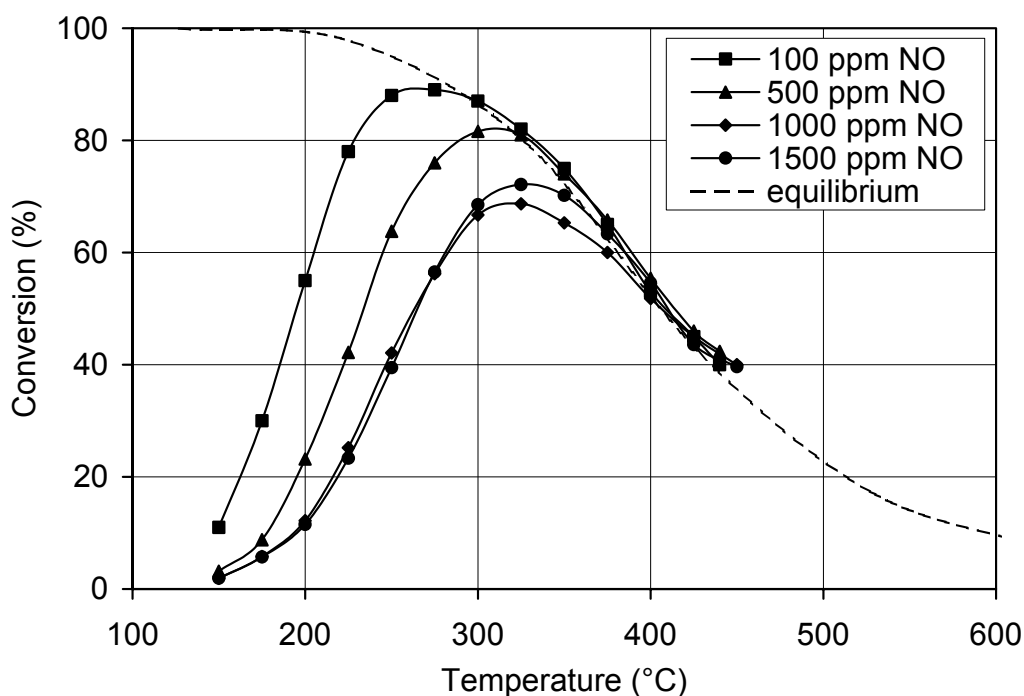


Figure 7-5: Conversion of various concentrations of NO in a humid feed on Pt/SiO_2 as a function of temperature. Sample weight = 0.8 g, $V^* = 150 \text{ L}_N/\text{h}$, feed: 100 - 1500 ppm NO, 10 % O_2 , 5 % H_2O , and balance N_2 .

Figure 7-6 depicts the influence of the NO feed concentration on the oxidation rate at 150, 175, and 200 °C. It can be observed that the rate increases for NO concentrations between 100 and 500 ppm. Above 500 ppm, the increase of the rate is much less pronounced. The apparent reaction order for NO was calculated using the values of conversion below 30 %. The apparent reaction order β for NO was found to be 0.3 and 0.29 at 150 and 175 °C, respectively. At 200 °C, its value was 0.36.

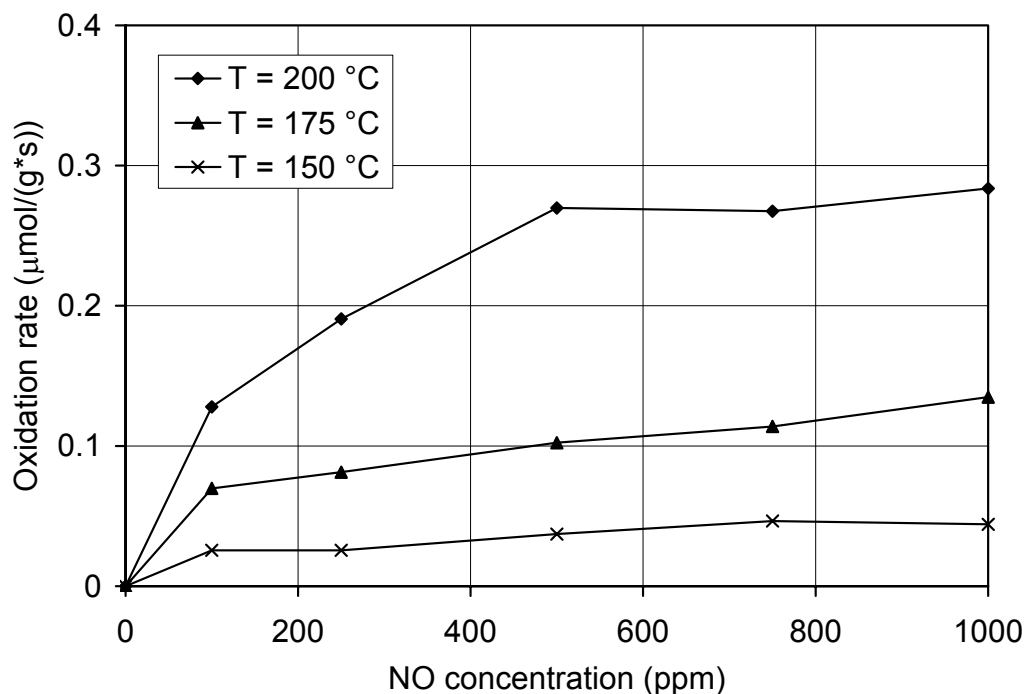


Figure 7-6: Influence of the concentration of nitric oxide on the reaction rate of NO oxidation at 150, 175 and 200 °C. Sample weight = 0.8 g, $V^* = 150 \text{ L}_N/\text{h}$, feed: 0 - 1000 ppm NO, 10 % O_2 , 5 % H_2O , and balance N_2 .

7.3.4 Influence of water

The oxidation of NO was investigated in a feed consisting of 500 ppm NO and 10 % O_2 under dry and humid (5 % H_2O) conditions. The influence of water was also studied with 20 and 30 % O_2 in the gas feed. Table 7-1 gives the conversions measured at 150, 175, and 200 °C. With 10 % O_2 in the feed, the conversion is almost identical under dry and humid conditions. However, with 20 and 30 % O_2 , the conversion is slightly higher in a dry feed than in a humid feed.

Table 7-1: Conversion of NO in dry and humid feeds as a function of O₂ feed concentration.

T (°C)	O ₂ (%)	Conversion ^{a)}	
		Dry feed	Humid feed ^{b)}
150	10	5.0	5.6
	20	8.8	6.0
	30	9.6	6.0
175	10	14.0	13.6
	20	21.0	14.4
	30	18.8	14.6
200	10	29.6	29.2
	20	40	30.6
	30	41.8	29.0

^{a)} NO concentration = 500 ppm.

^{b)} H₂O concentration = 5 %.

The oxidation of varying concentrations of NO in a dry feed was also investigated. For this study, the O₂ feed concentration was 10 %. Figure 7-7 shows the conversion over Pt/SiO₂ as a function of temperature. It can be seen that the conversion of NO decreases again with increasing concentrations of NO. This behavior has already been observed in humid conditions. It indicates that water is not responsible for the decreasing conversions at increasing NO feed concentrations.

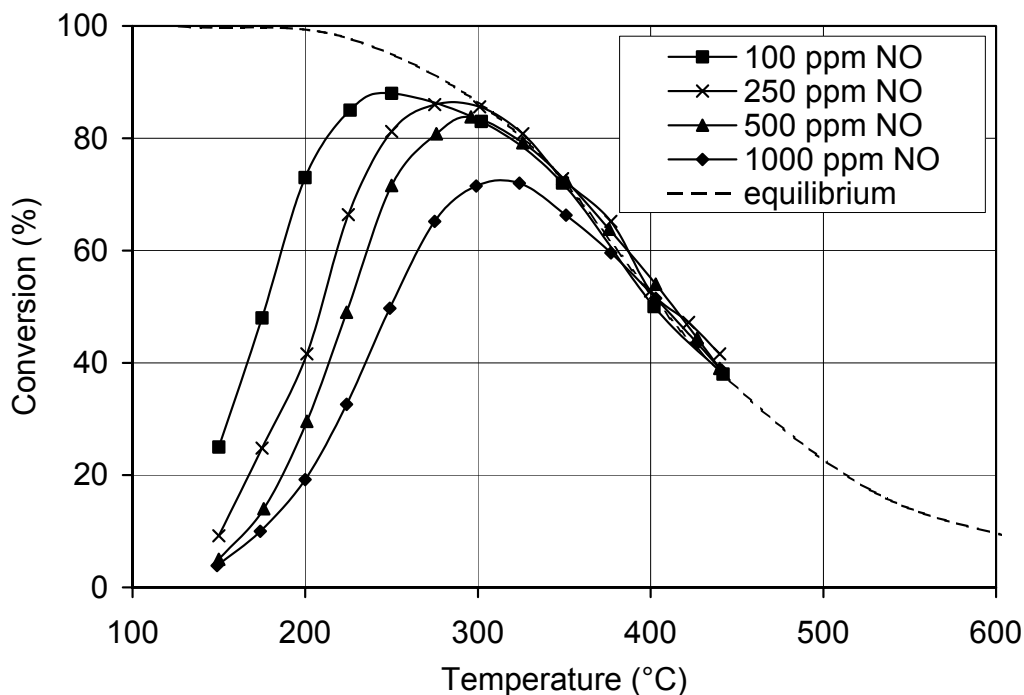


Figure 7-7: Conversion of various concentrations of NO in a dry feed on Pt/SiO₂ as a function of temperature. Sample weight = 0.8 g, V* = 150 L_N/h, feed: 100 - 1000 ppm NO, 10 % O₂, and balance N₂.

7.3.5 Influence of the NO₂ concentration

The oxidation of 500 ppm NO was studied in the presence of various concentrations of NO₂ in the base feed. The O₂ concentration was kept constant at 10 %. Figure 7-8 displays the concentrations of NO and NO₂ as a function of temperature for NO_x feeds consisting of 500 ppm NO (referred to as feed 1) and of 500 ppm NO + 100 ppm NO₂ (referred to as feed 2). Figure 7-9 compares the NO_x concentrations measured for feed 1 and for a NO_x feed consisting of 500 ppm NO + 500 ppm NO₂ (referred to as feed 3).

In feed 1, the highest concentrations of NO₂ are observed at 300 °C, whereas it is observed at 325 °C in feed 2. At higher temperatures, the concentrations of NO₂ and NO are fixed by the thermodynamic equilibrium. The different concentrations of NO₂ observed for feed 1 and feed 2 are due to the different total NO_x concentrations. For feed 1, it amounts to 500 ppm NO_x. For feed 2, it amounts to 600 ppm NO_x.

In feed 2, the concentration of NO_2 behind catalyst is 100 ppm at 150 °C. At the same temperature, the concentration of NO is about 500 ppm NO. It indicates that, at 150 °C, NO is not oxidized in feed 2. Between 150 and 300 °C, it can be seen that the conversion is inhibited by the presence of NO_2 in the feed.

A similar behavior has been observed for feed 3 containing 500 ppm NO and 500 ppm NO_2 (Figure 7-9). Between 150 and 200 °C, the concentrations of NO and NO_2 behind catalyst are 500 ppm each, thus indicating the absence of NO oxidation. On the other hand, it can be seen that NO_2 is already produced in the temperature range 150 – 200 °C when the NO_x feed contains only NO (feed 1). Between 200 and 325 °C, the concentration of NO decreases, thus showing the oxidation of NO in both feeds 1 and 3.

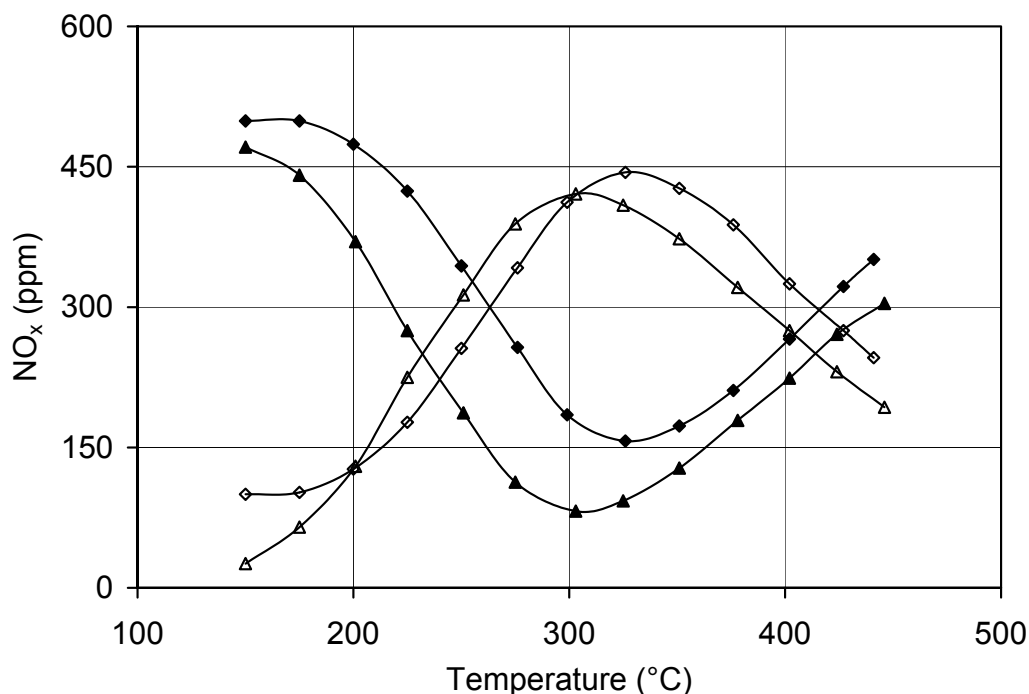


Figure 7-8: Concentrations of NO (full symbols) and NO_2 (open symbols) during NO oxidation. Feed 1 (triangles): 500 ppm NO in base feed, feed 2 (diamonds): 500 ppm NO and 100 ppm NO_2 in base feed.

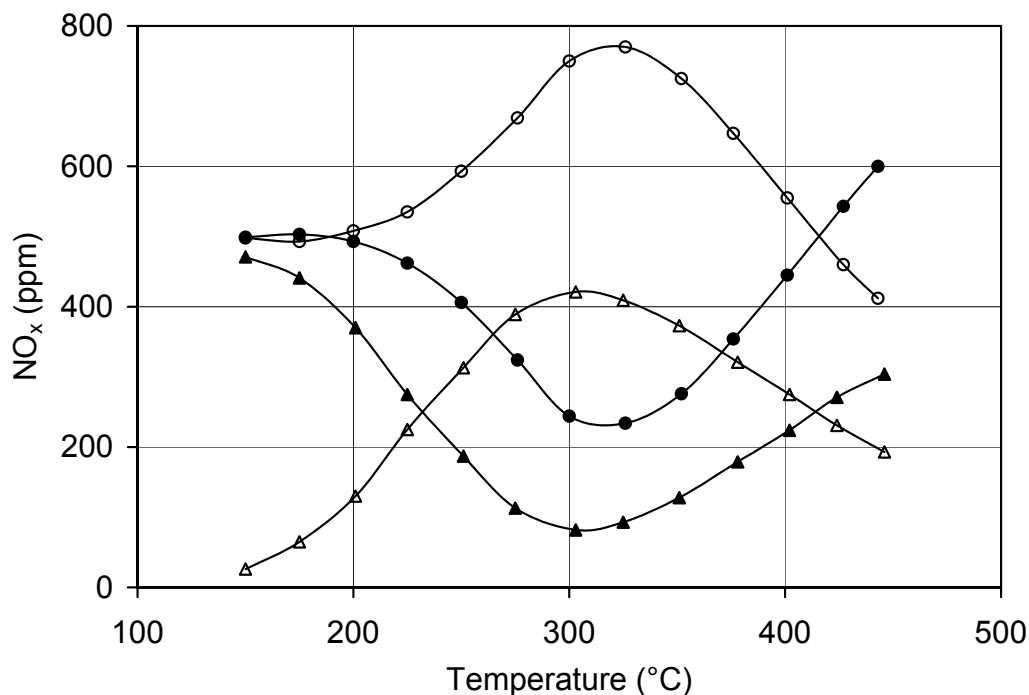


Figure 7-9: Concentrations of NO (full symbols) and NO₂ (open symbols) during NO oxidation. Feed 1 (triangles): 500 ppm NO in base feed, feed 3 (spheres): 500 ppm NO and 500 ppm NO₂ in base feed.

Figure 7-10 shows the conversion of NO at 200 and 225 °C evaluated according to equation (7.2) as a function of the inlet concentration of NO₂. The influence of NO₂ on the conversion is not reported for 150 and 175 °C because, at these low temperatures, the oxidation of NO is completely suppressed when NO₂ is added to the feed. At 200 and 225 °C, a decrease in conversion is observed at increasing concentrations of NO_{2,in}. At 225 °C, for NO_{2,in} = 0, the conversion is 41 %. If the oxidation test is performed with NO_{2,in} equals to 100 ppm, the conversion at 225 °C drops to 15 %. A similar drop in conversion is observed at 200 °C. The addition of a small quantity of NO₂ to the feed proved to have a strong inhibiting effect on the oxidation of NO. Attempts to find the reaction order for NO₂ were not successful because the plot (ln r) versus (ln c_{NO_{2,in}}) did not show a linear dependence. The difficulties regarding this estimation probably arise from the fact that NO₂ is also produced during the reaction itself.

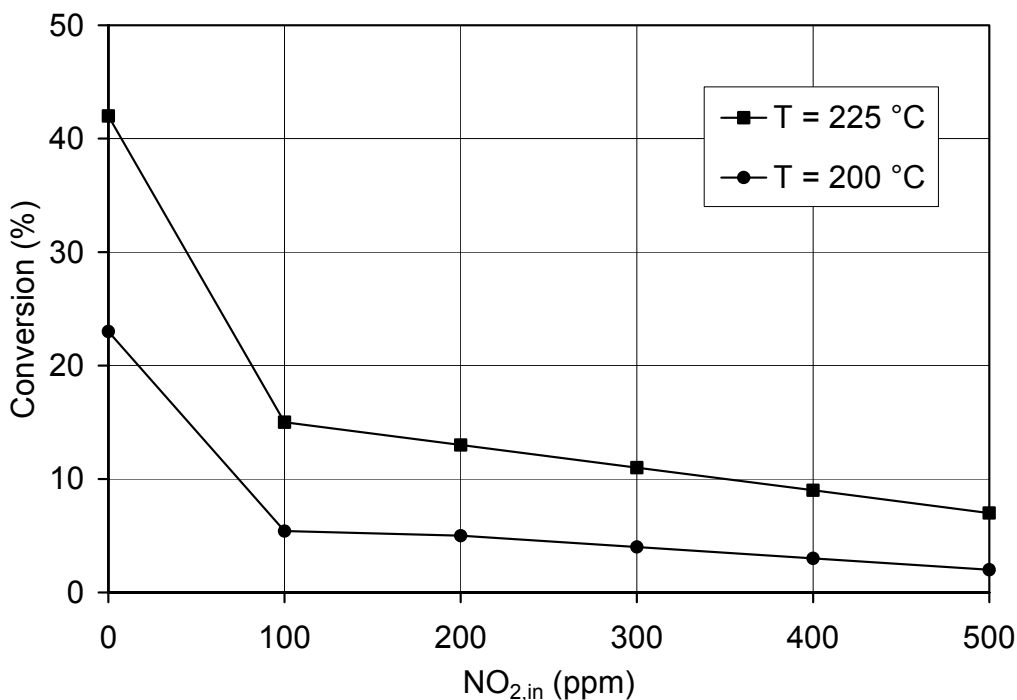


Figure 7-10: Influence of NO_2 on the conversion of NO at 200 and 225 °C. Sample weight = 0.8 g, $V^* = 150\text{ L}_\text{N}/\text{h}$, feed: 500 ppm NO, 10 % O_2 , 0 - 500 ppm NO_2 , 5 % H_2O , and balance N_2 .

7.4 Discussion

At constant temperature and constant NO feed concentration, the oxidation of NO first increases at increasing O_2 feed concentrations. Then, at oxygen feed content higher than 10 %, it levels off. Results obtained at low temperatures reflect a saturation effect with increasing oxygen feed concentration. This is consistent with the adsorption of oxygen on platinum. When the adsorption sites are saturated with oxygen, increasing the O_2 concentration will no longer enhance the reaction rate. Due to the dissociative adsorption of oxygen on platinum at the investigated temperatures (150 - 450 °C) [1], the reaction order for O_2 should be about 0.5. This value was found at the temperature of 150 °C. However, a lower reaction order was found at 175 and 200 °C. This shows that the reaction rate depends less on the oxygen feed concentrations at higher temperatures.

At constant temperature and at constant O₂ feed concentration, the conversion of NO is highest at low concentrations of NO and decreases with increasing NO feed concentration. The decrease is most pronounced if NO_{in} is below 500 ppm. This behavior has been observed in both dry and humid feeds. This influence of NO concentrations on the oxidation rate was not expected. In the literature, the mechanism proposed by Burch et al. [2] and by Olsson et al. [3] is an Eley-Rideal mechanism where oxygen reacts from an adsorbed state and NO reacts from the gas phase according to reaction (7.6):



In this case, the conversion should not depend on the concentration of NO, and the reaction order should be approximately 1. However, in our study, a fractional reaction order was found. A Langmuir-Hinshelwood mechanism with NO and oxygen adsorbing on platinum could explain the order lower than 1. However, such a mechanism seems very unlikely due to the fact that the Pt-NO bond is very weak compared to the Pt-O bond [4]. However, the influence of the concentration of NO could be explained by the inhibiting effect of NO₂ on the oxidation of NO.

At constant concentrations of oxygen and NO in the feed, the addition of NO₂ strongly inhibits the conversion of NO. J. Seifert [5] observed a similar inhibition effect of NO₂ on the NO oxidation over MnO₂/FeO₃ in dry feeds. This inhibition by NO₂ could explain the negative effect of rising NO concentrations in the feed (reaction order lower than 1). At low NO concentrations, the concentrations of NO₂ produced are small. For example, with NO_{in} = 100 ppm, only 55 ppm NO₂ are formed at 200 °C. The effect of these low NO₂ concentrations on the oxidation of NO is then weak. However, if higher input concentrations of NO are used, higher concentrations of NO₂ will be produced. This will cause in an increasing inhibition of the oxidation reaction.

The inhibition of the reaction by NO₂ can be attributed to the formation of strongly bound species at the catalyst surface. Xue et al. [6] analyzed the sample of Pt/SiO₂ after the oxidation reaction using X-ray electron spectroscopy. The catalytic tests were performed in the presence of SO₂. They concluded that surface species of the type [N_x-S_y-O_x] are formed at the platinum surface.

Another explanation is the formation of platinum oxides due to the dissociation of NO₂ on platinum. Studies of the interaction of NO₂ with model surfaces such as Pt(111) have shown that NO₂ easily dissociates into NO and atomic oxygen [7]. The dissociation of NO₂ leads to an increase of the oxygen coverage. Additional experiments to support this mechanism of deactivation will be presented in chapter 8.

7.5 Conclusions

The catalytic tests have shown that the oxidation of NO over Pt/SiO₂ depends strongly on the concentration of O₂ and NO in the feed. The presence of water in the feed has only a minor influence on the kinetics of the reaction. At oxygen concentrations below $\approx 10\%$, a strong dependence of the conversion on oxygen concentration is observed. However, above 10 % O₂, only a minor dependence is found. This is consistent with the reaction of oxygen from an adsorbed state. It has also been found that increasing concentrations of NO will lower the conversion. This behavior could be explained by the increasing concentrations of NO₂ produced by the reaction at increasing concentrations of NO and an inhibiting effect of NO₂ on the oxidation reaction.

7.6 References

- [1] C.T. Campbell, G. Ertl, H. Kuipers and J. Segner, *Surf. Sci.* **107** (1981), 220
- [2] R. Burch and T.C. Watling, *J. Catal.* **169** (1997), 45
- [3] L. Olsson, B. Westerberg, H. Persson, E. Fridell, M. Skodlundh and B. Andersson, *J. Phys. Chem B* **103** (1999), 10433
- [4] M.E. Bartram, B.E. Koel and E.A. Carter, *Surf. Sci.* **219** (1989), 467
- [5] J. Seifert, *Untersuchung der heterogen katalysierten NO-Oxidation in einer rechnergesteuerten, echtzeitkontrollierten Versuchsanlage*, Thesis, Erlangen (1989)
- [6] E. Xue, K. Seshan, J.G. Oommen and J.R.H. Ross, *Appl. Catal. B: Environ.* **2** (1993), 183

- [7] J. Segner, W. Vielhaber and G. Ertl, *Israel. J. Chem.* **22** (1982), 375

Deactivation and regeneration of Pt/SiO₂

8.1 Introduction

Platinum catalyst supported on silica showed the best activity for the oxidation of NO at low temperatures. These results prompted us to investigate the kinetics of the oxidation of NO over the catalyst Pt/SiO₂ (chapter 7). However, with increasing number of catalytic tests at various NO feed concentrations, the activity of Pt/SiO₂ decreased. Figure 8-1 shows the conversion of 500 ppm NO measured over the freshly reduced sample and over the used sample. It can be seen that the catalyst suffered from deactivation during the reaction. Xue et al. [1] also observed the deactivation of Pt/SiO₂ during the oxidation of NO. Therefore, investigations were carried out to understand the mechanism of deactivation, and strategies to regenerate the catalyst were investigated.

In our investigations, the gas feed consists of N₂, H₂O, O₂ and NO. The concentration of oxygen in the feed (typically 10 %) is much higher than the concentration of NO (e.g. 500 ppm). During the reaction, nitrogen dioxide is produced on the oxidation catalyst. We have shown in chapter 7 that NO₂ has an inhibiting effect on the oxidation of NO, probably due to its strong oxidizing properties [2]. Olsson and Fridell [3] observed the oxidation of platinum to platinum oxide by NO₂. Therefore, it was necessary to investigate the effect of pretreatments in feeds containing O₂, or both O₂

and NO_2 . Other investigations focused on the effect of the pretreatment temperature and of the pretreatment time in feeds containing NO_2 . After pretreatment, the samples were analyzed using X-ray photoelectron spectroscopy.

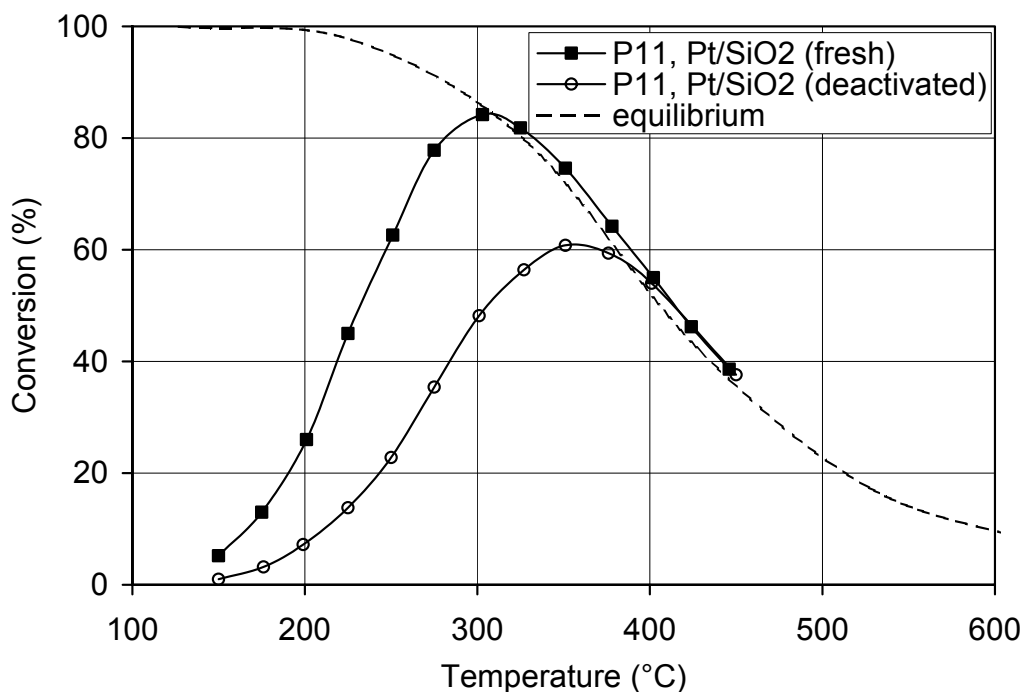


Figure 8-1: Conversion of NO over freshly reduced and used samples of Pt/SiO_2 . Sample weight = 0.8 g. $V^* = 150 \text{ L}_\text{N}/\text{h}$, feed: 500 ppm NO, 10 % O_2 , 5 % H_2O , and balance N_2 . Positive deviations of the NO conversion to the thermodynamic equilibrium can be attributed to the limited accuracy of the temperature measurements.

8.2 Experimental

8.2.1 Catalyst sample

The sample of Pt/SiO_2 with 2.5 w.% Pt was prepared in house according to the recipe described in chapter 6. This sample was referred to as sample **P11**.

8.2.2 Pretreatments of the samples

The reduced samples were pretreated using the following conditions:

- Pretreatment A: at 440 °C for 2 h in a feed consisting of 10 % O₂, 5 % H₂O and balance N₂ (denoted as base feed in the following).
- Pretreatment B: at 250 °C for 2 h in a feed consisting of 500 ppm NO₂ in the base feed.
- Pretreatment C: at 250 °C for 6 h in a feed consisting of 500 ppm NO₂ in the base feed.

In order to investigate the influence of pretreatment temperature, Pt/SiO₂ was pretreated at 150, 250, 350 and 450 °C for 6 hours in the base feed with 500 ppm NO₂.

8.2.3 Experimental setup and oxidation tests

The experimental setup has been described in chapter 3. The catalytic tests were performed in the stainless steel reactor having an internal diameter of 16 mm. The tests were performed with 0.8 g of Pt/SiO₂ at a flow rate of 150 L_N/h with a feed consisting of 500 ppm NO, 10 % O₂, 5 % H₂O, and balance N₂.

8.2.4 X-ray photoelectron spectroscopy measurements

XPS spectra were recorded with an ESCALAB 220i XL (Thermo VGScientific), using non-monochromatic Mg K α radiation at 300 W. The apparatus has been described in chapter 3. In order to correct for the sample charging, binding energies were referred to the peak of Si 2p at 103.5 eV. The composition of the samples was determined by quantitative analysis using the cross sections given by Scofield [4].

The XPS investigations were carried out on the freshly reduced Pt/SiO₂ and samples after pretreatments. Pt/SiO₂ was pretreated in the reactor at the conditions described previously and then transferred to the spectrometer.

8.3 Results

8.3.1 Oxidation of NO over reduced and pretreated samples

Figure 8-2 shows the conversion of NO to NO₂ over the freshly reduced sample and after pretreatment. After pretreatment A at 440 °C in the base feed, the sample has the same activity as the freshly reduced sample. However, pretreatment B at 250 °C with 500 ppm NO₂ leads to a lower conversion.

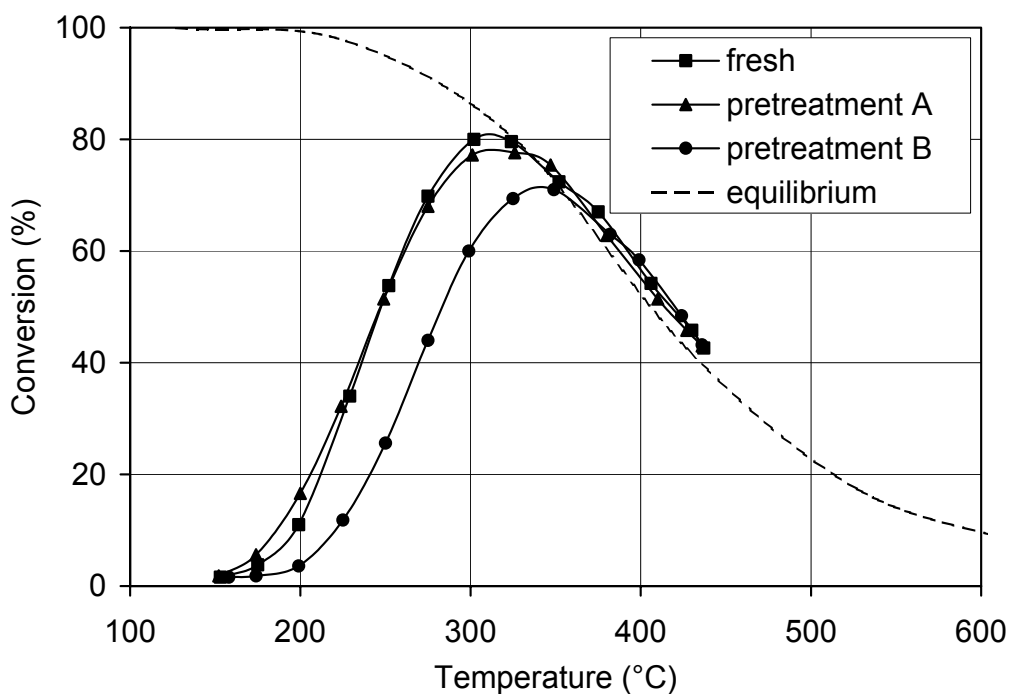


Figure 8-2: Oxidation of NO over reduced and pretreated samples. Sample weight = 0.8 g, $V^* = 150 \text{ L}_N/\text{h}$, feed: 500 ppm NO, 10 % O₂, 5 % H₂O, and balance N₂.

8.3.2 Pretreatment with NO₂

The effect of NO₂ on the activity of Pt/SiO₂ was further investigated for pretreatments of varying duration and temperature.

Influence of pretreatment duration

The deactivation of Pt/SiO₂ was investigated for an increased pretreatment time of 6 hours (pretreatment C) at 250 °C in the base feed containing 500 ppm NO₂. After pretreatment C, the conversion of NO measured at 200 °C was 3 %, whereas the conversion was 4 % after pretreatment B. Therefore, the sharpest drop of the conversion is observed after the pretreatment B for 2 hours.

Influence of pretreatment temperature

The oxidation of NO was investigated with samples pretreated for 6 hours at 150, 250, 350 and 450 °C in the base feed containing 500 ppm NO₂. The catalytic tests were performed between 150 and 450 °C. Figure 8-3 shows the conversion of NO at 200 °C as a function of the pretreatment temperature. The strongest deactivation is observed after a pretreatment at 250 °C. On the other hand, the pretreatments at 150 and 450 °C have no effect on the conversion. For the pretreatment temperature of 350 °C, the deactivation is less prominent.

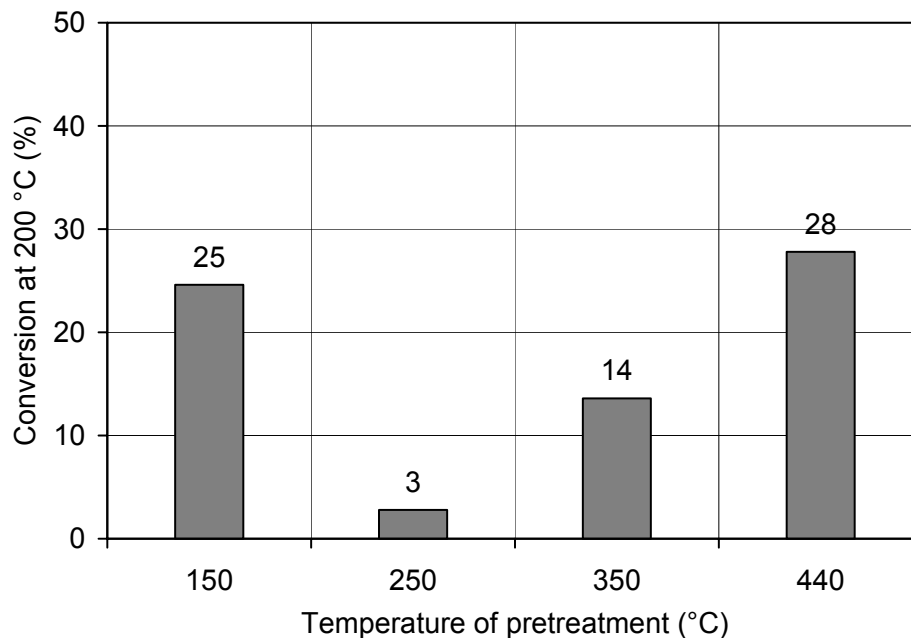


Figure 8-3: Influence of pretreatment temperature on the oxidation of NO at 200 °C. Feed during pretreatment (6 hours): 500 ppm NO₂ + base feed. Feed during oxidation: 500 ppm NO + base feed.

Table 8-1 gives the efflux concentrations of NO and NO₂ measured at steady state during the pretreatments with NO₂ in the feed. These concentrations were reached about 4 minutes after NO₂ was added to the feed. The concentrations of NO and NO₂ expected from the equilibrium are also given in Table 8-1. At 150 and 250 °C, the efflux concentration of NO₂ is 500 ppm. However, during the pretreatment at higher temperatures, the NO₂ concentration decreases with increasing temperature. Conversely, the relative amount of NO in the feed increases from 20 % at 350 °C to 60 % at 450 °C. The concentrations of NO and NO₂ are close to the values given by the thermodynamic equilibrium.

Table 8-1: Concentrations of NO and NO₂ measured during the pretreatment and expected from the thermodynamic equilibrium. Feed: 500 ppm NO₂, 10 % O₂, 5 % H₂O, and balance N₂.

T (°C)	NO _x concentration measured during pretreatment ^{a)}		NO _x concentrations according to equilibrium ^{b)}	
	NO ₂ (ppm)	NO (ppm)	NO ₂ (ppm)	NO (ppm)
150	500 (100 %)	0 (0 %)	500 (100 %)	0 (0 %)
250	500 (100 %)	0 (0 %)	475 (95 %)	25 (5 %)
350	400 (80 %)	100 (20 %)	360 (72 %)	140 (28 %)
450	200 (40 %)	300 (60 %)	180 (36 %)	320 (64 %)

^{a)} concentrations at steady state.

^{b)} extrapolated from Figure 2-5 in chapter 2.

Hysteresis effect

The catalytic tests with the sample pretreated for six hours were first performed with increasing temperatures from 150 to 450 °C. Subsequently, the oxidation of NO was determined with decreasing temperatures from 450 to 150 °C. As may be seen in Figure 8-4, the conversion with increasing temperatures is lower than the conversion with decreasing temperatures. Therefore, a hysteresis over the pretreated sample can be observed when the temperature is cycled up and down. A similar effect was observed over the sample pretreated for 2 hours.

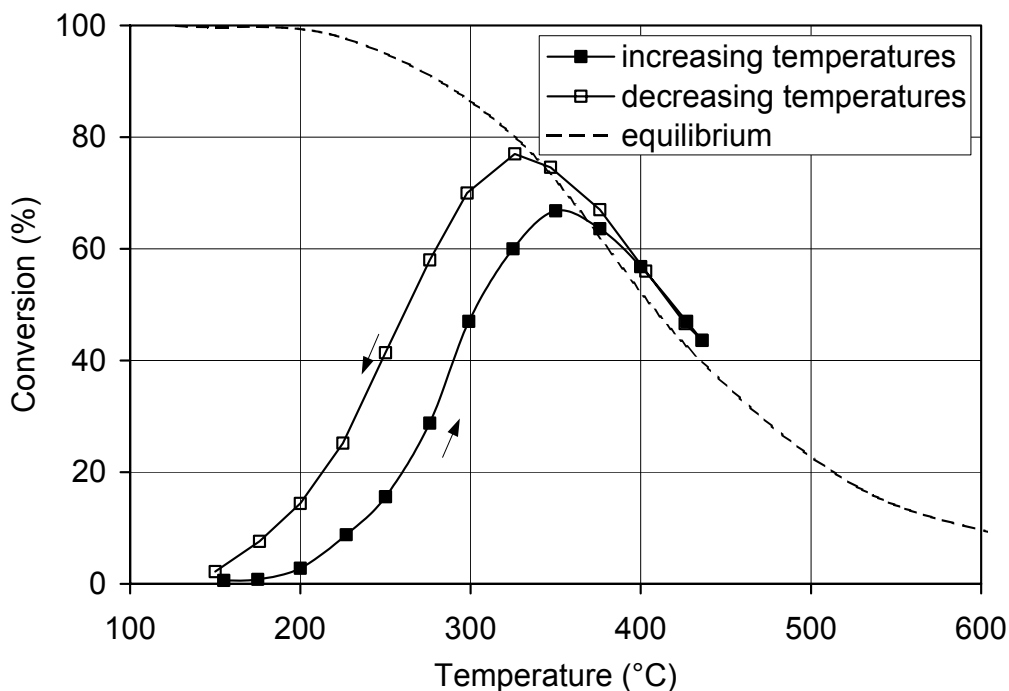


Figure 8-4: Hysteresis in NO conversion over Pt/SiO₂ pretreated at 250 °C. Feed during pretreatment C (6 hours): 500 ppm NO₂ + base feed. Feed during oxidation: 500 ppm NO + base feed.

8.3.3 Regeneration of the samples

Various strategies were tested to restore the initial activity of the sample after deactivation. Before applying a regeneration procedure, the sample of Pt/SiO₂ was pretreated at 250 °C for 2 hours in a feed consisting of 500 ppm NO₂ and base feed (pretreatment B).

Thermal regeneration

The deactivated sample was regenerated in an oven at various temperatures ranging from 450 to 650 °C. The regeneration was performed in static air for 1 hour. Figure 8-5 shows the performance of Pt/SiO₂ after regeneration at 650 °C. Lower temperatures than 650 °C were not sufficient to restore the initial activity.

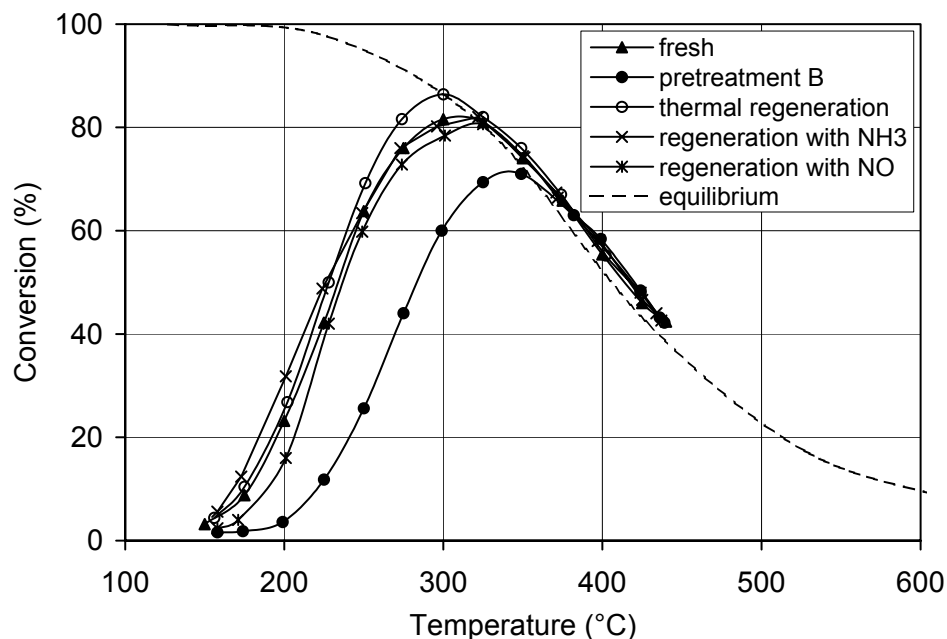


Figure 8-5: Oxidation of NO over freshly reduced sample, after pretreatment with NO₂ and after regeneration. Sample weight = 0.8 g, V* = 150 L_N/h, feed: 500 ppm NO, 10 % O₂, 5 % H₂O, and balance N₂.

Regeneration under reducing conditions

As shown also in Figure 8-5, the pretreated sample was also fully regenerated at 250 °C for 1 hour in a feed consisting of 200 ppm NH₃ and balance N₂. Figure 8-6 shows the consumption of NH₃ during the first minutes of the regeneration. The total NH₃ consumed amounts to 105 μmol/g_{cat}. However, a part of NH₃ may also have reacted on the wall of the reactor. During the regeneration, a formation of N₂O and NO was not observed. Therefore, NH₃ must have been oxidized to N₂, which is not detectable by the IR gas analyzer.

NO can also be used as a reducing agent to regenerate the sample. The regeneration of Pt/SiO₂ was performed at 250 °C for one hour in a feed consisting of 200 ppm NO, 5 % H₂O and balance N₂. Figure 8-7 shows the evolution of NO and NO₂ during the first minutes of the regeneration. The formation of NO₂ is observed, indicating the oxidation of NO in the absence of oxygen in the feed. The consumption of NO amounts to 130 μmol/g_{cat}, and the amount of NO₂ formed is 93 μmol/g_{cat}. Figure 8-5 shows the activity of Pt/SiO₂ after regeneration in the feed containing NO. The regenerated sample shows the same activity as the freshly reduced sample.

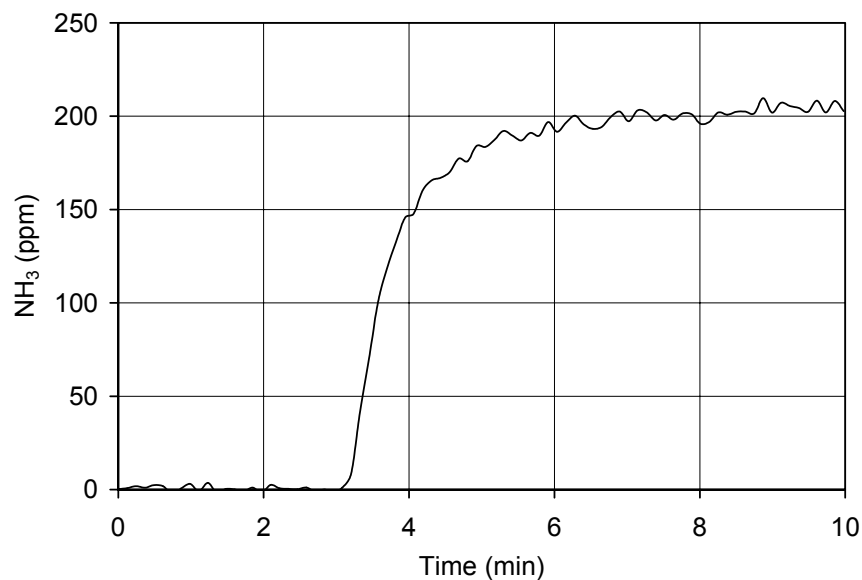


Figure 8-6: Evolution of NH_3 during the regeneration of samples pretreated with NO_2 (pretreatment B). Sample weight = 0.8 g, $V^* = 150 \text{ L}_\text{N}/\text{h}$, $T = 250 \text{ }^\circ\text{C}$, feed: 200 ppm NH_3 in N_2 .

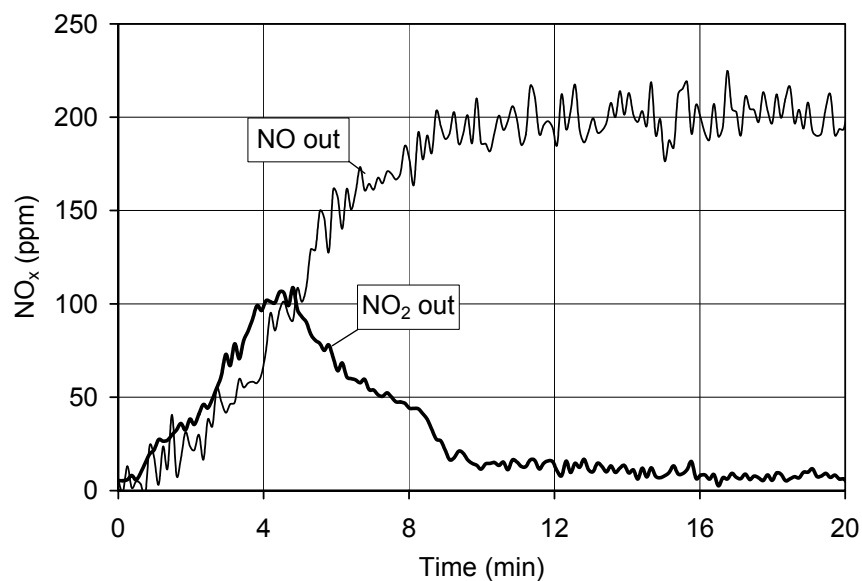


Figure 8-7: Evolution of NO_x during the regeneration with NO of samples pretreated with NO_2 (pretreatment B). Sample weight = 0.8 g, $V^* = 150 \text{ L}_\text{N}/\text{h}$, $T = 250 \text{ }^\circ\text{C}$, feed: 200 ppm NO , 5 % H_2O , and balance N_2 .

8.3.4 XPS analysis

The XPS spectra of the freshly reduced sample Pt/SiO₂ and after various pretreatments are shown in Figure 8-8. The binding energies (BE) indicating the peak position of Pt 4f_{5/2} and Pt 4f_{7/2} are listed in Table 8-2. The BE values for the sample after reduction are slightly higher than the values characteristic of bulk platinum due to the low coverage of platinum [5]. After pretreatment A in the feed containing O₂ at 450 °C, the BE values remain unchanged. The XPS spectrum after pretreatment B at 250 °C in the feed containing both O₂ and NO₂ does not show significant change of the Pt 4f peak. Even the longer pretreatment of 12 hours does not influence the binding energies. The intensity ratio between the XPS signal from Pt and the XPS signal from SiO₂ is ≈0.045 and is constant for all pretreatments.

Table 8-2: XPS data of freshly reduced Pt/SiO₂ and after pretreatments.

Samples	Pretreatment	Binding energies (eV)		I (Pt 4f)/ I (Si 2p)	d _{Pt} ^{a)} (nm)
		Pt 4f _{5/2}	Pt 4f _{7/2}		
Pt		74.60 ^{b)}	71.20 ^{b)}	-	-
PtO		75.60 ^{b)}	72.30 ^{b)}	-	-
Pt/SiO ₂ (P11)	Reduction	74.80	71.60	0.045	7.0
	Oxidation in O ₂ ^{c)}	74.75	71.40	0.046	6.8
	Oxidation in O ₂ +NO ₂ (2h) ^{d)}	75.00	71.50	0.049	6.8
	Oxidation in O ₂ +NO ₂ (12h)	74.75	71.4	0.048	6.7

^{a)} platinum particle size d_{Pt} determined using the model of Kerkhof and Moulijn [6].

^{b)} from reference [7].

^{c)} pretreatment A.

^{d)} pretreatment B.

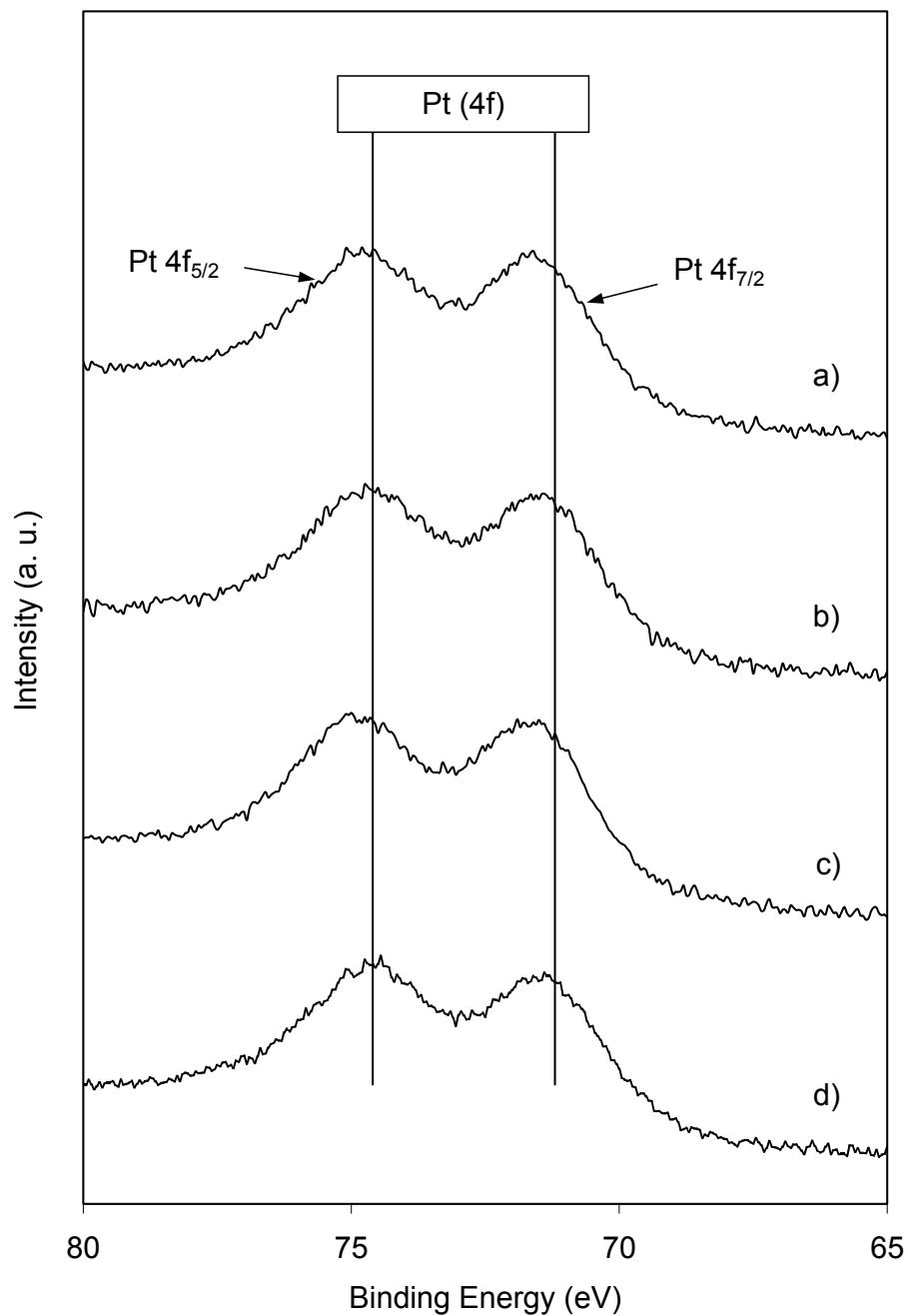


Figure 8-8: XPS spectra of the Pt 4f core-level of Pt/SiO₂: a) freshly reduced, b) after pretreatment A at 450 °C in the base feed, c) after pretreatment B at 250 °C with NO₂ and base feed, d) after pretreatment for 12 h at 250 °C in the same feed as pretreatment B.

In order to check if the observed deactivation by NO₂ can be attributed to a change of the size of the platinum particles, their size was estimated from the XPS intensities using the model of Kerkhof and Moulijn [6] described in Annex 1. The model compares the experimental value of I_{Pt}/I_{Si} (reported in Table 8-2) with the ratio I_{Pt}/I_{Si} expected for a monolayer of platinum. If the experimental value is lower than the theoretical ratio for a monolayer, platinum is in the form of particles. The ratio I_{Pt}/I_{Si} for a monolayer was calculated using the following data:

- The BET surface area (S_{SiO_2}) and the density (ρ_{SiO_2}) of silica are 160 m²/g and 2.2·10⁶ g/m³ [8] respectively. The escape depth of electrons from silica (λ_{SiO_2}) is 3.8 nm [6]. The sheet thickness t ($= 2 / (\rho_{SiO_2} \cdot S_{SiO_2})$) of the supporting oxide has thus a value of 5.7 nm. The dimensionless support thickness β ($= t / \lambda_{SiO_2}$) is 1.5.
- The photoelectron cross-sections of silica (σ_{SiO_2}) and of platinum (σ_{Pt}) are 0.865 and 15.860 respectively [4]. Using equation (A.5) in Annex 1, the intensity ratio for a monolayer can then be expressed as:

$$\left(\frac{I_{Pt}}{I_{SiO_2}} \right)_{\text{monolayer}} = 21.6 \cdot \left(\frac{Pt}{SiO_2} \right)_{\text{bulk}} \quad (8.1)$$

where $(Pt/Si)_{\text{bulk}}$ is the bulk atomic ratio of platinum and SiO₂. The platinum loading of Pt/SiO₂ is 2.5 w.%, thus giving a value of 0.079 for $(Pt/SiO_2)_{\text{bulk}}$. Therefore, the ratio of intensities expected for a monolayer is equal to 0.171.

For the freshly reduced sample, the experimental ratio is 0.045. This value corresponds to about 26 % of the monolayer. In Annex 1, the fraction of monolayer intensity is plotted as a function of the dimensionless particle size α ($= d_{Pt}/\lambda_{Pt}$). For a fraction equal to 0.26, α is evaluated to be 3.7. Using the escape depth value λ_{Pt} of 1.9 nm reported by Kerkhof and Moulijn [6], the particle size d_{Pt} of the freshly reduced sample is about 7.0 nm.

Table 8-2 gives the particle size of the samples after pretreatments. It can be seen that the pretreatments does not affect the size of the platinum particles. A XRD line broadening analysis has confirmed that the size does not change during pretreatment. Therefore, the deactivation of the catalyst after pretreatment in a feed containing NO₂ cannot be attributed to a modification of the particle size.

8.4 Discussion

The results show that the sample consisting of Pt/SiO₂ deactivates after a pretreatment in a feed containing NO₂. The temperature of pretreatment has a strong influence on the oxidation activity. As may be seen in Figure 8-3, the deactivation of the sample is strongest at 250 °C. The longer pretreatment time of 6 hours leads to a stronger deactivation of Pt/SiO₂. The initial activity of the sample could be recovered by a thermal regeneration in air at 650 °C or under reducing conditions.

The NO₂ molecule has strong oxidizing properties and dissociates on platinum into NO and atomic oxygen [9]. Olsson and Fridell [3] have shown that NO₂ can also oxidize platinum supported on Al₂O₃. Therefore, the deactivation of Pt/SiO₂ by NO₂ observed by us could be due to the formation of platinum oxide. R.J. Berry [10] studied the surface oxidation of a platinum wire in a feed consisting of oxygen. He showed that platinum oxide can dissociate rapidly into platinum and oxygen, in air at atmospheric pressure and temperatures ranging from 600 to 650 °C. Therefore, the thermal regeneration procedure at 650 °C in air of Pt/SiO₂ causes the destruction of the oxide layer at the surface of the particle.

The pretreated sample was also regenerated at 250 °C in a feed containing ammonia, where NH₃ is used as a reducing agent. During the reduction, ammonia is consumed (Figure 8-6) without the formation of byproducts like N₂O or NO. Therefore, NH₃ is selectively oxidized to N₂ according to the selective catalytic oxidation (SCO) reaction as following:



Due to the fact that the feed did not contain oxygen, the oxygen must have been supplied by platinum oxide, which in turn was reduced to platinum by ammonia.

The deactivated sample can even be regenerated in an oxygen-free feed by nitrogen monoxide. NO can thus act as a reducing agent, reacting with platinum oxide to form NO₂ (Figure 8-7) according to:



The regeneration using NO can explain the hysteresis effect observed in Figure 8-4. After pretreatment C, platinum oxide is formed at the surface of the particle. During the oxidation reaction of NO to NO₂ with increasing temperatures, the platinum surface is regenerated by the reaction of NO with platinum oxide according to reaction (8.2), yielding a more active surface. Therefore, by cycling down the temperature, Pt/SiO₂ shows a higher activity. A hysteresis effect by cycling up and down has also been reported for the catalytic oxidation of methane over palladium oxide [11,12]. The different conversions observed at increasing and decreasing temperatures were explained by a change of the oxygen content in palladium oxide due to the reaction and to the temperature. Methane could play the role of reducing agent, and palladium oxide decomposes into palladium and oxygen at high temperatures. However, in the combustion of methane, palladium oxide is more active than palladium [11,12].

The effect of the pretreatment temperature (Figure 8-3) can also be attributed partly to NO. At 450 °C, the relative amount of NO and NO₂ during the pretreatment, i.e. 60 % NO and 40 % NO₂ reach almost the thermodynamic equilibrium. Therefore, even if the dissociation of NO₂ is fast, NO can also react rapidly with oxygen, thus preventing the formation of platinum oxide. At the lower pretreatment temperature of 350 °C, the relative amounts of NO and NO₂ are 20 % and 80 % respectively, again close to the thermodynamic equilibrium. The surface reactions of NO₂ dissociation and NO oxidation are slower due to the lower temperature. However, the temperature is probably high enough to cause formation of platinum oxide. At 150 and 250 °C, the NO_x feed during the pretreatment consists only of NO₂. However, only the latter temperature is probably sufficiently high to yield platinum oxide.

The formation of platinum oxide could not be shown by X-ray photoelectron spectroscopy, which is quite unexpected. The binding energies of Pt 4f peaks after pretreatment in the feed containing NO₂ remain close to the BE values of bulk platinum. This is probably due to the fact that the fraction of PtO that may form on large particles is very low compared to the fraction of platinum metal [13]. In order to illustrate this, the following calculations were performed. The intensity I of the radiation emitted after irradiation with an X-ray beam of intensity I_0 can be calculated from:

$$I = I_0 \int_0^d \exp\left(-\frac{t}{\lambda_{Pt}}\right) dt \quad (8.4)$$

$$I = I_0 \cdot \lambda_{Pt} \cdot \left[1 - \exp\left(-\frac{d}{\lambda_{Pt}}\right) \right] \quad (8.5)$$

with t thickness of platinum analyzed using XPS
 d thickness of a platinum oxide layer
 λ_{Pt} escape depth of electrons in platinum equal to 1.9 nm [6]

After deactivation at 250 °C, a monolayer of platinum oxide could form at the surface of the particle. The lengths of the unit cell edges in PtO are equal to $3.05 \pm 3 \text{ \AA}$ and to $5.35 \pm 5 \text{ \AA}$ [14]. The fraction of the XPS signal arising from platinum oxide is estimated from the following equation:

$$\frac{I(t)}{I_\infty} = 1 - \exp\left(-\frac{d}{\lambda_{Pt}}\right) \quad (8.6)$$

If a platinum oxide monolayer with a thickness of 0.535 nm is formed on the surface, the fraction of Pt XPS signal arising from PtO would be 24.5 %. Taking into account the large platinum particle size of the sample (i.e. $\approx 7 \text{ nm}$), such a fraction of platinum oxide is close to the detection limit. However, it is more likely that the surface of the platinum particle is only partly oxidized to platinum oxide [15], or that only a fraction of the total Pt particles are covered with this thin oxide layer [16]. The small concentration of platinum oxide and the low dispersion could explain why the XPS Pt 4f peak remains unchanged after pretreatment B in the presence of NO₂.

8.5 Conclusions

Platinum supported on silica is a very active catalyst for the oxidation of NO to NO₂. However, the sample suffers from deactivation by NO₂ formed during the oxidation reaction. The deactivation is strongest at intermediate temperatures ranging from 250 to 350 °C. The deactivation is due either to the oxidation of part of the platinum surface, or to the formation of a thin platinum oxide layer at the surface of a fraction of the platinum particles. After deactivation, NO can be used in order to regenerate the sample. Therefore, also nitrogen monoxide present during the oxidation reaction will slow down the deactivation process due to the redissociation of NO₂.

8.6 References

- [1] E. Xue, K. Seshan and J.R.H. Ross, *Appl. Catal. B: Environ.* **11** (1996), 65
- [2] B.J. Cooper, H.J. Jung and E.J. Thoss, US Patent 4,902,487 (1990), Assignee: Johnson Matthey Inc.
- [3] L. Olsson and E. Fridell, *J. Catal.* **210** (2002), 340
- [4] J.H. Scofield, *J. Electron. Spectrosc. Relat. Phenom.* **8** (1976), 129
- [5] M.G. Mason, *Phys. Rev. B* **27** (1983), 748
- [6] F.P.J.M. Kerkhof and J.A. Moulijn, *J. Phys. Chem.* **83** (1979), 1612
- [7] V. Pitchon and A. Fritz, *J. Catal.* **186** (1999), 64
- [8] *Handbook of chemistry and physics*, D.R. Lide (Ed.), 75th Edition, CRC Press, (1995)
- [9] J. Segner, W. Vielhaber and G. Ertl, *Israel. J. Chem.* **22** (1982), 375
- [10] R.J. Berry, *Surf. Sci.* **76** (1978), 415
- [11] P. Salomonson, S. Johansson and B. Kasemo, *Cat. Lett.* **3** (1995), 1
- [12] T. Kenelly, R.J. Farrauto, M.C. Hobson and E.M. Waterman, EU Patent 0,886,107 (1998), Assignee: Engelhard Corporation
- [13] C.B. Wang and C.T. Yeh, *J. Catal.* **178** (1998), 450
- [14] *Crystal structure data of inorganic compounds*, in: K.H. Hellwege and A.M. Hellwege (Eds), *Landolt-Börnstein, Numerical data and functional relationships in Science and technology*, New series, Vol. 7, Springer-Verlag, Berlin, (1975), Part b, p. 604
- [15] A.P. Markusse, *Platinum catalyst deactivation and reactivation during aqueous oxidation of alcohols*, Thesis, Technical University Eindhoven, (2000)
- [16] J.L. Freysz, J. Saussey, J.C. Lavalley and P. Bourges, *J. Catal.* **197** (2001), 131

Oxidation of NO over Pt/Al₂O₃ and Pt/ZrO₂

9.1 Introduction

Platinum supported on Al₂O₃ and ZrO₂ is less active than Pt/SiO₂ for the oxidation of nitrogen oxide to nitrogen dioxide under lean conditions (chapter 6) [1,2]. Xue et al. [1] suggested that the strong interaction of NO and NO₂ with Al₂O₃ and ZrO₂ can influence the NO oxidation reaction. Recently, Yoshida et al. [3] observed a similar reactivity sequence of supported platinum catalysts for the oxidation of methane at 250 °C. On the basis of XANES measurements, the authors claimed that Pt is more easily oxidized to PtO or PtO₂ if platinum is supported on supporting oxides like Al₂O₃ or ZrO₂. Yazawa et al. [4] observed an analogous influence of the supporting oxide on the oxidation state of palladium.

Olsson and Fridell [5] investigated the NO oxidation reaction on Pt/Al₂O₃ and Pt/BaO/Al₂O₃, a typical NO_x storage and reduction catalyst. The authors reported higher conversions of NO over Pt/Al₂O₃ than on Pt/BaO/Al₂O₃. They attributed the difference of conversion to the formation of a higher fraction of platinum oxide on Pt/BaO/Al₂O₃ than on Pt/Al₂O₃.

In contrast to these groups, we have investigated the adsorption of NO and NO₂ in humid feeds, representing realistic conditions in the diesel exhaust. In chapter 4, we

have shown that NO does not interact with supporting oxides, but under these conditions, NO₂ does. From these findings, the question arises, how does the NO₂ adsorbed influence the NO oxidation reaction on Pt, present in these systems. In order to compare with Pt/SiO₂, the oxidation state of platinum for freshly reduced Pt/ZrO₂ and Pt/ZrO₂ after pretreatments in feeds containing O₂, or a mixture of O₂ and NO₂ is also studied. The effect of these pretreatments on the oxidation state of platinum is correlated with the activity of the freshly reduced samples and of the pretreated samples.

9.2 Experimental

9.2.1 Catalyst samples

The samples were prepared according to the methods described in chapter 6. The sample of Pt/Al₂O₃ has been referred to as sample **P8**, and Pt/ZrO₂ as sample **P21**. As has already been described in chapter 6, the preparation of both samples included a final reduction at 450 °C for 1 h in a feed consisting of 5 % H₂/N₂.

9.2.2 NO₂ adsorption experiments

The experimental setup has been described in detail in chapter 3. The adsorption experiments were performed in a stainless steel reactor using 0.8 g of Pt/Al₂O₃, Al₂O₃, Pt/ZrO₂ or ZrO₂ held between quartz wool plugs. All experiments were carried out at a flow rate of 150 L_N/h in a humid gas feed with 5 % H₂O. The adsorption of NO₂ was performed at 250 °C, using a feed consisting of 500 ppm NO₂, 10 % O₂, 5 % H₂O, and balance N₂. For the samples of pure Al₂O₃ and pure ZrO₂, the desorption of adsorbed NO_x species was subsequently studied by temperature programmed desorption from 250 to 450 °C at a heating rate of 8 °C/min.

9.2.3 NO oxidation tests

The catalytic tests were carried out with 0.8 g of samples at a flow rate of 150 L_N/h. A feed gas consisting of 500 ppm NO, 10 % O₂, 5 % H₂O and balance N₂ was used, and the temperature ranged from 150 to 450 °C.

The oxidation of NO was investigated with freshly reduced samples of Pt/Al₂O₃ and Pt/ZrO₂, and after performing the following pretreatments:

- Pretreatment A: at 440 °C for 2 h in a feed consisting of 10 % O₂, 5 % H₂O and balance N₂ (referred to in the following as “base feed”)
- Pretreatment B: at 250 °C for 2 h in the feed consisting of 500 ppm NO₂ and base feed.

It must be noted that pretreatment B was performed at the same temperature and in the same feed as the NO₂ adsorption experiments.

9.2.4 X-ray photoelectron spectroscopy

The samples of Pt/ZrO₂ freshly reduced and after pretreatments were analyzed by XPS. The spectra were recorded with an ESCALAB 220i XL (Thermo VGScientific) apparatus and further details have been described in chapter 3. In order to correct for sample charging, binding energies were referred to the signal of Zr 3d at 182.2 eV. The composition of the samples was determined by quantitative analysis using the cross sections given by Scofield [6].

9.3 Results

9.3.1 NO₂ adsorption experiments

Pt/Al₂O₃ (P8) and Al₂O₃

Figure 9-1 shows the stationary concentrations of NO_x in the first 30 minutes of NO₂ adsorption on Pt/Al₂O₃. After addition of NO₂ to the feed, the concentration of NO₂ behind catalyst first increases rapidly to a value of about 200 ppm, but then much slower to reach the inlet NO₂ concentration, i.e. 500 ppm, after about 20 minutes. At the same time, NO is produced. The amount of NO produced and NO₂ adsorbed on the sample are given in Table 9-1. The production of NO is due to the disproportionation of three molecules of NO₂ into one molecule of NO released to the gas phase and two nitrate species. However, the stoichiometric ratio between NO₂ adsorbed and NO produced amounts to 3 : 1.33 with Pt/Al₂O₃.

In order to analyze the influence of platinum, the adsorption of NO₂ was investigated with a sample consisting of pure γ -Al₂O₃. The production of NO was observed during the adsorption of NO₂, thus indicating the disproportionation of NO₂ into gaseous NO and nitrate species. The amounts of NO₂ adsorbed and NO produced are higher with pure Al₂O₃ than with Pt/Al₂O₃. In Table 9-1, it can be seen that the interaction of NO₂ with pure Al₂O₃ leads to a ratio of 3 : 0.93 between NO_{2,adsorbed} and NO_{produced}. During the following TPD with Al₂O₃, the NO_x desorption arising from the decomposition of nitrate species amounts to 218 μ mol/g, thus yielding a stoichiometric ratio of 3 : 1.27 between NO_{2,adsorbed} and NO_{x,desorbed}.

Pt/ZrO₂ (P21) and ZrO₂

The NO₂ adsorption was also studied with samples of Pt/ZrO₂ (P21) and pure ZrO₂. The evolution of NO was observed during the adsorption of NO₂ with both samples. The NO₂ adsorption was significantly lower on Pt/ZrO₂ than on ZrO₂. In the case of ZrO₂, the stoichiometric ratio between NO_{2,adsorbed} and NO_{produced} amounted to approximately 3 : 1, whereas it was 3 : 1.68 over Pt/ZrO₂ (Table 9-1). During the following temperature programmed desorption, the desorption of nitrogen oxides from ZrO₂ yields a ratio of 3 : 1.75 between NO_{2,adsorbed} and NO_{x,desorbed}.

Table 9-1: Adsorption of NO₂ on various samples. Sample weight = 0.8 g, V* = 150 L_N/h.

Samples	Adsorption ^{a)}			TPD ^{b)}	
	NO _{2,adsorbed} (μ mol/g _{cat.})	NO _{produced} (μ mol/g _{cat.})	NO _{2,adsorbed} : NO _{produced}	NO _{x,desorbed} (μ mol/g _{cat.})	NO _{2,adsorbed} : NO _{x,desorbed}
Pt/Al ₂ O ₃ (P8)	256	114	3 : 1.33	^{c)}	^{c)}
Al ₂ O ₃	516	161	3 : 0.93	128	3 : 1.27
Pt/ZrO ₂ (P21)	265	148	3 : 1.68	^{c)}	^{c)}
ZrO ₂	402	149	3 : 1.11	235	3 : 1.75

^{a)} T = 250 °C, feed during adsorption = 500 ppm NO₂ + base feed.

^{b)} T = 250 - 450 °C, feed during TPD = base feed.

^{c)} not determined.

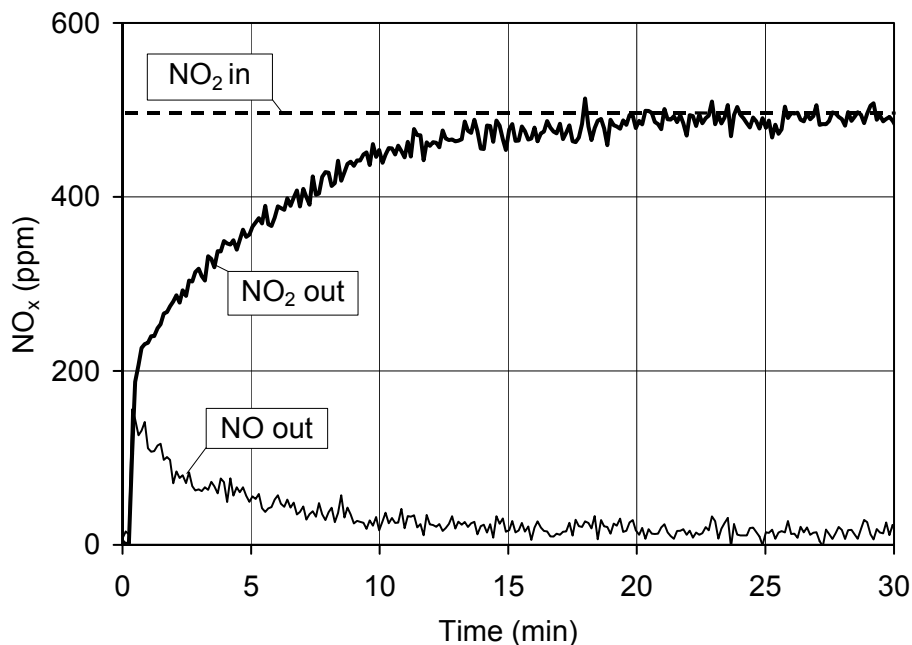


Figure 9-1: Adsorption of NO_2 at 250 °C on freshly reduced $\text{Pt}/\text{Al}_2\text{O}_3$ (P8). Sample weight = 0.8 g, $V^* = 150 \text{ L}_\text{N}/\text{h}$, feed = 500 ppm NO_2 , 10 % O_2 , 5 % H_2O , and balance N_2 .

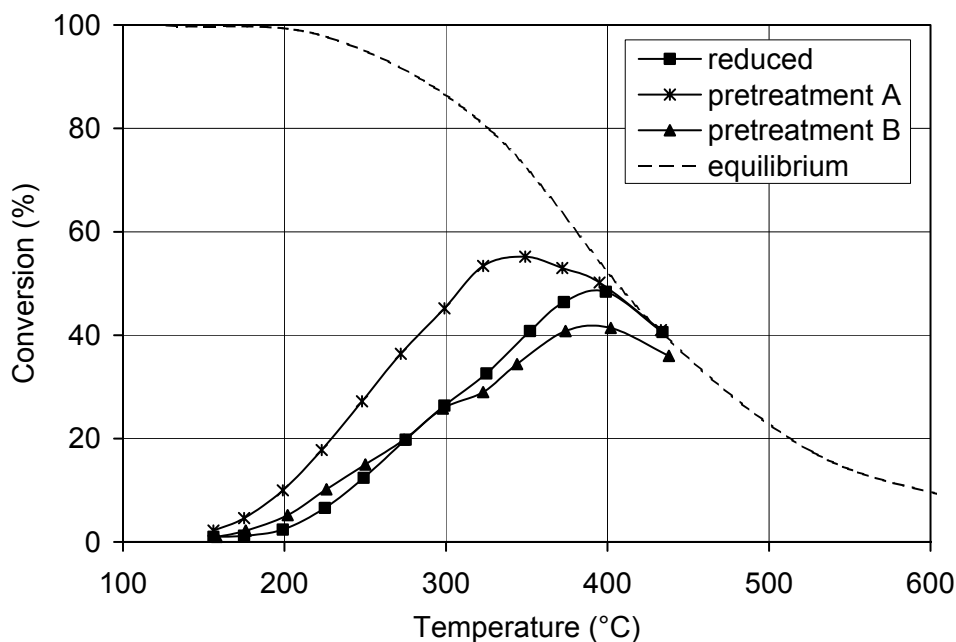


Figure 9-2: Conversion of NO as a function of temperature over reduced and pretreated samples of $\text{Pt}/\text{Al}_2\text{O}_3$. Sample weight = 0.8 g, $V^* = 150 \text{ L}_\text{N}/\text{h}$, feed: 500 ppm, 10 % O_2 , 5 % H_2O , and balance N_2 .

9.3.2 Oxidation of NO over reduced and pretreated samples

Pt/Al₂O₃ (P8)

Figure 9-2 shows the performance of catalyst **P8** after reduction and after pretreatments A and B. The dotted line gives the highest possible conversions set by the thermodynamic equilibrium at an oxygen partial pressure of 0.1 bar.

It can be observed that the conversion traces a parabolic curve. Over the freshly reduced sample, the maximum of conversion is reached at 400 °C. Pretreatment A at 450 °C in the base feed leads to a substantial improvement of the conversion. The maximum of conversion shifts to 350 °C after pretreatment A. On the other hand, pretreatment B at 250 °C in a feed containing additionally NO₂ leads only to minor changes of the conversion. At temperatures above 300 °C, the activity of the pretreated sample is slightly lower than the freshly reduced sample.

The catalytic oxidation of NO over the freshly reduced Pt/Al₂O₃ was first investigated from 150 to 450 °C. Subsequently, the oxidation of NO was investigated with decreasing temperatures from 450 °C down to 150 °C. A hysteresis effect was observed by cycling up and down the temperature (Figure 9-3). The conversions were higher with decreasing temperatures than with increasing temperatures.

Pt/ZrO₂ (P21)

Figure 9-4 shows the conversion of NO to NO₂ over Pt/ZrO₂ (**P21**) after reduction and after pretreatments A and B. As already mentioned in chapter 6, Pt/ZrO₂ is less active than Pt/Al₂O₃. At 300 °C, the conversion amounts only to 19 % over sample **P21** (Figure 9-4), compared to 26 % for Pt/Al₂O₃ (Figure 9-2).

After pretreatment A, an increase in the conversion of NO to NO₂ has been observed. Conversely, pretreatment B does not change the activity of Pt/ZrO₂, except at temperatures above 300 °C. Therefore, after pretreatments A and B, the samples of Pt/ZrO₂ behave similarly to Pt/Al₂O₃. The oxidation of NO over the freshly reduced sample **P21** was also investigated with increasing temperatures and then with decreasing temperatures. A hysteresis effect has also been observed, but only in the temperature range between 300 and 440 °C.

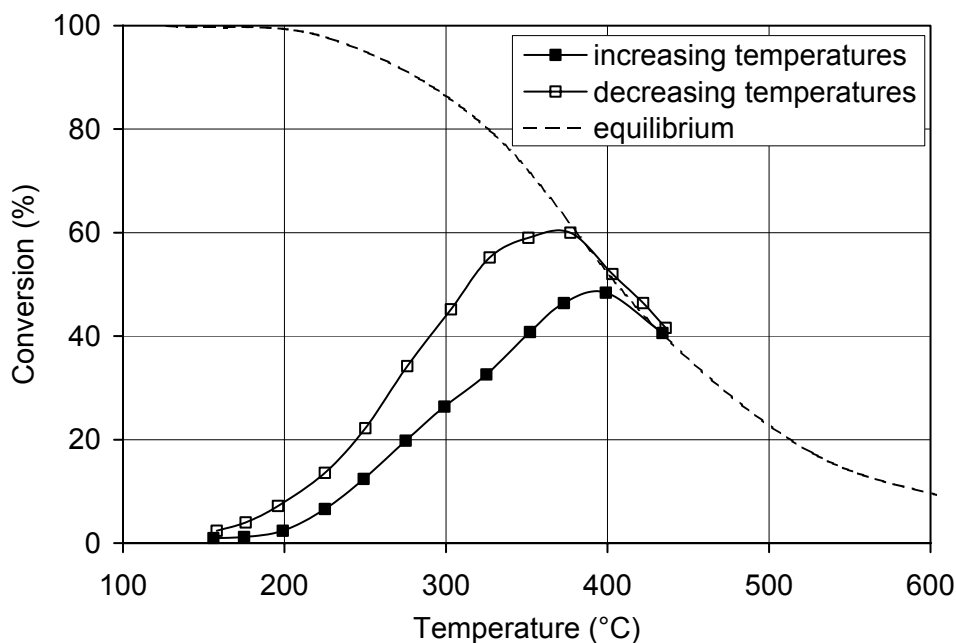


Figure 9-3: Conversion of NO over freshly reduced Pt/Al₂O₃ with increasing temperatures and decreasing temperatures. Sample weight = 0.8 g, V* = 150 L_N/h, feed: 500 ppm, 10 % O₂, 5 % H₂O, and balance N₂.

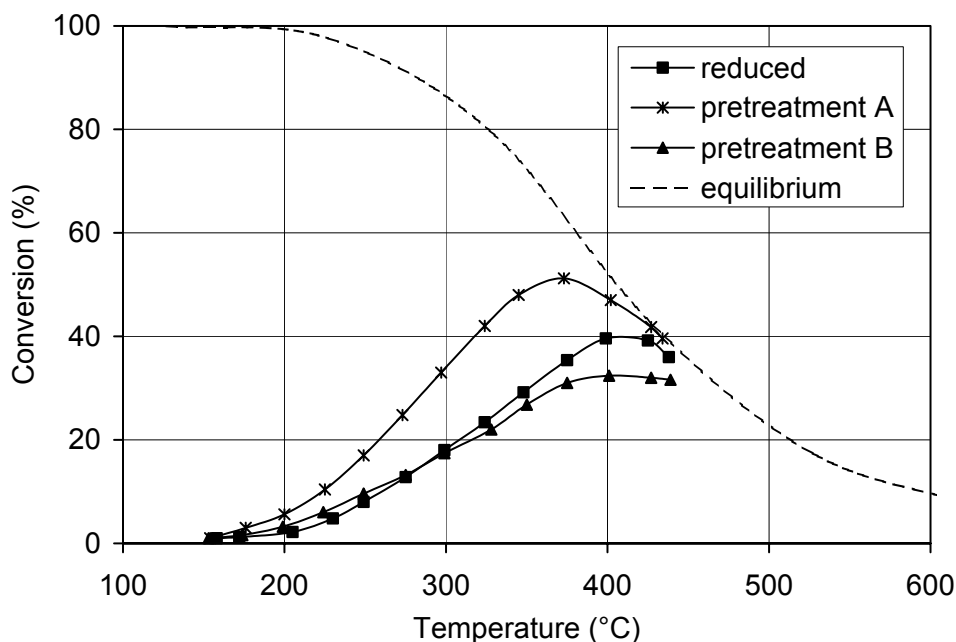


Figure 9-4: Conversion of NO as a function of temperature over reduced (P21) and pretreated samples of Pt/ZrO₂. Sample weight = 0.8 g, V* = 150 L_N/h, feed: 500 ppm, 10 % O₂, 5 % H₂O, and balance N₂.

9.3.3 X-ray photoelectron spectroscopy analysis

Due to the very low activity of Pt/ZrO₂, the oxidation state of platinum supported on zirconia was investigated using X-ray photoelectron spectroscopy. Figure 9-5 shows the XPS spectra of the Pt 4f core-level for the reduced and pretreated samples. Table 9-2 lists the binding energy values at maximum intensity of Pt 4f_{5/2} and of Pt 4f_{7/2}, and the ratio between the peak intensity of Pt 4f and of Zr 3d. The binding energies of Pt 4f_{7/2} and Pt 4f_{5/2} assigned to platinum or platinum oxides, according to the values reported by Pitchon and Fritz [7] are given in Table 9-2.

Table 9-2: Binding energy values of Pt 4f core-level and intensity ratios for various samples.

Species		Binding energies (eV)		I(Pt 4f) / I(Zr 3d)
		Pt 4f _{5/2}	Pt 4f _{7/2}	
Pt		74.60 ^{a)}	71.20 ^{a)}	-
PtO		75.60 ^{a)}	72.30 ^{a)}	-
PtO ₂		76.80 ^{a)}	73.60 ^{a)}	-
P21	Reduced	74.65	71.50	0.063
	Pretreatment in O ₂ ^{b)}	75.30	72.35	0.080
	Pretreatment in O ₂ + NO ₂ ^{c)}	75.70	72.85	0.063

^{a)} from reference [7].

^{b)} pretreatment A.

^{c)} pretreatment B.

For the reduced sample **P21**, the peaks of Pt 4f core-level were observed at a binding energy of 74.65 eV for Pt 4f_{5/2} and 71.50 eV for Pt 4f_{7/2}. The peak positions are in good agreement with values reported for bulk platinum metal [7]. After pretreatment A at 440 °C in a feed containing oxygen, a shift of the Pt 4f peaks towards higher binding energies can be observed, suggesting the formation of platinum oxide. Pretreatment B yields a further shift of the binding energies of Pt 4f_{5/2} and Pt 4f_{7/2} levels to 75.70 and 72.85 eV. A small shoulder at 76.80 eV in the Pt 4f_{5/2} peak is observed, indicating the possible formation of platinum dioxide.

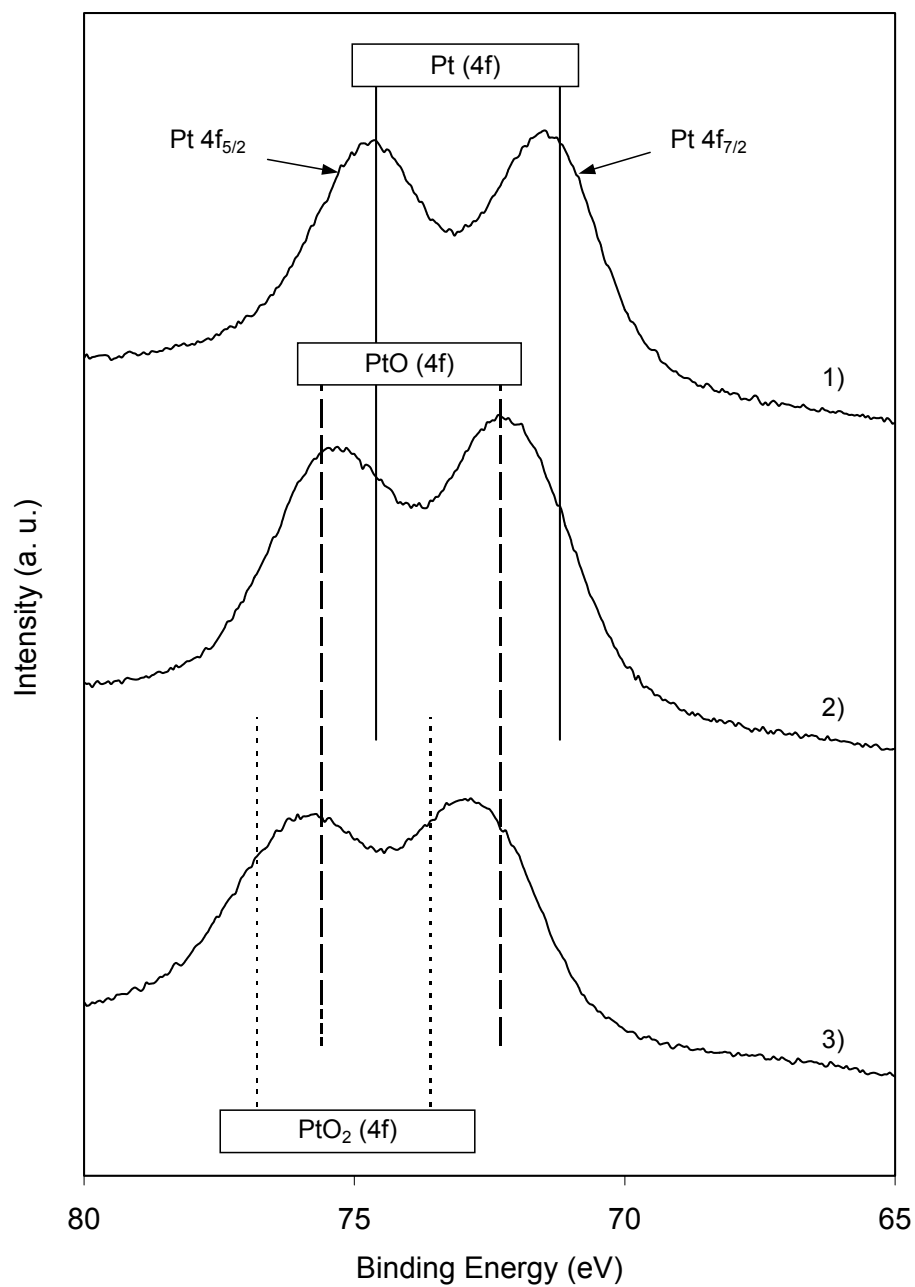


Figure 9-5: XPS spectra of the Pt 4f core-level of Pt/ZrO₂ (P21): 1) freshly reduced, 2) after pretreatment A at 450 °C in the base feed, 3) after pretreatment B at 250 °C in NO₂ + base feed.

In order to estimate the dispersion of platinum on zirconia, the ratio of intensities $I(\text{Pt } 4f)/I(\text{Zr } 3d)$ expected for a monolayer of platinum was calculated using the model of Kerkhof and Moulijn [8] described in Annex 1. The BET surface area of zirconia was $75 \text{ m}^2/\text{g}$. Pretreatments A and B had no influence on S_{BET} . The density of zirconia is $5.6 \cdot 10^6 \text{ g/m}^3$ [9]. The sheet thickness $t (= 2 / (\rho_{\text{ZrO}_2} \cdot S_{\text{ZrO}_2}))$ of the supporting oxide is thus equal to 4.8 nm. In order to calculate the dimensionless support thickness of ZrO_2 , the escape depth λ of the electrons from SiO_2 was used. This approximation is possible because the kinetic energy of electrons from the Zr 3d level is about the same as the kinetic energy of electrons from the Si 2p level. The value of λ_{SiO_2} reported by Kerkhof and Moulijn is 3.8 nm for the Mg K α source [8]. This leads to a dimensionless support thickness $\beta (= t / \lambda_{\text{ZrO}_2})$ of 1.3. The photoelectron cross-sections σ_{Pt} and σ_{Zr} are equal to 15.86 and 7.30 respectively [6]. The ratio of intensities for a monolayer of platinum on zirconia can thus be calculated from the following equation:

$$\left(\frac{I_{\text{Pt}}}{I_{\text{ZrO}_2}} \right)_{\text{monolayer}} = 2.45 \cdot \left(\frac{\text{Pt}}{\text{ZrO}_2} \right)_{\text{bulk}} \quad (9.1)$$

where $(\text{Pt}/\text{ZrO}_2)_{\text{bulk}}$ is the atomic ratio of platinum and zirconia. For our study, the platinum loading was 2.5 w.%, thus yielding a theoretical value for a monolayer of Pt equal to 0.040.

The experimental values of $I(\text{Pt } 4f)/I(\text{Zr } 3d)$ for the samples of Pt/ZrO_2 are reported in Table 9-2. In the case of the freshly reduced sample **P21**, the ratio amounts to 0.063, indicating that the platinum coverage is higher than a monolayer. A second or third monolayer can recover partially the first monolayer. An analysis of sample **P21** using TEM did not evidence the formation of Pt particles. Oi-Uchisawa et al. [2] measured also a very high Pt dispersion for Pt/ZrO_2 by CO chemisorption. After pretreatment A in the feed containing O_2 , an increase in the intensity ratio to a value of 0.08 was observed, thus indicating a better spreading of platinum. According to the model used to predict XPS intensity ratios, this value would be expected in the case of two monolayers. Therefore, we suggest that platinum from the third monolayer diffuses and completes the second monolayer. On the other hand, after pretreatment B, the intensity ratio is the same as for the freshly reduced sample, indicating that pretreatment B does not modify the platinum spreading.

9.4 Discussion

The oxidation of NO over Pt/Al₂O₃ and Pt/ZrO₂ was studied over freshly reduced samples and after various pretreatments. Pretreatment A was performed at 450 °C in a feed consisting of 10 % O₂, 5 % H₂O and balance N₂. Pretreatment B was performed at 250 °C in a feed containing additionally 500 ppm NO₂. As may be seen in Figure 9-2, the activity of Pt/Al₂O₃ is improved after pretreatment A. On the other hand, pretreatment B has no influence on the activity of Pt/Al₂O₃. The pretreated sample exhibits the same activity as the freshly reduced sample. The sample consisting of Pt/ZrO₂ after pretreatment behave similarly to the sample of Pt/Al₂O₃. The conversion of NO to NO₂ is higher after pretreatment A than after reduction. Pretreatment B has no influence on the activity of Pt/ZrO₂.

As has been reported in chapter 8, Pt/SiO₂ showed a complete opposite behavior compared to Pt/Al₂O₃ and Pt/ZrO₂. Pretreatment A of Pt/SiO₂ had no influence on the NO oxidation activity. However, after pretreatment B with NO₂, Pt/SiO₂ showed a strong deactivation of the NO oxidation. Although platinum oxide was not evidenced using XPS, the deactivation process with NO₂ was attributed to the formation of platinum oxide at the surface of the Pt particle.

The XPS study performed on Pt/ZrO₂ showed that pretreatments A and B lead to the formation of platinum oxide. Therefore, the low activity of Pt/ZrO₂ for the oxidation of NO is thus attributed to the easy formation of platinum oxide in a feed containing oxygen. Pitchon and Fritz [7] have also reported the oxidation of platinum in lean conditions when platinum is supported on lanthanum-doped zirconia.

Due to the fact that pretreatments A and B had the same influence on the NO oxidation activity on Pt/Al₂O₃ and on Pt/ZrO₂, the formation of platinum oxide on Pt/Al₂O₃ may also be expected. Olsson and Fridell [5] have shown that platinum supported on Al₂O₃ was oxidized either by a pretreatment at 350 °C in NO₂ or a pretreatment at 400 °C in O₂.

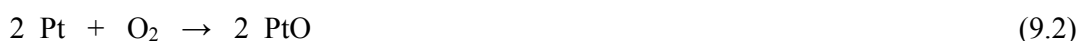
Pretreatment A at 450 °C led to an increase in NO conversion both on Pt/Al₂O₃ and Pt/ZrO₂. This effect is attributed to a rearrangement of platinum oxide at the surface of the supporting oxide. This rearrangement can be favored by the high temperature during

pretreatment A. The enhanced activity after pretreatment A could explain the hysteresis effect observed when the oxidation of NO was investigated over the freshly reduced sample of Pt/Al₂O₃ by cycling up and down the temperature (Figure 9.3). The reaction was studied from 150 to 450 °C, thus leading to a more active platinum catalyst at 450 °C. Therefore, higher conversions were observed with decreasing temperatures after activating the catalyst at 450 °C.

After pretreatment B, a shoulder at 76.8 eV in the peak of Pt 4f_{5/2} can be observed, thus evidencing the possible formation of PtO₂. The higher oxidation state of platinum after pretreatment B could be explained by either the different temperatures of pretreatment, or the presence of NO₂ during pretreatment B. Pretreatment A was performed at 450 °C, whereas pretreatment B was carried out at 250 °C. Platinum dioxide is less stable than PtO. The melting point of PtO₂ and PtO are 450 °C and 550 °C respectively [9]. Therefore, the formation of PtO₂ cannot be expected at the high temperature of pretreatment A. However, Pitchon and Fritz [7] observed the formation of PtO₂ on Pt/La₂O₃-ZrO₂ after DeNO_x at 550 °C.

During pretreatment B, NO₂ was added to the base feed. NO₂ is known to be a stronger oxidizer than O₂, which easily dissociates on platinum into NO and atomic oxygen [5,7,10-11]. Therefore, platinum could first be oxidized by O₂, then by NO₂ according to the following scheme:

Reaction during pretreatment A with O₂:



Additional reactions during pretreatment B with O₂ and NO₂:



During pretreatment B of Pt/Al₂O₃ and Pt/ZrO₂, the decomposition of NO₂ on platinum was not observed. Actually, the production of NO during the pretreatment is observed because NO₂ reacts with the supporting oxide, either Al₂O₃ or ZrO₂, according to the following disproportionation reaction:



where X represents an adsorption site.

Such a 3 : 1 stoichiometric ratio between NO₂ adsorbed and NO produced has already been observed with Al₂O₃ [12,13], and with Cu-ZSM-5 or BaO/TiO₂ (chapter 4 and 5 respectively). However, the stoichiometric ratio was 3 : 1.33 for Pt/Al₂O₃ and 3 : 1.68 for Pt/ZrO₂ (Table 9-1). Therefore, platinum modifies the stoichiometry of the overall adsorption scheme. A part of NO produced during the adsorption is probably reoxidized to NO₂ over platinum, thus decreasing the amount of NO_{produced}.

Pretreatment B was performed at the same temperature and in the same feed gas as the NO₂ sorption experiments. Therefore, pretreatment B leads also to the formation of nitrates on the supporting oxide. However, the samples of Pt/ZrO₂ and Pt/Al₂O₃ exhibit the same activity for NO oxidation after reduction and after pretreatment B. Therefore, the adsorption of NO₂ on the supporting oxide does not influence the NO oxidation reaction.

9.5 Conclusions

The most decisive factor explaining the low NO oxidation activity of Pt/Al₂O₃ and Pt/ZrO₂ is the formation of platinum oxide. Platinum supported on ZrO₂ is easily oxidized to platinum oxide in a feed containing O₂. If the feed contains oxygen and NO₂, platinum is oxidized to platinum oxide, and likely to platinum dioxide. Pretreatment A at 450 °C of Pt/Al₂O₃ and Pt/ZrO₂ (2.5 w.% Pt) in a feed containing oxygen yields an enhanced activity for the oxidation of NO. The increase in activity can be attributed to a rearrangement of platinum oxide on the supporting oxide due to the high temperature of pretreatment. The formation of nitrate species on the supporting oxides during pretreatment B showed no influence on the NO oxidation reaction.

9.6 References

- [1] E. Xue, K. Seshan and J.R.H. Ross, *Appl. Catal. B: Environ.* **11** (1996), 65
- [2] J. Oi-Ushisawa, A. Obuchi, R. Enomoto, S. Liu, T. Nanba and S. Kushiyaama, *Appl. Catal. B: Environ.* **26** (2000), 17
- [3] H. Yoshida, Y. Yazawa, N. Takagi, A. Satsuma, T. Tanaka, S. Yoshida and T. Hattori, *J. Synchrotron Rad.* **6** (1999), 471
- [4] Y. Yazawa, H. Yoshida, N. Takagi, S.I. Komai, A. Satsuma and T. Hattori, *J. Catal.* **187** (1999), 15
- [5] L. Olsson and E. Fridell, *J. Catal.* **210** (2002), 340
- [6] J.H. Scofield, *J. Electron. Spectrosc. Relat. Phenom.* **8** (1976), 129
- [7] V. Pitchon and A. Fritz, *J. Catal.* **186** (1999), 64
- [8] F.P.J.M. Kerkhof and J.A. Moulijn, *J. Phys. Chem.* **83** (1979), 1612
- [9] *Handbook of chemistry and physics*, D.R. Lide (Ed.), 75th Edition, CRC Press, (1995)
- [10] J. Segner, W. Vielhaber and G. Ertl, *Israel J. Chem.* **22** (1982), 375
- [11] W. Huang, Z. Jiang, J. Jiao, D. Tan, R. Zhai and X. Bao, *Surf. Sci.* **506** (2002), L287
- [12] M.R. Lee, E.R. Allen, J.T. Wolan and G.B. Hoflund, *Ind. Eng. Chem. Res.* **37** (1998), 3375
- [13] N.W. Cant and M.J. Paterson, *Catal. Today* **73** (2002), 271

Proposed mechanisms for the oxidation of NO to NO₂ over supported platinum catalysts

10.1 Introduction

Only few mechanistic studies on the oxidation of NO to NO₂ over platinum catalysts have been performed [1-3]. In all these studies, the proposed mechanism suggests the reaction of a gaseous molecule of nitrogen monoxide with an oxygen atom adsorbed on platinum, according to an Eley-Rideal mechanism. Therefore, the resulting reaction order for NO should be about 1. However, the kinetic investigations on Pt/SiO₂ reported in chapter 7 have shown that the reaction order for NO is lower than 1. We attributed the lower reaction order to the inhibiting effect of NO₂ produced during the reaction. Moreover, we have shown in chapter 9 that the catalytic surface is platinum oxide in the case of Pt/Al₂O₃ and Pt/ZrO₂.

In this chapter, possible reaction mechanisms for the oxidation of nitrogen monoxide over supported platinum catalyst are proposed, which are in accordance with the experimental results.

10.2 Langmuir-Hinshelwood or Eley-Rideal mechanism ?

The oxidation of NO to NO₂ involves the reaction of NO with oxygen at the surface of platinum or platinum oxide. Oxygen is strongly adsorbed on platinum and desorbs only at high temperatures. Saliba et al. [4] calculated the activation energy of oxygen desorption from Pt(111) after exposure to ozone. This activation energy varies with the oxygen coverage. For oxygen coverages between 0.2 and 1 monolayer (ML), the activation energy for O₂ desorption decreases from 45 kcal/mol to a value of about 26 kcal/mol. At these coverages up to a monolayer, atomic oxygen is only adsorbed at the surface.

Saliba et al. [4] were also able to obtain coverages exceeding a monolayer of oxygen on Pt(111). Due to the strong oxidizing properties of ozone, coverages greater than 1 ML were attributed to the formation of platinum oxide. For coverages between 1.2 and 2.4 ML, the desorption of oxygen takes place at higher temperatures. The activation energy for O₂ desorption reached a value of 38 kcal/mol at the oxygen coverage of 2.4 ML.

Nitrogen monoxide is only weakly adsorbed on platinum. Campbell et al. [5] found an activation energy for NO desorption from Pt(111) of about 27 kcal/mol, but only at very low coverages. The activation energy strongly decreases at higher NO coverages. For NO coverage of 0.25, it decreases to 19 kcal/mol. Precovering the Pt(111) surface with oxygen leads to a weakening of the bond between platinum and NO [5,6].

Summarizing, the results obtained on model surfaces like Pt(111) have shown that the bond between Pt and NO is rather weak compared to the bond between platinum and oxygen. Therefore, a Langmuir-Hinshelwood mechanism may be ruled out in favor of an Eley-Rideal mechanism.

10.3 Proposed mechanisms

10.3.1 Mechanism of NO oxidation over Pt/Al₂O₃ and Pt/ZrO₂

We have shown in chapter 6 that platinum supported on alumina and zirconia is less active for NO oxidation than platinum supported on SiO₂. The formation of platinum oxide was evidenced on Pt/ZrO₂ using X-ray photoelectron spectroscopy (chapter 9). In the same chapter, we have also concluded that platinum oxide was formed on Pt/Al₂O₃ because Pt/Al₂O₃ and Pt/ZrO₂ showed identical reactivity after pretreatments in various feeds. The oxidation of platinum to platinum oxide or platinum dioxide involves the following reactions:

Dissociative adsorption of O₂ or NO₂ on platinum:



Formation of platinum oxide:



It is possible that platinum oxide is further oxidized to platinum dioxide according to:



Whether PtO or PtO₂ is formed depends on oxygen coverage [4] and temperature.

The bond between oxygen and platinum in platinum oxide is very strong, thus leading to a high activation energy for O₂ desorption and to a lower reactivity of oxygen. Therefore, the oxidation of nitrogen monoxide to nitrogen dioxide is expected to involve the reduction of platinum oxide by NO to platinum according to the following reaction [7,8], followed by its reoxidation:



10.3.2 Mechanism of NO oxidation over Pt/SiO₂

The sample of Pt/SiO₂ showed a much higher activity for NO oxidation at low temperatures than Pt/Al₂O₃ and Pt/ZrO₂. The higher activity of Pt/SiO₂ may be attributed to the fact that the Pt surface remains mainly in the form of platinum under lean conditions (chapter 8).

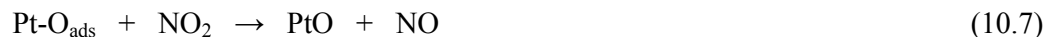
Platinum is able to dissociate easily the O₂ molecule according to reaction (10.1). Therefore, we propose a mechanism involving a surface reaction between adsorbed oxygen and nitrogen monoxide. Because the bond strength between platinum and adsorbed oxygen is much weaker than the Pt–O bond in platinum oxide, this adsorbed oxygen is much more reactive than oxygen in platinum oxide. Therefore, the higher reactivity of oxygen results in the faster oxidation of NO over Pt/SiO₂.

Nitrogen monoxide will react either from the gas phase or from a weakly adsorbed state according to an Eley-Rideal mechanism:



The free platinum sites are again available for the dissociation of O₂ or NO₂ according to reactions (10.1) and (10.2).

However, nitrogen dioxide produced during the reaction causes the deactivation of Pt/SiO₂ (chapter 8). We suggest that a higher oxygen coverage of the Pt surface is obtained due to the dissociation of NO₂ according to reaction (10.2) [9]. Such a high oxygen coverage favors the formation of platinum oxide on the Pt surface, thus leading to the deactivation of Pt/SiO₂. The formation of platinum oxide could occur according to:



We have shown in chapter 9 that platinum oxide is less active than platinum metal, thus explaining the decrease in activity for NO oxidation. The fact that nitrogen monoxide can also react with platinum oxide as a reducing agent can explain the hysteresis effect observed after pretreating Pt/SiO₂ with NO₂.

10.4 Conclusions

The oxidation of NO to NO₂ proceeds with a higher rate on platinum than on platinum oxide due to the weaker bonding of the oxygen atom. The supporting oxides Al₂O₃ or ZrO₂ are prone to form platinum oxide under lean conditions, resulting in a lower rate of NO oxidation. On Pt/Al₂O₃ and Pt/ZrO₂, the mechanism for NO oxidation requires the reduction of platinum oxide by nitrogen monoxide to form nitrogen dioxide.

Platinum supported on SiO₂ is much less susceptible to form platinum oxide in the presence of oxygen. However, dissociation of NO₂ may lead to partial platinum oxide formation on a fraction of the platinum surface. Therefore, the oxidation of NO on Pt/SiO₂ involves two concurring reactions: a classical Eley-Rideal mechanism between NO and adsorbed oxygen, and NO₂ dissociation on platinum resulting in the formation of platinum oxide.

10.5 References

- [1] J. Seifert, Untersuchung der heterogen katalysierten NO-Oxidation in einer rechnergesteuerten, echtzeitkontrollierten Versuchsanlage, Thesis, University of Erlangen, (1989)
- [2] J. Seifert and G. Emig, Chem. Ing. Tech. **61** (1989), 560
- [3] L. Olsson, B. Westerberg, H. Persson, E. Fridell, M. Skodlundh and B. Andersson, J. Phys. Chem B **103** (1999), 10433
- [4] N.A. Saliba, Y.L. Tsai, C. Panja and B.E. Koel, Surf. Sci. **419** (1999), 79
- [5] C.T. Campbell, G. Ertl and J. Segner, Surf. Sci. **115** (1982), 309
- [6] M.E. Bartram, B.E. Koel and E.A. Carter, Surf. Sci. **219** (1989), 467
- [7] A.P. Markusse, B.F.M. Kuster and J.C. Schouten, J. Mol. Catal. A: Chemical **158** (2000), 215
- [8] P. Denton, A. Giroir-Fendler, Y. Schuurman, H. Praliaud, C. Mirodatos and M. Primet, Appl. Catal. A: General **220** (2001), 141
- [9] J. Segner, W. Vielhaber and G. Ertl, *Israel. J. Chem.* **22** (1982), 375

Conclusions and Outlook

Adsorption of nitrogen oxides

Various adsorbents have been tested for a possible adsorption of NO at 200 °C. The conclusion from these tests is that the NO molecule itself cannot be adsorbed. On the other hand, NO₂ could be adsorbed on a variety of adsorbents over a wide temperature range of temperatures. Therefore, the adsorption of NO must be preceded by its oxidation to NO₂.

Mass balances have shown that the adsorption of NO₂ generally involves the disproportionation reaction of three NO₂ molecules into two nitrate species and one molecule of NO. This reaction has been observed on Cu-ZSM-5, γ -Al₂O₃, TiO₂ (anatase), ZrO₂ and BaO.

The reverse reaction of the NO₂ disproportionation has also been observed: if NO is added to the feed, nitrates previously formed on the sorbent will decompose into NO₂. Therefore, the above disproportionation of NO₂ must be considered as an equilibrium reaction and can probably be described by thermodynamic equilibrium calculations. We propose that this reaction plays an important role in the behavior of NO_x storage and reduction catalysts although the situation is complicated in this case at higher temperatures by the presence of platinum. Due to its redox properties, platinum will accelerate the attainment of the thermodynamic equilibrium $\text{NO}_2 \rightleftharpoons \text{NO} + \frac{1}{2} \text{O}_2$ thus modifying the original concentrations of NO and NO₂.

Oxidation of NO

Because the oxidation of NO is essential to many future aftertreatment techniques for lean exhaust gases, its oxidation has been studied in detail. It could be confirmed that the commercial catalysts presently used for this purpose containing platinum on silica are probably the best choice. Compared to other supports (γ -Al₂O₃, ZrO₂), silica yields definitely the most active catalysts. It could be shown that the better activity of Pt/SiO₂ is due to its ability to remain longer in the reduced state whereas platinum supported on

the other two oxides tends to form platinum oxide easily. However, the very strong oxidizing effect of NO_2 will lead also to the deactivation of Pt/SiO_2 . Because NO_2 is the desired product of the NO oxidation reaction, this may be considered as an autoinhibition which cannot be avoided. Although the formation of platinum oxide on Pt/SiO_2 could not be proved by any characterization technique, we believe that a thin layer of platinum oxide is formed which covers at least a fraction of the total platinum surface. The lower activity of platinum oxide compared to adsorbed oxygen atoms on platinum may be easily understood by the higher binding energy of oxygen in the oxide.

A deactivated Pt/SiO_2 catalyst was easily regenerated by a thermal treatment in air at $\approx 650^\circ\text{C}$ (dissociation of PtO) or by a reducing treatment with NH_3 or even NO at lower temperatures. Therefore, it is possible that such a catalyst will also be regenerated in real exhaust gases which usually contain small amounts of reducing agents (CO , hydrocarbons). Unfortunately, due to limited time, experiments with realistic test gas mixtures could not be included in the present work.

Future work should focus on the problem of deactivation of these catalysts and look for possibilities to impede the deeper oxidation of platinum. The addition of a second metal or metal oxide might be one possible approach. Due to the metal-metal interaction, bimetallic catalysts could yield an enhanced and more stable catalytic activity. Such an improved NO oxidation catalyst would be welcome in helping to fulfill future emission standards of lean internal combustion engines for both NO_x and soot.

Annex 1

A Determination of the platinum particle size

XRD line broadening analysis

The particle size can be estimated from X-ray line broadening analysis. It relies on the fact that the width of a diffraction line depends on the particle size. A broad peak will be obtained in the case of small particles. Conversely, large particles will give a sharp peak. Scherrer [1] has shown that the size d of the particles is obtained from the width β of the diffraction line using the equation:

$$d = \frac{k \cdot \lambda}{\beta \cdot \cos \theta} \quad (\text{A.1})$$

with	k	a constant taken as unity
	λ	the wavelength of the X-ray radiation (\AA)
	β	the width of a diffraction line (rad)
	θ	the angular position of the peak maximum ($^\circ$)

Determination of the size of a particle with XPS intensities [2]

The intensity ratio between the XPS signal from the particles and the XPS signal from the support reflects the dispersion of the metal over the support. The highest ratio is expected for a monolayer of catalytic promoter. Crystallite growth and clustering will lower the intensity ratio. The model of Kerkhof and Moulijn [2] predicts the expected ratio for a monolayer catalyst on top of a support. The particle size is derived by comparing the XPS intensity ratio of a measured sample with the expected intensity ratio in the case of a monolayer of catalyst.

In this model [2], the sample consists of sheets of support (s), with cubic crystallites of catalytic promoter (p) with dimension c in between. The thickness of the sheets t in meter can be estimated from the following equation:

$$t = \frac{2}{\rho_s \cdot S_{\text{BET}}} \quad (\text{A.2})$$

with ρ_s the density of the support (g/m^3)
 S_{BET} the surface area of the support (m^2/g)

The dimensionless support thickness β is calculated from the following equation:

$$\beta = \frac{t}{\lambda_s} \quad (\text{A.3})$$

with λ_s the escape depth of the electrons from the support

The dimensionless crystallite size α is given by:

$$\alpha = \frac{c}{\lambda_p} \quad (\text{A.4})$$

with c the crystallite size
 λ_p the escape depth of the electrons from the promoter

The XPS intensity ratio for a monolayer is predicted by equation (A.5) for electrons with small differences of kinetic energy:

$$\left(\frac{I_p}{I_s} \right)_{\text{monolayer}} = \left(\frac{p}{s} \right)_{\text{bulk}} \cdot \frac{\sigma_p}{\sigma_s} \cdot \frac{\beta}{2} \cdot \frac{(1 + e^{-\beta})}{(1 - e^{-\beta})} \quad (\text{A.5})$$

with $\left(\frac{p}{s} \right)_{\text{bulk}}$ the atomic ratio of promoter and support
 σ_p, σ_s the photoelectron cross sections of the promoter and the support
 β the dimensionless support thickness

The XPS intensity ratio in the case of crystallite growth is given by the following equation:

$$\left(\frac{I_p}{I_s}\right)_{\text{crystallites}} = \left(\frac{p}{s}\right)_{\text{bulk}} \cdot \frac{\sigma_p}{\sigma_s} \cdot \frac{\beta}{2} \cdot \frac{(1+e^{-\beta})}{(1-e^{-\beta})} \cdot \frac{(1-e^{-\alpha})}{\alpha} \quad (\text{A.6})$$

with α the dimensionless crystallite size

The quotient between the intensity ratio in the case of crystallite growth and the intensity ratio for a monolayer is given by equation (A.7). It is plotted against α in Figure A-1.

$$\left(\frac{I_p}{I_s}\right)_{\text{crystallites}} / \left(\frac{I_p}{I_s}\right)_{\text{monolayer}} = \frac{(1-e^{-\alpha})}{\alpha} \quad (\text{A.7})$$

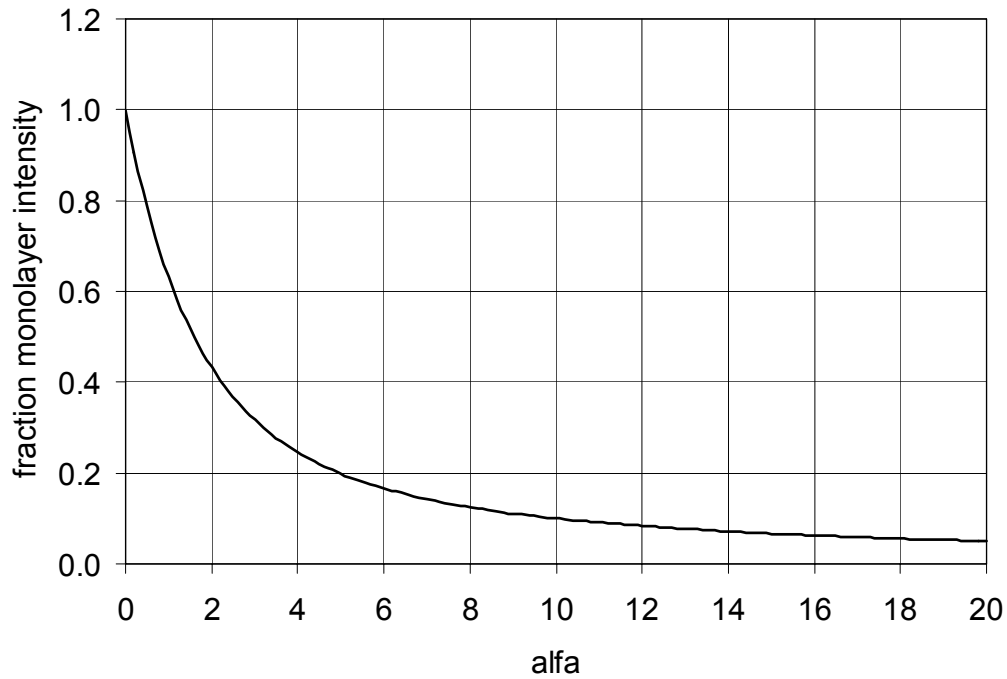


Figure A-6: Intensity ratio in case of crystallite growth (fraction of the monolayer prediction) as a function of the dimensionless crystallite size α ($=c/\lambda_{pt}$).

Procedure to determine the particle size of supported platinum:

In order to predict the crystallite size of platinum particles, the following procedure is used [2]. It includes the calculation using the data given in Table A-1 of:

- 1) the XPS intensity ratio $(I_{\text{pt}}/I_{\text{support}})_{\text{crystallites}}$ measured for the sample,
- 2) the XPS intensity ratio $(I_{\text{pt}}/I_{\text{support}})_{\text{monolayer}}$ expected for a monolayer using the data listed in Table A-1,
- 3) the quotient of the two ratios.

From the curve plotted in Figure A-1, the dimensionless crystallite size α ($= c / \lambda_{\text{pt}}$) is estimated, and the crystallite size of the platinum particles then is calculated from equation (A.4).

Table A-3: Data used for the estimation of the platinum particle size of Pt/SiO₂ and Pt/ZrO₂.

Symbols	Units	Compounds		
		SiO ₂	ZrO ₂	Pt
S_{BET}	(m ² /g)	160	75	
ρ_{S}	(g/m ³)	$2.2 \cdot 10^6$ ^{a)}	$5.6 \cdot 10^6$ ^{a)}	
λ_{S}	(nm)	3.8 ^{b)}	3.8 ^{b)}	
λ_{p}	(nm)			1.9 ^{b)}
σ_{S}	-	0.865 ^{c)}	7.3 ^{c)}	
σ_{p}	-			15.86 ^{c)}

^{a)} from [4], ^{b)} from [2], ^{c)} from [3].

B References

- [1] K.S.W. Sing, J. Rouquerol, P. Gallezot and G. Bergeret, in: G. Ertl, H. Knözinger and J. Weitkamp (Eds.), *Handbook of heterogeneous catalysis*, Vol. 2, Wiley-VCH, Weinheim (1997), pp. 427-475
- [2] F.P.J.M. Kerkhof and J.A. Moulijn, *J. Phys. Chem.* **83** (1979), 1612
- [3] J.H. Scofield, *J. Electron. Spectrosc. Relat. Phenom.* **8** (1976), 129
- [4] *Handbook of chemistry and physics*, D.R. Lide (Ed.), 75th Edition, CRC Press, (1995)

List of Publications

The following list summarizes the papers which resulted from this study. Further publications based on the work presented in chapters 6-10 are in preparation.

Publications

J. Despres, M. Koebel, O. Kröcher, M. Elsener and A. Wokaun, "Storage of NO₂ on BaO/TiO₂ and the influence of NO", *Appl. Catal. B: Environ.*, submitted

J. Despres, M. Koebel, O. Kröcher, M. Elsener and A. Wokaun, "Adsorption and desorption of NO and NO₂ on Cu-ZSM-5", *Microporous Mesoporous Mater.*, in press

J. Despres, M. Koebel, M. Elsener and A. Wokaun, "Investigation of the oxidation of NO over platinum catalysts", *PSI Scientific report 2001*, Volume V (2002), 64

Poster

J. Despres, M. Elsener, M. Koebel and A. Wokaun, "Oxidation of NO on a catalyst Pt/SiO₂", Fall meeting of the Swiss chemical society, ETH Zurich, Switzerland, October 12, 2001.

Curriculum Vitae

Name : Despres, Joël
Date of birth : March 9, 1973
Place of birth : Saint-Rémy (France)
Nationality : French

Education :

1979-1983	Primary School, Lux (Saône-et-Loire), France
1983-1987	Secondary School <i>Collège Louis Pasteur</i> , Saint-Rémy (Saône-et-Loire), France
1987-1988	High School <i>Lycée Agricole</i> , Tournus (Saône-et-Loire), France
1988-1991	High School <i>Lycée Ponthus de Thiard</i> , Saint-Rémy (Saône-et-Loire), France
1991-1994	DEUG (Diplôme d'Etudes Universitaires Générales) Nature and Life Sciences, University of Burgundy, Dijon (Côte d'Or), France
1994-1997	Licence, Maîtrise, Chemistry, University Louis Pasteur, Strasbourg (Alsace), France
1997-1998	DEA (Diplôme d'Etudes Approfondies) Chimie des Métaux de Transition et d'Ingénierie Moléculaire, University Louis Pasteur, Strasbourg, (Alsace), France
1998-2003	Ph.D. Thesis under the supervision of Prof. Dr. A. Wokaun (ETH Zurich) at the Paul Scherrer Institute in Villigen (Aargau), Switzerland